SCALING AND SELF-SIMILARITY IN MULTI-DIMENSIONAL FLOW THROUGH UNSATURATED POROUS MEDIA

A THESIS SUBMITTED TO
THE GRADUATE SCHOOL OF NATURAL AND APPLIED SCIENCES
OF
MIDDLE EAST TECHNICAL UNIVERSITY

BY

MUSTAFA MAZHAR BASA

IN PARTIAL FULFILLMENT OF THE REQUIREMENTS
FOR
THE DEGREE OF DOCTOR OF PHILOSOPHY
IN
CIVIL ENGINEERING

FEBRUARY 2026

Approval of the thesis:

SCALING AND SELF-SIMILARITY IN MULTI-DIMENSIONAL FLOW THROUGH UNSATURATED POROUS MEDIA

submitted by **MUSTAFA MAZHAR BASA** in partial fulfillment of the requirements for the degree of **Doctor of Philosophy** in **Civil Engineering, Middle East Technical University** by,

Prof. Dr. Naci Emre Altun
Dean, **Graduate School of Natural and Applied Sciences** _____

Prof. Dr. Erdem Canbay
Head of the Department, **Civil Engineering** _____

Assoc. Prof. Dr. Ali Ercan
Supervisor, **Civil Engineering, METU** _____

Examining Committee Members:

Prof. Dr. Ayşe Burcu Altan Sakarya
Civil Engineering, METU _____

Assoc. Prof. Dr. Ali Ercan
Civil Engineering, METU _____

Prof. Dr. Mete Köken
Civil Engineering, METU _____

Prof. Dr. Mustafa Levent Kavvas
Civil and Env. Engineering, Univ. of California Davis, USA _____

Assoc. Prof. Dr. Kei Ishida
Civil and Env. Engineering, Kumamoto University, Japan _____

Date: 27.02.2026

I hereby declare that all information in this document has been obtained and presented in accordance with academic rules and ethical conduct. I also declare that, as required by these rules and conduct, I have fully cited and referenced all material and results that are not original to this work.

Name Last name : Mustafa Mazhar Basa

Signature :

ABSTRACT

SCALING AND SELF-SIMILARITY IN MULTI-DIMENSIONAL FLOW THROUGH UNSATURATED POROUS MEDIA

Basa, Mustafa Mazhar
Doctor of Philosophy, Civil Engineering
Supervisor: Assoc. Prof. Dr. Ali Ercan

February 2026, 114 pages

Researchers have been exploring scaling and self-similarity within hydrologic and hydraulic processes governed by nonlinear partial differential equations to better understand and model their complex nature. In this study, a theoretical scaling framework is developed using the Lie group of point transformations, under which one-, two-, and three-dimensional unsteady flow in unsaturated porous media exhibits self-similarity. This work extends scaling and self-similarity analysis to the initial and boundary value problem of unsteady flow in multi-dimensional unsaturated porous media, linking a critical gap between classical hydrodynamic scaling and porous media flow. Lie group theory, originally formulated by Sophus Lie in the nineteenth century for solving differential equations, provides a powerful mathematical foundation for identifying symmetries and invariance properties of the governing equations in complex physical processes. Main contribution of this study is the derivation of scaling conditions that simultaneously preserve form of the governing equations in scaled domain and associated initial and boundary conditions, yielding self-similarity in multi-dimensional unsteady unsaturated flow. Numerical simulations are used to demonstrate the existence of self-similar solutions across multiple space-time domains under the derived scaling transformations.

Performed numerical examples confirm that self-similarity across multiple space-time domains of unsaturated flow can be achieved under the proposed scaling conditions. In engineering practice, configuration of experimental studies is constrained by factors such as the available laboratory space, accessible materials, and feasible experimental durations. The derived scaling relations enhance spatial, temporal, and economic flexibility in design and implementation of physical models, offering new insights into unsteady unsaturated porous media flow.

Keywords: Scaling Laws, Self-similarity, Unsaturated Porous Media, Unsteady Multi-dimensional Flow, Lie Group Transformations

ÖZ

DOYMAMIŞ GÖZENEKLİ ORTAMDAKİ ÇOK BOYUTLU AKIŞTA ÖLÇEKLENDİRME VE ÖZ BENZERLİK

Basa, Mustafa Mazhar
Doktora, İnşaat Mühendisliği
Tez Yöneticisi: Doç. Dr. Ali Ercan

Şubat 2026, 114 sayfa

Araştırmacılar, hidrolojik ve hidrolik süreçlerin karmaşık doğasını daha iyi anlamak ve modellemek için, doğrusal olmayan kısmi diferansiyel denklemlerin yönettiği bu süreçlerde ölçeklendirme ve özbenzerliği araştırmaktadır. Bu çalışmada, Lie Noktasal Ölçekleme Dönüşümleri Grubu kullananılarak, doymamış gözenekli ortamlarda bir, iki ve üç boyutlu kararsız (zamanla değişen) akışların özbenzerlik sergilediği yeni bir ölçeklendirme yaklaşımı önerilmektedir. Bu çalışma, ölçeklendirme ve özbenzerlik analizini çok boyutlu doymamış gözenekli ortamlarda kararsız akışın başlangıç ve sınır değer problemine genişleterek, klasik hidrodinamik ölçeklendirme ile gözenekli ortam akışı arasındaki kritik boşluğu doldurmaktadır. 19. yüzyılda Sophus Lie tarafından diferansiyel denklemleri çözmek için geliştirilen Lie grubu teorisi, karmaşık fiziksel süreçlerde özbenzerlik koşullarını belirlemek için güçlü bir temel sağlar. Bu çalışmanın literatüre ana katkısı, ölçeklendirilmiş alanda (domainde) yönetici denklemlerin ve ilgili başlangıç ve sınır koşullarının formunu aynı anda koruyan ölçeklendirme koşullarının türetilmesidir. Bu, çok boyutlu kararsız doymamış gözenekli ortamdaki akışta özbenzerlik sağlar. Sayısal simülasyonlar, türetilen ölçeklendirme dönüşümleri altında birden fazla uzay-zaman alanında özbenzer çözümlerin varlığını göstermek için kullanılmıştır.

Gerçekleştirilen sayısal örnekler, önerilen ölçeklendirme koşulları altında doymamış akışın birden fazla uzay-zaman alanında özbenzerliğin elde edilebileceğini doğrulamaktadır. Mühendislik uygulamalarında, deneysel çalışmaların düzenlenmesi mevcut laboratuvar alanı, erişilebilir malzemeler ve uygulanabilir deney süreleri gibi faktörlerle sınırlıdır. Türetilen ölçeklendirme ilişkileri, fiziksel modellerin tasarımı ve uygulanmasında mekansal, zamansal ve ekonomik esnekliği artırarak, doymamış gözenekli ortamlarda kararsız akışa ilişkin yeni öngörüler sunmaktadır.

Anahtar Kelimeler: Ölçekleme Yasaları, Özbenzerlik, Doymamış Gözenekli Ortamlar, Kararsız Çok Boyutlu Akış, Lie Grubu Dönüşümleri

Dedication

For my beloved mother, for my amazing wife, for my baby.

ACKNOWLEDGMENTS

First and foremost, I would like to express my sincere gratitude to my advisor, Assoc. Prof. Dr. Ali Ercan for his invaluable support, insightful guidance, patience, and continuous encouragement throughout the course of my PhD studies. I would never accomplish such complicated tasks without his support, I wish him all the best for his future research career and happiness in his personal life and health for his family

I am deeply grateful to the members of my thesis monitoring committee members Assoc. Prof. Dr. Elif Oğuz for her honest, direct and professional guidance and Assoc. Prof. Dr. Kei Ishida for his original and different perspective and also his patience and not complaining about the time difference between Turkey and Japan. We were deeply saddened by the passing of Dr. Elif Oğuz , who will always be remembered.

I would also like to thank Prof. Dr. Ayşe Burcu Altan Sakarya, Prof. Dr. Mete Köken, and Prof. Dr. Levent Kavvas for being part of my dissertation jury and for their valuable time, insightful comments, and contributions to the final evaluation of my dissertation.

I would like to extend my heartfelt thanks to Prof. Dr. İsmail Aydın for his initial guidance and patience in this long journey and wish him healthy and peaceful retirement.

TABLE OF CONTENTS

ABSTRACT v

ÖZ vii

ACKNOWLEDGMENTS x

TABLE OF CONTENTS xi

LIST OF TABLES xiv

LIST OF FIGURES xvi

LIST OF ABBREVIATIONS xx

LIST OF SYMBOLS xxi

CHAPTERS

1 INTRODUCTION 1

1.1 Research Motivation and Novelty 4

1.2 Research Objectives 6

1.3 Description of Chapters 7

2 LITERATURE REVIEW 11

2.1 Applications of Unsteady Flow Through Unsaturated Porous Media 11

2.2 Scaling in Flow Through Unsaturated Porous Media 15

2.3 Scaling and Self-similarity by Lie group Scaling Transformation in Hydraulics and Hydrology 18

3 GOVERNING EQUATIONS 21

3.1 Introduction 21

3.2 Three-Dimensional Unsteady Flow Through Porous Media 22

3.3 Two-Dimensional Unsteady Flow Through Porous Media 22

3.4 One-Dimensional Unsteady Flow Through Porous Media 23

3.5 Unsaturated Hydraulic Conductivity Models 23
3.6 Initial and Boundary Conditions 25
3.7 Evaluation Metrics 26
3.7.1 Root Mean Square Error (RMSE) 26
3.7.2 R-value (Correlation Coefficient) 27
3.7.3 Nash-Sutcliffe Efficiency (NSE) 27
4 NOVEL SCALING AND SELF-SIMILARITY CONDITIONS BY ONE-PARAMETER LIE GROUP POINT SCALING TRANSFORMATIONS 29
4.1 Introduction 29
4.2 One Parameter Lie Group Point Scaling Transformations 30
4.2.1 One-dimensional unsteady flow through porous media 30
4.2.2 Two-dimensional unsteady flow through porous media 33
4.2.3 Three-dimensional unsteady flow through porous media 35
4.3 Novel scaling and self-similarity conditions 36
4.3.1 One-dimensional unsteady flow through porous media 36
4.3.2 Two-dimensional unsteady flow through porous media 36
4.3.3 Three-dimensional unsteady flow through porous media 37
4.4 Usage of Scaling of Richards Equation in Engineering Practice 37
5 NUMERICAL VERIFICATION OF SCALING ONE-DIMENSIONAL UNSTEADY FLOW THROUGH POROUS MEDIA 39
5.1 Scaling Using Identical Hydraulics Conductivities in One-Dimensional Flow 40
5.2 Scaling Using Different Hydraulic Conductivities in One-Dimensional Flow 58

6 NUMERICAL VERIFICATION OF SCALING TWO-DIMENSIONAL UNSTEADY FLOW THROUGH POROUS MEDIA 75

6.1 Scaling Using Identical Hydraulics Conductivities in Two-Dimensional Flow …….77

6.2 Scaling Using Different Hydraulics Conductivities in Two-Dimensional Flow ……..90

7 CONCLUSIONS.....103

7.1 Summary and Concluding Remarks 103

7.2 Limitations and Recommendations for Future Research..... 105

REFERENCES 107

CURRICULUM VITAE……....114

LIST OF TABLES

TABLES

Table 5.1 Identification of original and scaled domains used for 1-dimensional flow through unsaturated porous media.....40
Table 5.2 Scaling conditions used to obtain scaled domains from the original domain while maintaining constant hydraulic conductivity for 1-dimensional flow through unsaturated porous media.....44
Table 5.3 Problem descriptions for the original and scaled domains with identical hydraulic conductivities for 1-dimensional flow through unsaturated porous media 45
Table 5.4 Scaling conditions used to obtain scaled domains from the original domain with different hydraulic conductivities for 1-dimensional flow through unsaturated porous media 61
Table 5.5 Problem descriptions for the original and scaled domains with different hydraulic conductivities for 1-dimensional flow through unsaturated porous media 62
Table 6.1 Identification of original and scaled domains used for 2-dimensional flow through unsaturated porous media.....77
Table 6.2 Scaling conditions used to obtain scaled domains from the original domain while maintaining constant hydraulic conductivity for 2-dimensional flow through unsaturated porous media.....80
Table 6.3 Problem descriptions for the original and scaled domains with identical hydraulic conductivities for 2-dimensional flow through unsaturated porous media 81
Table 6.4 Scaling conditions used to obtain scaled domains from the original domain with different hydraulic conductivities for 2-dimensional flow through unsaturated porous media 93

Table 6.5 Problem descriptions for the original and scaled domains with different hydraulic conductivities for 2-dimensional flow through unsaturated porous media 94

LIST OF FIGURES

FIGURES

Figure 1.1. A typical representation of flow through unsaturated porous media or vadose zone 3

Figure 4.1. Schematic representation of the transformation from the original domain to the scaled domain in one-dimensional flow through unsaturated porous media 32

Figure 4.2. Schematic representation of the transformation from the original domain to the scaled domain in two-dimensional flow through unsaturated porous media 34

Figure 5.1. Comparison of pressure head between original domain (1D-0) and scaled domains (1D-1, 1D-2, and 1D-3) at Times t = 0 to 4 Hours in original domain and corresponding scaled times in scaled domains for 1D flow with constant hydraulic conductivity. 47

Figure 5.2. Comparison of hydraulic head between original domain (1D-0) and scaled domains (1D-1, 1D-2, and 1D-3) at Times t = 0 to 4 Hours in original domain and corresponding scaled times in scaled domains for 1D flow with constant hydraulic conductivity. 49

Figure 5.3. Comparison of water content between original domain (1D-0) and scaled domains (1D-1, 1D-2, and 1D-3) at Times t = 0 to 4 Hours in original domain and corresponding scaled times in scaled domains for 1D flow with constant hydraulic conductivity. 51

Figure 5.4. Scatter plots comparing pressure head values in Original Domain (1D-0) and scaled domains (1D-1, 1D-2, 1D-3) at Times t = 1 to 4 hours in original domain and corresponding scaled times in scaled domains for 1D flow with constant hydraulic conductivity. The slope of the regression line reflects the pressure head scaling ratio between scaled and original domain. 54

Figure 5.5. Scatter plots comparing water content values in Original Domain (1D-0) and scaled domains (1D-1, 1D-2, 1D-3) at Times t = 1 to 4 hours in original domain and corresponding scaled times in scaled domains for 1D flow with constant hydraulic conductivity. The slope of the regression line reflects the pressure head scaling ratio between scaled and original domain. 57
Figure 5.6. Comparison of pressure head between original domain (1D-0) and scaled domains (1D-4, 1D-5, and 1D-6) at Times t = 0 to 4 Hours in original domain and corresponding scaled times in scaled domains for 1D flow with distinct hydraulic conductivity. 64
Figure 5.7. Comparison of hydraulic head between original domain (1D-0) and scaled domains (1D-4, 1D-5, and 1D-6) at Times t = 0 to 4 Hours in original domain and corresponding scaled times in scaled domains for 1D flow with distinct hydraulic conductivity. 66
Figure 5.8. Comparison of water content between original domain (1D-0) and scaled domains (1D-4, 1D-5, and 1D-6) at Times t = 0 to 4 Hours in original domain and corresponding scaled times in scaled domains for 1D flow with district hydraulic conductivity. 68
Figure 5.9. Scatter plots comparing pressure head values in Original Domain (1D-0) and scaled domains (1D-4, 1D-5, 1D-6) at Times t = 1 to 4 hours in original domain and corresponding scaled times in scaled domains for 1D flow with distinct hydraulic conductivity. The slope of the regression line reflects the pressure head scaling ratio between scaled and original domain. 71
Figure 5.10. Scatter plots comparing water content values in Original Domain (1D-0) and scaled domains (1D-4, 1D-5, 1D-6) at Times t = 1 to 4 hours in original domain and corresponding scaled times in scaled domains for 1D flow with distinct hydraulic conductivity. The slope of the regression line reflects the pressure head scaling ratio between scaled and original domain. 74
Figure 6.1. Sample 2D domain which represents the groundwater reservoir recharge from a drainage trench (List and Radu, 2016). 76

Figure 6.2. Temporal evolution of pressure head (m) from t = 0 to 3 days in Domain 2D-0 (prototype domain), and at the corresponding scaled times in Domains 2D-1, 2D-2, and 2D-3 for two-dimensional flow under identical hydraulic conductivity values (Case 1) 82
Figure 6.3. Temporal evolution of water content (%) from t = 0 to 3 days in Domain 2D-0 (prototype domain), and at the corresponding scaled times in Domains 2D-1, 2D-2, and 2D-3 for two-dimensional flow under identical hydraulic conductivity values (Case 1) 83
Figure 6.4. Scatter plots comparing pressure head (m) values in Domain 2D-0 (prototype domain) with those in scaled Domains 2D-1,2D-2, and 2D-3 at time steps from t = 0 to 3 days in the original domain and at the corresponding scaled times in the scaled domains for two-dimensional flow under identical hydraulic conductivity values (Case 1). The slope of the regression line represents the inverse of the pressure head scaling ratio ($S_{R\Psi}$). 86
Figure 6.5. Scatter plots comparing water content (%) values in Domain 2D-0 (prototype domain) with those in scaled Domains 2D-1, 2D-2, and 2D-3 at time steps from t = 0 to 3 days in the original domain and at the corresponding scaled times in the scaled domains for two-dimensional flow under identical hydraulic conductivity values (Case 1). The slope of the regression line is 1, reflecting the water content scaling ratio. 89
Figure 6.6. Temporal evolution of pressure head (m) from t = 0 to 3 days in Domain 2D-0 (prototype domain), and at the corresponding scaled times in Domains 2D-4, 2D-5, and 2D-6 for two-dimensional flow under different hydraulic conductivity values (Case 2). 95
Figure 6.7. Temporal evolution of water content (%) from t = 0 to 3 days in Domain 2D-0 (prototype domain), and at the corresponding scaled times in Domains 2D-4, 2D-5, and 2D-6 for two-dimensional flow under different hydraulic conductivity values (Case 2). 96
Figure 6.8. Scatter plots comparing pressure head (m) values in Domain 2D-0 (prototype domain) with those in scaled Domains 2D-4, 2D-5, and 2D-6 at time

steps from t = 0 to 3 days in the original domain and at the corresponding scaled times in the scaled domains for two-dimensional flow with different hydraulic conductivity values (Case 2). The slope of the regression line represents the inverse of the pressure head scaling ratio ($1/\mathrm{SR}\Psi$). 99
Figure 6.9. Scatter plots comparing water content (%) values in Domain 2D-0 (prototype domain) with those in scaled Domains 2D-4, 2D-5, and 2D-6 at time steps from t = 0 to 3 days in the original domain and at the corresponding scaled times in the scaled domains for two-dimensional flow with different hydraulic conductivity values (Case 2). The slope of the regression line is 1, reflecting the water content scaling ratio. 102

LIST OF ABBREVIATIONS

ABBREVIATIONS

ADR	Advective-Dispersive-Reactive
HYDRUS	Computational software for simulating water flow developed Šimůnek et al. (2016)
IBVP	Initial Boundary Value Problem
RANS	Reynolds Averaged Navier Stokes Equation
SWCC	Soil-Water Characteristic Curve
RMSE	Root Mean Square Error
NSE	Nash-Sutcliffe Efficiency

LIST OF SYMBOLS

SYMBOLS

t	time
x	distance in x direction
y	distance in y direction
z	distance in z direction
q	the water flux
K_z	the hydraulic conductivity in z-direction
h	the total hydraulic head
L	flow path length
q_x	water fluxes in x direction
q_y	water fluxes in y direction
q_z	water fluxes in z direction
θ	volumetric water content
K_s	saturated hydraulic conductivity
K_{s_x}	saturated hydraulic conductivity in x direction
K_{s_y}	saturated hydraulic conductivity in y direction
K_{s_z}	saturated hydraulic conductivity in z direction
$K_r(\theta)$	relative hydraulic conductivity as a function of water content
Ψ	matric head
θ_s	residual water content

θ_r saturated water content

α pore-size distribution parameter (van Genuchten, 1980)

m hydraulic conductivity function (van Genuchten, 1980)

L an empirical pore-connectivity parameter (Mualem, 1976)

S_e effective water saturation

λ pore-size distribution index

Ψ matric pressure head

Ψ_a air-entry head value

Γ_D a Dirichlet type boundary condition

Γ_N a Neumann type boundary condition

q_N flux across the boundary for Neumann type boundary condition

ϵ scaling parameter

α scaling exponent

SR_θ scaling ratio for water content

SR_t scaling ratio for time

SR_x scaling ratio for distance in x-direction

SR_y scaling ratio for distance in y-direction

SR_z scaling ratio for distance in z-direction

SR_Ψ scaling ratio for matric potential

SR_{K_x} scaling ratio for hydraulic conductivity in x-direction

SR_{K_y} scaling ratio for hydraulic conductivity in y-direction

SR_{K_z} scaling ratio for hydraulic conductivity in z-direction

$\bar{t}$ time in scaled domain

$\bar{x}$ distance in x direction in scaled domain

$\bar{y}$ distance in y direction in scaled domain

$\bar{z}$ distance in z direction in scaled domain

$\bar{q}$ the water flux in scaled domain

$\overline{K_z}$ the hydraulic conductivity in z-direction in scaled domain

$\bar{h}$ the total hydraulic head in scaled domain

$\bar{L}$ flow path length in scaled domain

$\overline{q_x}$ water fluxes in x direction in scaled domain

$\overline{q_y}$ water fluxes in y direction in scaled domain

$\overline{q_z}$ water fluxes in z direction in scaled domain

$\bar{\theta}$ volumetric water content in scaled domain

$\overline{K_s}$ saturated hydraulic conductivity in scaled domain

$\overline{K_{s_x}}$ saturated hydraulic conductivity in *x* direction in scaled domain

$\overline{K_{s_y}}$ saturated hydraulic conductivity in *y* direction in scaled domain

$\overline{K_{s_z}}$ saturated hydraulic conductivity in *z* direction in scaled domain

CHAPTER 1

INTRODUCTION

In the literature, extensive efforts have been made to model the behavior of fluids and solids to better understand their individual dynamics and interactions. These models aim to develop mathematical representations of natural phenomena to enable numerical predictions of system behavior. By applying governing equations, initial and boundary conditions, and relevant physical properties, researchers can simulate and analyze complex systems with greater precision.

In hydromechanics, one of the most challenging aspects of modeling fluid flow is the involvement of nonlinear differential equations. To address this complexity, techniques such as scaling and self-similarity have emerged as powerful tools. These methods simplify complicated processes by transferring quantitative data from one spatial or temporal domain to another, allowing scientists to utilize verified data from previously studied cases to solve new problems more efficiently.

One of the leading research areas within this field is the interaction between fluids and soils, commonly referred to as flow through porous media. Porous media are materials characterized by interconnected pores or voids that allow the movement of fluids such as water, air, or oil. These include natural substances like soils and rocks, as well as engineered materials such as concrete. Of particular importance is the unsaturated zone, also known as the vadose zone, which lies between the land surface and the water table. This zone plays a critical role in the hydrological cycle by regulating the transport of water, nutrients, and contaminants.

Within the vadose zone, complex interactions among solid, liquid, and gaseous phases give rise to highly nonlinear and spatially heterogeneous flow behaviors, as depicted in Figure 1.1. Traditional modeling approaches often fall short in capturing these intricacies, highlighting the need for more sophisticated and adaptive methods. One such modeling challenge involves predicting the water-retention curve, a topic that will be explored in detail in the following sections.

In many cases, flow through porous media can be approximated as steady; however, real-world conditions are rarely steady. Temporal variability in rainfall, groundwater levels, and irrigation practices introduce time-dependent changes in fluid movement. As a result, porous media flow is often unsteady, with velocity, pressure, and moisture content varying over time.

Understanding unsteady flow in porous media is fundamental to a wide range of environmental and engineering applications. These dynamic processes play a critical role in water resources management, soil remediation, agricultural planning, and infrastructure design. This study focuses on fluid-soil interactions, commonly referred to as flow through porous media. Unsaturated porous media are common in both natural and engineered environments, including soils, rocks, and construction materials. Accurately modeling water movement and its interactions within these media is essential for reliably predicting system behavior across key civil engineering disciplines such as hydraulics, hydrology, geotechnical engineering, groundwater engineering, and water resource management.

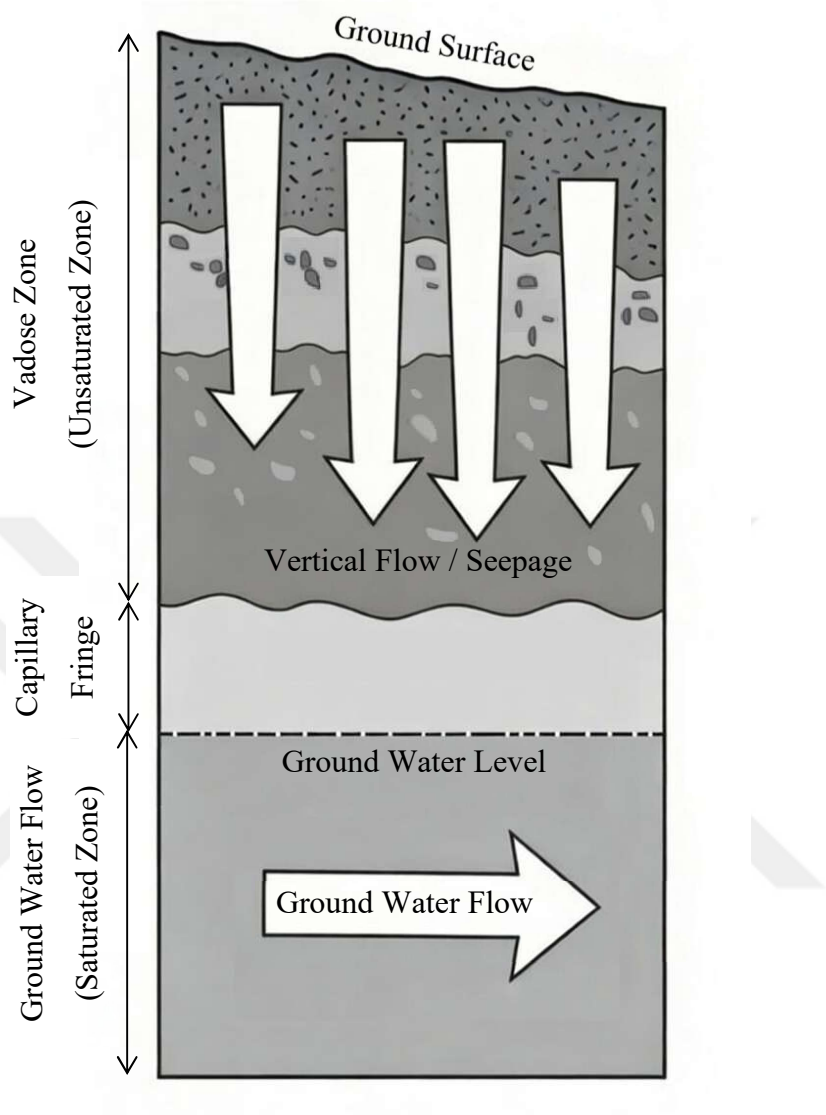

Figure 1.1. A typical representation of flow through unsaturated porous media or vadose zone (Adapted from Saeid and Faezeh, 2025)

1.1 Research Motivation and Novelty

Self-similarity is a concept closely related to scaling. It refers to the property of a system or object that exhibits similar patterns at different scales. In other words, two self-similar systems look essentially the same, regardless of the scale at which they are observed (Mandelbrot, 1982). This property is very common in nature, some examples can be the fractal patterns of coastlines (Turcotte, 1989).

Self-similarity and scaling are crucial for understanding and modeling various phenomena across different spatial and temporal scales. For instance, the patterns observed in river networks at a large scale can often be seen repeating in smaller tributary systems, exhibiting a degree of self-similarity (Rodriguez-Iturbe & Rinaldo, 1997).

Scaling and self-similarity serve as tools for transferring conditions, analyses, and quantitative insights from one spatial or temporal domain to another. Mandelbrot (1982) proposed the concept of fractal geometry to describe the irregularity and fragmentation found in nature and the patterns that remain consistent across different geometric scales. Fractals, along with dimensional analysis, symmetry, scale invariance, and self-similarity, form interconnected principles that provide valuable insight into the relationships between different scales in geophysical processes.

Similar to fractals, certain geophysical phenomena can exhibit self-similarity when subjected to appropriate scaling transformations across specific spatial and temporal dimensions. This study examines the conditions under which the multi-dimensional unsteady flow through porous media exhibits self-similar behavior by applying a one-parameter Lie group of point scaling transformations to the initial-boundary value problem (IBVP) of the governing process. Lie groups, originally developed by Sophus Lie in the 19th century (Lie, 1888), were introduced as a powerful mathematical tool for solving differential equations. These mathematical structures enable the reduction of nonlinear partial differential equations, such as

those governing fluid flow, into simpler, lower-order forms through point transformation techniques (Bluman and Cole, 1974; Ibragimov, 1994; and Bluman and Anco, 2002).

Lie group scaling transformation framework was recently applied to several hydraulic and hydrologic processes (Haltas and Kavvas, 2011; Ercan et al., 2014; Carr et al., 2015; Ercan and Kavvas, 2015a, 2015b; 2017; Ercan, 2020). However, it will be the first time in this study to apply it to initial and boundary value problem of unsteady flow through multi-dimensional unsaturated porous media.

Utilizing Lie group of point transformations framework, this study extends the application of scaling and self-similarity analysis to the initial and boundary value problem of unsteady flow in multi-dimensional unsaturated porous media, where such an approach has not previously been applied. This novel extension aims to bridge the gap between classical hydrodynamic scaling and porous media flow, offering new insights into the behavior of unsteady, multi-dimensional systems under varying spatial and temporal scales.

A key limitation of traditional Reynolds and Froude number similitude lies in its tendency to treat one parameter as dominant while disregarding the influence of the other. However, in many practical problems, both parameters play a critical role simultaneously. To ensure dynamic similarity between the prototype and the scaled model, whether in physical modeling or numerical simulation, both Reynolds and Froude numbers must be scaled concurrently.

A key strength of the proposed approach is its ability to examine self-similarity conditions not only arising from the governing equations but also from the initial and boundary conditions. By implementing the derived scaling laws to unsteady flow in multi-dimensional unsaturated porous media, the value of a flow variable at a specific time and location within a scaled domain can be reliably mapped to its corresponding value in the original domain at the equivalent relative time and spatial position. The scaling relations derived by the Lie group transformation approach offer enhanced spatial, temporal, and economic flexibility in the design

and implementation of physical hydraulic models for unsteady flow in multi-dimensional unsaturated porous media.

In engineering practice, the configuration of experimental studies is constrained by factors such as the available laboratory space, accessible materials, and feasible experimental durations. By applying the derived novel scaling conditions, the corresponding scaling parameters can be determined to match these practical limitations. As such, the derived scaling relations enhance spatial, temporal, and economic flexibility in the design and implementation of physical models, offering new insights into unsteady, multi-dimensional flow in unsaturated porous media.

1.2 Research Objectives

Within the above framework, the objectives of this study are:

1. To transform the governing equations of one-, two, three-dimensional Richards equation (Richards, 1931) to model unsteady flow through unsaturated porous media by Lie group of point transformations following the methodologies outlined in in Bluman and Anco, 2002; Polyanin and Manzhirov, 2006; and Haltas and Kavvas, 2011.
2. To transform empirical closure relations of the Richards equation, specifically those proposed by Brooks and Corey (1964), and Van Genuchten (1980). These closures define the relationships between volumetric water content, hydraulic conductivity, and matric potential.
3. To derive self-similarity and scaling conditions for unsaturated flow through porous media by Lie group of point transformations such that the transformed governing equations remain invariant, preserving the form of the original equations.
4. To conduct numerical simulations to represent original (prototype) domain of one-, two-dimensional cases of unsteady flow through unsaturated porous media.

5. To implement the derived self-similarity and scaling conditions to construct scaled domains from the original prototype domain.
6. To verify the proposed scaling framework by comparing numerical solutions for the original and scaled domains, and to assess the consistency and accuracy of the self-similarity conditions.

1.3 Description of Chapters

Chapter 1 serves as the introduction to this study, presenting the necessary background to understand the research problem. It begins by discussing the broader context of unsteady flow through unsaturated porous media, explaining why this topic is significant in the field of fluid mechanics and hydrology. The chapter also details the motivation for the investigation, describing the gaps in existing knowledge and the reasons for pursuing this line of research. Furthermore, it outlines the specific objectives that guide the study, such as transforming the governing equations of the Richards equation using Lie group point transformations, addressing empirical closure relations, and establishing self-similarity and scaling conditions. By clearly stating the aims and setting the groundwork for later chapters, Chapter 1 provides readers with a comprehensive overview of what the thesis seeks to achieve.

Chapter 2 provides a literature review, focusing on the application of scaling and self-similarity principles in fluid mechanics. It examines various established methods for scaling unsteady flow through porous media, as well as other types of flows encountered in hydromechanics. The chapter also highlights the innovative use of Lie point group transformations for scaling, as introduced in this thesis, and discusses instances where this novel approach has been applied to other fluid mechanics processes. By presenting both conventional and emerging scaling techniques, Chapter 2 establishes a solid foundation for the methodologies developed and implemented in subsequent chapters.

Chapter 3 outlines the main methodologies adopted in this study. It introduces the selected models, governing equations, and the initial and boundary conditions relevant to unsteady flow through unsaturated porous media. The chapter then describes how the one-parameter Lie group of point scaling transformations is applied to these equations, transforming both the partial differential equations and their corresponding initial and boundary conditions. Solutions to the transformed initial boundary value problem are then presented for both upscaled and downscaled domains, providing a comprehensive framework for analyzing flow behavior under different scaling scenarios.

The first three chapters of this study covering the introduction, literature review, and the development of methodologies set the groundwork and provide essential background, but do not encompass the novel aspects of this research. The true innovation begins after Chapter 3, where this thesis introduces a new approach to scaling the Richards Equation, presenting the original contribution of this thesis study. So, the next chapters following Chapter 3, introduces its novel contribution by presenting an innovative method for scaling the Richards Equation.

Chapter 4 presents the application of the new scaling method developed in this study. It explains how the one-parameter Lie point group transformations are used in scaling of different flow scenarios in 1D, 2D, and 3D unsteady unsaturated porous media. Chapter 4 highlights the advantages and reliability of this innovative approach.

Chapter 5 and 6 is dedicated to the verification of the novel scaling method introduced for unsteady flow through porous media in 1D and 2D, respectively. In both chapters, a previously verified example problem in literature will be used to apply the novel scaling approach explained in Chapter 4. By using this novel scaling approach, new self-similar domains will be generated from the original domain and the numerical simulations will be performed for the new domains and the results will be compared with the original domain to verify the success of scaling approach.

Chapter 7 concludes the thesis by summarizing the main findings, discussing the significance of the results, and providing recommendations for future research. It reflects on the methods and results presented in earlier chapters, emphasizing the contributions made to the understanding of scaling and self-similarity in unsaturated flow. The chapter also suggests potential improvements and areas where the proposed methodology can be further applied or developed.

CHAPTER 2

LITERATURE REVIEW

In this chapter, literature survey that summarizes the previous academic studies on the subject of thesis will be presented.

2.1 Applications of Unsteady Flow Through Unsaturated Porous Media

The vadose zone, representing the initial layer of infiltration above the saturated groundwater zone, is widely recognized as a typical example of unsaturated porous media. Such media are commonly present in soils, rocks, and certain building materials. Following precipitation, rainwater does not immediately descend to deeper aquifers; instead, it moves downward through the vadose zone. This region exemplifies unsaturated porous media (Selker et al., 1999).

Unsteady flow through unsaturated porous media often occurs within the vadose zone due to variable rainfall or irrigation, resulting in changing moisture content over time. In addition to natural soils, such unsteady flows can be observed in engineered landfill covers, concrete structures exposed to intermittent water infiltration, and even in oil reservoirs during secondary recovery processes. These examples demonstrate how fluctuations in source input or boundary conditions lead to dynamic changes within unsaturated porous systems, making them important across a variety of environmental and industrial contexts.

An unsaturated porous medium refers to a material, domain, or environment that consists of interconnected spaces containing both air and liquid (Bear, 1972). In the vadose zone, these spaces include voids between soil particles, holes, openings, gaps, cracks in rocks, and root channels. They hold a combination of air and water,

resulting in an unsaturated condition. The vadose zone extends from the ground surface down to the water table. The water table marks the lower boundary of the vadose zone; below it, the ground is fully saturated with water. The term "unsaturated" is used because the pore spaces within soil particles in this zone are not entirely filled with water but contain both air and water. This contrasts with the saturated zone (or phreatic zone) located beneath the water table, where all pore spaces are occupied by water (Fetter, 2001).

The presence of an unsaturated vadose zone is primarily due to capillary forces. Capillary forces originate from the surface tension of water and its interaction with the solid surfaces of soil particles or rock fractures (Nimmo, 2004). These forces pull water upward against gravity in small spaces. Within the vadose zone, water remains in smaller pores and as films coating soil particles because of these capillary forces, which are also known as matric forces or soil suction. In contrast, larger pores generally contain air, as the gaps are too wide for capillary forces to retain water against gravity. As depth increases from the water table through the vadose zone, gravity's influence on water retention becomes more significant than that of capillary forces. This leads to a reduction in water content, making the upper portions of the vadose zone less saturated compared to areas near the capillary fringe, the region above the water table where capillary action can still result in near-saturation under sub-atmospheric pressure. The coexistence of air and water in the vadose zone arises from the interplay between gravity pulling water downward and capillary forces retaining water within the porous medium. The degree of saturation or unsaturation, typically defined as water content by percentage, at any point in the vadose zone depends mainly on the material's pore size distribution and the relative magnitudes of capillary and gravitational forces.

As a summary, the vadose zone is "unsaturated" or "not fully saturated", because the capillary forces can only hold a certain amount of water within the pore spaces against the gravity, leaving the remaining space to be filled with air. The distribution of water and air within this zone is largely determined by the magnitude of capillary forces, which are strongest in smaller pores and close to the

groundwater table. The movement of water through the soil particles is influenced by factors like soil particle sizes and texture, presence of organic matter, and forces acting on water particles like gravity and surface tension. Some of the water is caught and retained by the soil particles due to adhesive forces, while the rest continues its downward movement, which is also called vertical filtration, until it reaches the saturated zone and becomes part of groundwater.

Another example of an unsaturated porous media can be concrete in building materials. It has a complex internal structure consisting of pores of varying sizes. These pores can hold water in different states: free water in larger pores, adsorbed water on the surfaces of the cement particles, and chemically bound water within the hydration products. Baroghel-Bouny (2007), has demonstrated how different water states exist in the concrete pore structure. The moisture content within these pores varies with the ambient humidity and temperature, impacting the material's properties and durability. Its behavior under varying moisture conditions is a critical aspect of its performance, impacting durability, thermal properties, and structural integrity. Understanding and modeling these characteristics can lead to improved construction practices and more durable buildings. Concrete can absorb and desorb moisture from the environment, affecting its thermal and mechanical properties. Hall (1989), provided comprehensive analysis of water absorptivity in concrete and mortars.

Another practical application of flow through porous materials can be groundwater recharge which is a fundamental process in the hydrologic cycle where water moves from the surface into subsurface aquifers, serving as a critical component in water resource management and engineering applications. This process involves the infiltration of precipitation, surface water, or artificially applied water through soil and rock layers to replenish underground water supplies. Scanlon et al. (2002) has discussed various methods, highlighting the importance of understanding unsaturated flow for accurate recharge estimation. Nimmo (2004) emphasized the role of “unsaturated flow pathways”, “pore space" and its "pore-size distribution” in influencing recharge.

In water resource management, by studying the topic of flow through porous media, scientists can develop and improve models that predict water movement in different scenarios. This allows for development of more accurate hydrological models for better management of water resources, assessment of risks like drought or flooding, and design of irrigation systems. Šimůnek et al. (2016) has described development and application of HYDRUS models, which are widely used to simulate water flow in unsaturated media for irrigation design, water resource management, and flood risk assessment.

For contaminant transport, materials like fertilizers or pollutants, may be dissolved in water. We can forecast the environmental spread of these dissolved substances or contaminants and create pollution control and remediation plans with the aid of research in flow through porous media. In order to forecast pollutant movement and create remediation plans, Toride et al. (1995) provided techniques for modeling contaminant transport, particularly through unsaturated porous media. In-depth mathematical frameworks for comprehending and forecasting the movement of contaminants in porous media were presented by Bear and Cheng (2010) and Bear (2018).

Climate change is changing precipitation patterns and increasing the risk of extreme weather events. In recent years, effect of climate change has become obvious as it has started to affect the whole global population. Studying unsaturated flow helps us understand how these changes will affect water availability, storage and movement in different regions in the long run. Taylor et al. (2013) examined how climate change affects groundwater systems through altered precipitation patterns and increased extreme events, highlighting the importance of unsaturated zone processes in determining future water availability. Trenberth (2011) discussed the effect of precipitation patterns on soil moisture and unsaturated flow.

2.2 Scaling in Flow Through Unsaturated Porous Media

In simple terms, the idea of "scaling" or "similitude" in how water moves through unsaturated porous materials (like soils or concrete) means looking for patterns, similarities, trends or rules that stay the same, even if the material or its parts change size. Such methods can be used to generate new solutions from existing solutions, or predict the results from already obtained and verified results. Early scientists like Miller and Miller (1956) noticed that if you compare soils made up of particles of different sizes, but keep other properties similar, their water behavior can look the same when you adjust (or scale) for size. This is useful for predicting how water moves in different kinds of soils or materials.

However, this only works well for very uniform materials, like well-sorted sand, not for natural soils that contain a variety of particle sizes, complex structures, organic matter, and other heterogeneities. The presence of aggregates, macropores, clay lenses, and even biological activity adds additional layers of complexity, making direct comparisons and predictions more challenging. As a result, researchers recognized the need for more advanced scaling techniques that could account for this real-world variability and provide better tools for predicting unsaturated flow in diverse soil environments.

Because natural soils are more complicated, later researchers developed new ways to group or "scale" data so that it's possible to compare and predict water movement in much more varied and real-world conditions. They found that sometimes you need to use several scaling factors, not just one, because soils in the field are made up of many different layers and particle sizes. These advances allowed for better models and predictions, which are important for things like managing water resources, irrigating crops, and understanding how contaminants move through the ground.

Miller-similar porous media are considered to be in similar states when they exhibit the same values in a characteristic length or size that applies to both pores and solid particles (Miller and Miller, 1956).

Later researches recognized the limitations of the microscopic similar-media concept for heterogeneous field soils and shifted towards more macroscopic and empirical approaches, often based on functional normalization (Reichardt et al., 1972; Warrick et al., 1977; Simmons et al., 1979; Sharma et al., 1980; Russo and Bresler, 1980). These approaches sought to combine multiple soil-water characteristic curves into one reference curve (Sposito and Jury, 1985). The importance of a scaled Richards equation for solving vadose-zone hydrology problems, by reducing the complexity of field-soil spatial heterogeneity, was emphasized (Warrick, 1990). Warrick and Amoozegar-Fard (1979) scaled the one-dimensional Richards equation using the similar media concept for constant-head boundary conditions.

Using Lie-group techniques, soil-water properties must be expressed in analytically defined forms for the Richards equation to remain mathematically consistent under scaling transformations (Sposito, 1990). In particular, the two transport coefficients, soil-water diffusivity and hydraulic conductivity, must follow power-law or exponential relationships with volumetric water content (Sposito, 1990). In addition, relative saturation is required to be scale invariant, which leads to a power-law relationship between relative saturation and matric potential (Sposito, 1990). Under certain conditions, this relationship is equivalent to the Brooks-Corey model (Brooks and Corey, 1964), as demonstrated by Sposito (1990). A generalized concept of similitude was introduced, suggesting that pore-size distribution remains unchanged under scaling, instead of the volumetric water content (Sposito and Jury, 1990). This approach aligns with the variety of particle sizes and the non-uniform porosity commonly found in field soils.

Similitude applied to centrifugal scaling of unsaturated flow was explored by Barry et al. (2001), showing that Miller-similar media allow scaling for arbitrary

boundary conditions. They also introduced Lisle-similar media as a more general class, based on the equivalence mapping of Richards' equation onto itself.

More recently, research has aimed to extend scaling methods to dissimilar soils. Dissimilar soils are those that differ significantly in properties such as texture, structure, pore-size distribution, or composition. Unlike similar soils, which share comparable physical characteristics and often respond to scaling laws in predictable ways, dissimilar soils can vary widely in their ability to hold and transmit water, their organic content, or their mineral make-up. This variability poses unique challenges, as scaling approaches developed for uniformly behaving soils do not always translate well. As a result, new scaling frameworks are needed to effectively capture water flow and retention in such heterogeneous environments. Sadeghi et al. (2011) proposed a method for scaling the Richards equation for soil water redistribution that is not restricted to specific hydraulic functions, making it applicable to dissimilar soils (Sadeghi et al., 2011). They further developed invariant solutions for Richards' equation for water movement in dissimilar soils, using exponential-power functions to reduce dependence on soil hydraulic properties (Sadeghi et al., 2012a). However, these scaled solutions can deviate when gravitational force increases or column depth increases (Sadeghi et al., 2012a). Sadeghi et al. (2012b) also added new scaled solutions to the Warrick and Hussen (1993) method, extending its applicability to a wider range of soils for specific hydraulic functions (Sadeghi et al., 2012b).

Wang (2021) conducted a scaling analysis of Richards' equation for horizontal infiltration, demonstrating that admissible scaling transformations can reduce the Richards equation to ordinary differential equations through scale symmetry analysis (Wang, 2021). This work introduced a shape factor that is independent of boundary moisture and directly related to the Brooks-Corey power exponent (Wang, 2021). Other researchers have focused on the estimation of intrinsic length scales of flow in unsaturated porous media, which are crucial for defining the range of applicability of the Richards equation and for governing phenomena such as soil evaporation and drainage (Assouline et al., 2017).

2.3 Scaling and Self-similarity by Lie group Scaling Transformation in Hydraulics and Hydrology

Lie group of point transformations framework was recently applied to several hydraulic and hydrologic processes (Haltas and Kavvas, 2011; Ercan et al., 2014; Carr et al., 2015; Ercan and Kavvas, 2015a, 2015b; 2017; Ercan, 2020). However, this study represents the first application of the approach to the initial and boundary value problem associated with unsteady flow in unsaturated porous media.

Haltas and Kavvas (2011) investigated scale invariance in various hydrologic processes as IBVP and performed a numerical demonstration to groundwater flow in confined aquifers with various initial and boundary conditions.

Ercan et al. (2014) investigated the scaling and self-similarity for one-dimensional open channel flow problem. In contrast to conventional methods, this study presents a distinction between longitudinal-horizontal and transverse-horizontal length scales. The scaled domain derived from the proposed approach, particularly when the scaling ratios of channel width and water depth are equal, plays a critical role in preserving the similarity of flow characteristics within the cross-section in one-dimensional open channel flow. This is because the width-to-depth ratio and the bank inclination angles remain consistent under such scaling conditions.

Ercan and Kavvas (2015a) examined the scaling and self-similarity properties of depth-averaged two-dimensional hydrodynamic equations system formulated as an IBVP in addition to two-dimensional k-e turbulence model. Numerical applications were performed for a contracting open channel flow scenario. Ercan and Kavvas (2015b) extended the analysis to full Navier-Stokes equations. Building on this framework, Ercan and Kavvas (2017) investigated the scaling and self-similarity characteristics of the three-dimensional Reynolds Averaged Navier Stokes (RANS) equations, also framed as an IBVP. Numerical demonstrations were carried out for a rigid-lid cavity flow problem for both up-scaled and down-scaled domains. Given that the three-dimensional RANS equations (Ercan and Kavvas, 2017) represent

time-averaged forms of the general Navier-Stokes equations (Ercan and Kavvas, 2015b), the self-similarity conditions for the primary flow variables in both systems were found to be consistent. However, the incorporation of turbulence closure in the RANS framework required additional scaling conditions.

Building on the application of Lie group scaling transformations to the Saint-Venant equations to identify self-similarity conditions for unsteady open channel flow (Ercan et al., 2014), Carr et al. (2015) investigated the self-similarity of one-dimensional unsteady suspended sediment transport, both for the general case and with unscaled sediment diameters. Their study further explored the scaling conditions associated with unscaled sediment material properties.

Polsinelli and Kavvas (2016) examined the relationship between the Lie group scaling framework and classical scaling approaches based on dimensional analysis, non-dimensionalization, and the Buckingham-Π theorem (Buckingham, 1914). They outlined the fundamental principles of Lie group theory and demonstrated the application of Lie scaling transformations. A comparative analysis was conducted using two classical models: one addressing unconfined groundwater flow and the other focused on contaminant transport. Their results showed that the Lie scaling method yields invariant transformations of prototype variables while preserving dynamic similarity between model and prototype systems.

Ercan (2020) investigated the self-similar behavior of contaminant fate and transport in groundwater using the three-dimensional advective-dispersive-reactive (ADR) transport equation system. The derived self-similarity criteria enhance the conceptual understanding of ADR transport processes and offer spatial, temporal, and cost-effective flexibility for developing scaled models that accurately replicate field conditions governed by three-dimensional ADR dynamics.

The Lie-group-based point-scaling transformation method does not rely on a single dimensionless number, in contrast to traditional scaling approaches that are formulated in terms of specific dimensionless parameters. This distinction has also been demonstrated in the studies of Catucci et al. (2021, 2023), who showed that

conventional Froude-based scaling laws often fail for air-water flows. For compressible air-water flows, this method applies to continuity, momentum, heat transfer, and state equations, treating air as a perfect gas. For incompressible air-water flows, it applies to the Reynolds-averaged Navier-Stokes equations, incorporating surface tension effects. Unlike traditional Froude scaling laws, which frequently introduce scale effects due to an incorrect representation of viscosity, surface tension, air compressibility, and heat transfer, Lie-group-based scaling laws are specifically designed to ensure self-similarity.

Utilizing the framework of Lie groups of point transformations, this study extends scaling and self-similarity analysis to the initial and boundary value problem of unsteady flow in multi-dimensional unsaturated porous media, in which this approach has not previously been applied. This novel extension bridges classical hydrodynamic scaling with porous-media flow theory, offering new insights into the behavior of unsteady, multi-dimensional systems across varying spatial and temporal scales.

The novelty of the proposed method lies in the direct application of one-parameter Lie group point-scaling transformations to the governing equations, together with the corresponding initial and boundary conditions. This unified framework enables the derivation of a complete set of scaling conditions that all variables, including fluid properties, flow variables, and initial and boundary conditions, must satisfy to achieve self-similarity across different scales.

CHAPTER 3

GOVERNING EQUATIONS

In this chapter, governing equations for unsteady flow through porous media will be summarized.

3.1 Introduction

The Richards equation, developed by Richards (1931), describes water movement in unsaturated soil by combining the continuity equation with Darcy's law. It characterizes how soil moisture varies over time and space, accounting for changes in hydraulic conductivity that occur with varying moisture content.

According to Darcy's law based on the experiments of Darcy (1856), the water flux q through a porous medium is proportional to the hydraulic gradient, dh/dL, where h is the hydraulic head and L is the flow path length.

Darcy's law is a fundamental principle governing the flow of water through porous media (Freeze and Cherry, 1979):

$$q = -K_z \frac{\mathrm{dh}}{\mathrm{dL}} \dots\dots\dots\dots\dots\dots\dots\dots\dots\dots\dots\dots\dots\dots (3.1)$$

where

q is the water flux [L/T].

K_z is the hydraulic conductivity in z-direction [L/T].

h is the total hydraulic head [L]..

L is the flow path length [L].

3.2 Three-Dimensional Unsteady Flow Through Porous Media

Starting with conservation of mass, the derivation begins by considering a controlled volume in a soil column. For a three-dimensional case, the continuity principle states that changes in moisture content over time (∂θ/∂t) must be balanced by the changes in fluxes (q) across x, y, z coordinate directions:

$$\frac{\partial \theta}{\partial t} + \frac{\partial q_x}{\partial x} + \frac{\partial q_y}{\partial y} + \frac{\partial q_z}{\partial z} = 0 \ldots\ldots\ldots\ldots\ldots\ldots\ldots\ldots\ldots\ldots (3.2)$$

where q_x, q_y, and q_z are the water fluxes in x, y, z directions.

Incorporating Darcy's law, by replacing these fluxes using Darcy's law in the continuity equation, we obtain:

$$\frac{\partial \theta}{\partial t} = \frac{\partial}{\partial x}\left(K_x(\theta)\frac{\partial h}{\partial x}\right) + \frac{\partial}{\partial y}\left(K_y(\theta)\frac{\partial h}{\partial y}\right) + \frac{\partial}{\partial z}\left(K_z(\theta)\frac{\partial h}{\partial z}\right) \ldots\ldots (3.3)$$

where h represents the total hydraulic head [L], $h = \psi(\theta) + z$ and $\psi(\theta)$ is the soil matric potential or capillary pressure head as a function of water content θ.

Expressing total hydraulic head in terms of pressure and gravitational potential and replacing $h = \psi(\theta) + z$, we obtain governing equations of three-dimensional flow

$$\frac{\partial \theta}{\partial t} = \frac{\partial}{\partial x}\left(K_x(\theta)\frac{\partial \psi}{\partial x}\right) + \frac{\partial}{\partial y}\left(K_y(\theta)\frac{\partial \psi}{\partial y}\right) + \frac{\partial}{\partial z}\left(K_z(\theta)\frac{\partial \psi}{\partial z}\right) + \frac{\partial K_z(\theta)}{\partial z} \ldots\ldots (3.4)$$

3.3 Two-Dimensional Unsteady Flow Through Porous Media

Simplifying to two-dimensional flow, we can exclude one of the horizontal terms (∂/∂y) to yield:

$$\frac{\partial \theta}{\partial t} = \frac{\partial}{\partial x}\left(K_x(\theta)\frac{\partial \psi}{\partial x}\right) + \frac{\partial}{\partial z}\left(K_z(\theta)\frac{\partial \psi}{\partial z}\right) + \frac{\partial K_z(\theta)}{\partial z} \ldots\ldots\ldots\ldots (3.5)$$

3.4 One-Dimensional Unsteady Flow Through Porous Media

Simplifying to one-dimensional vertical flow, for vertical infiltration only, we can exclude the horizontal terms (∂/∂x and ∂/∂y) to yield:

$$\frac{\partial \theta}{\partial t} = \frac{\partial}{\partial z}\left(K_z(\theta)\frac{\partial \psi}{\partial z}\right) + \frac{\partial K_z(\theta)}{\partial z} \quad \ldots\ldots\ldots\ldots\ldots\ldots\ldots\ldots\ldots\ldots\ldots\ldots (3.6)$$

3.5 Unsaturated Hydraulic Conductivity Models

The relationships between ψ-θ and K-θ are nonlinear, posing significant challenges in applying the Richards equation. The hydraulic conductivity is a nonlinear function of volumetric water content (θ). This nonlinearity arises from the complex pore structure of soils and the complex relationship between water content and the ability of water to flow through the pores. Also, the water retention curve, which relates water content to pressure head, is also nonlinear, further complicating the Richards equation to become a complex nonlinear partial differential equation

To overcome these challenges, approximations like Van Genuchten (1980), and Brooks and Corey (1964) could be employed. These approximations provide empirical relationships between volumetric soil water content and hydraulic conductivity, allowing to express these parameters as functions of a single variable (e.g., pressure head). However, it is important to note that these approximations have limitations and may not be accurate for all soil types and hydrological conditions.

The hydraulic conductivity function $K(\theta) = (K_x(\theta), K_y(\theta), K_z(\theta))$ is commonly expressed as

$$K(\theta) = K_s\, K_r(\theta) \quad \ldots\ldots\ldots\ldots\ldots\ldots\ldots\ldots\ldots\ldots\ldots\ldots\ldots (3.7)$$

where $K_s = \left(K_{s_x}, K_{s_y}, K_{s_z}\right)$ is saturated hydraulic conductivity and $K_r(\theta)$ is the relative hydraulic conductivity.

Hydraulic properties are commonly characterized by the pore-size distribution model proposed by Mualem (1976) for hydraulic conductivity, coupled with the water retention function introduced by van Genuchten (1980):

$$\theta = \begin{cases} \theta_r + \dfrac{\theta_s - \theta_r}{\left[1 + |\alpha\Psi|^n\right]^m}, & \Psi \le 0 \\ \theta_s, & \Psi > 0 \end{cases} \quad \ldots\ldots\ldots\ldots\ldots\ldots\ldots\ldots (3.8)$$

Where θ is volumetric water content at pressure (matric) head Ψ, θ_s and θ_r are the residual and saturated water contents, respectively; α (> 0, in $1/L$) is related to the inverse of the air-entry pressure; n (>1) is a measure of the pore-size distribution (van Genuchten, 1980); and $m = 1 - \frac{1}{n}$. The hydraulic conductivity function is

$$K = \begin{cases} K_s S^L{}_e \left[1 - \left(1 - S_e^{\frac{1}{m}}\right)^m\right]^2, & \Psi \le 0 \\ K_s, & \Psi > 0 \end{cases} \quad \ldots\ldots\ldots\ldots\ldots\ldots\ldots (3.9)$$

where L is an empirical pore-connectivity parameter which is 0.5 (Mualem, 1976), and S_e is the effective saturation

$$S_e = \frac{\theta - \theta_r}{\theta_s - \theta_r}, \quad \ldots\ldots\ldots\ldots\ldots\ldots\ldots\ldots\ldots\ldots\ldots (3.10)$$

According to Brooks-Corey, (1964):

$$\frac{\theta - \theta_r}{\theta_s - \theta_r} = S_e = \begin{cases} (\frac{\Psi_a}{\Psi})^\lambda, & \Psi < \Psi_a \\ 1, & \Psi \ge \Psi_a \end{cases} \quad \ldots\ldots\ldots\ldots\ldots\ldots\ldots\ldots (3.11)$$

$$K = K_s S_e{}^{3+2/\lambda} \quad \ldots\ldots\ldots\ldots\ldots\ldots\ldots\ldots\ldots\ldots (3.12)$$

where, θ_r and θ_s are residual and saturated soil water contents, respectively. Here

K_s	saturated hydraulic conductivity
S_e	effective water saturation
λ	pore-size distribution index

Ψ matric pressure head

Ψ_a air-entry head value

3.6 Initial and Boundary Conditions

When utilizing Lie point transformations to establish self-similarity for unsaturated flow, transformation of initial and boundary conditions should also be performed alongside the governing equations.

The strength of Lie group theory lies in its capacity not only to transform the differential equations themselves but also to dictate how the associated conditions must transform to preserve the underlying symmetry

For unsteady flow through unsaturated porous media, modeled by the Richards equation, the initial condition typically specifies the pressure head (or water content) distribution throughout the domain at time *t = 0*. Boundary conditions define the behavior of the flow at the domain's boundaries. These can include prescribed pressure heads (Dirichlet conditions), prescribed fluxes (Neumann conditions), (Bear and Cheng, 2010).

The initial condition in the original domain can be specified as

$$\Psi(x, y, z, t = 0) = \Psi_0(x, y, z) \ldots\ldots\ldots\ldots\ldots\ldots\ldots\ldots\ldots (3.13)$$

Dirichlet boundary conditions, also known as first-type boundary conditions, specify the value of the dependent variable (in this case, pressure head Ψ) directly at the boundary. For example, if a specific section of the domain's boundary, denoted as Γ_D, has a prescribed head that may vary with time, the condition is given by:

$$\Psi(x, y, z, t) = \Psi_D(x, y, z, t) \quad on \quad \Gamma_D \ldots\ldots\ldots\ldots\ldots\ldots\ldots\ldots (3.14)$$

Compared to Dirichlet type boundary conditions, what is different in Neumann boundary conditions, or second-type boundary conditions, is that it does not

enforce a fixed value, but it specifies the flux across the boundary. In the example of unsaturated flow, this often relates to the water flux or inflow normal to the boundary. For a boundary Γ_N, a Neumann condition can be expressed as:

$$q_N(x,y,z,t) = -K(x,y,z)(\nabla h((x,y,z,t)) \cdot n \text{ on } \Gamma_N \ldots\ldots\ldots\ldots\ldots\ldots\ldots (3.15)$$

where *K* is the hydraulic conductivity, *n* is the outward normal vector to the boundary, and q_N is the prescribed flux across the boundary.

3.7 Evaluation Metrics

In order to compare the results obtained from scaled domain solution with the existing original domain solution, following statistical evaluation metrics will be used.

These methods compare the observed (simulated), or in this case, scaled values to the original (real) values to calculate a score that evaluates how well the results from the numerical solution of the original (prototype) and the results obtained from the numerical solution of scaled domain correlate with each other.

If the correlation score is within the acceptable limits, it means that the scaling method proposed in this study works as expected.

3.7.1 Root Mean Square Error (RMSE)

RMSE is widely used in hydrological studies, meteorology, air quality, and climate research studies (Hodson, 2022). It is calculated as shown in equation 3.16. It determines the average numerical difference between the real and observed data. Solution data set is defined as 1D array for each point as y_i in the original domain and $\hat{y}_i$ as the projected (scaled) domain where *n* is the total number of data points. RMSE = 0 indicates a perfect fit (no error).

$$RMSE = \sqrt{\frac{1}{n}\sum_{i=1}^{n}(y_i - \hat{y}_i)^2} \quad \text{.....(3.16)}$$

3.7.2 R-value (Correlation Coefficient)

Developed by Pearson (1896), it measures the statistical linear relationship between two set of variables (x_i and y_i) and is calculated as shown in equation 3.17. $\bar{x}$ and $\bar{y}$ are the mean values. Calculated R value ranges from -1 to 1, where a value close to 1 indicates a strong linear relationship and suggests model robustness.

$$R = \frac{\sum(x_i - \bar{x})(y_i - \bar{y})}{\sqrt{(\sum(x_i - \bar{x})^2 \sum(y_i - \bar{y})^2)}} \quad \text{.....(3.17)}$$

3.7.3 Nash-Sutcliffe Efficiency (NSE)

The NSE is calculated as in equation 3.18 and is frequently used to evaluate model accuracy in climate studies and hydrological simulations. $Q_{obs,i}$ is the ith value of observed data and $Q_{sim,i}$ is the simulated data. And *n* is the total number of data points. A perfect match is indicated by an NSE of 1. According to Knoben et al. (2019), a value of more than 0.5 is assumed acceptable, while Newman et al. (2015) suggests values greater than 0.55 are suitable for hydrological models. Moriasi et al. (2007) classifies performance as:

- Very Good: > 0.75
- Good: 0.65 - 0.75
- Satisfactory: 0.5 - 0.65
- Poor: < 0.5

$$NSE = 1 - \frac{\sum_{i=1}^{n}\left(Q_{obs,i} - Q_{sim,i}\right)^2}{\sum_{i=1}^{n}\left(Q_{obs,i} - \overline{Q_{obs}}\right)^2} \quad \text{.....(3.15)}$$

CHAPTER 4

NOVEL SCALING AND SELF-SIMILARITY CONDITIONS BY ONE-PARAMETER LIE GROUP POINT SCALING TRANSFORMATIONS

This chapter presents the novel scaling method introduced in this thesis, based on one-parameter Lie point group scaling transformations, and explains its application to unsteady flow through porous media.

4.1 Introduction

The one-parameter Lie group of point scaling transformations of the unsteady flow through porous media can be defined as

$$\theta = \epsilon^{\alpha_\theta}\bar{\theta} \text{ (volumetric water content)}$$
$$t = \epsilon^{\alpha_t}\bar{t} \text{ (time)}$$
$$x = \epsilon^{\alpha_x}\bar{x} \text{ (distance in x direction)}$$
$$y = \epsilon^{\alpha_y}\bar{y} \text{ (distance in y direction)}$$
$$z = \epsilon^{\alpha_z}\bar{z} \text{ (distance in z direction)} \quad \ldots\ldots\ldots (4.1)$$
$$\Psi = \epsilon^{\alpha_\Psi}\overline{\Psi} \text{ (Matric potential)}$$
$$K_x = \epsilon^{\alpha_{K_x}}\overline{K_x} \text{ (hydraulic conductivity in x direction)}$$
$$K_y = \epsilon^{\alpha_{K_y}}\overline{K_y} \text{ (hydraulic conductivity in y direction)}$$
$$K_z = \epsilon^{\alpha_{K_z}}\overline{K_z} \text{ (hydraulic conductivity in z direction)}$$

The transformations were discussed in Bluman and Anco (2002); Polyanin and Manzhirov (2006). It was first applied to hydrological processes by Haltas and Kavvas (2011). These transformations in unsteady flow through porous media map the variables in the original domain (θ, x,y z, Ψ, K_x, K_y, K_z) to variables in scaled domain ($\bar{\theta}$, $\bar{x}$, $\bar{z}$, $\overline{\Psi}$, $\overline{K_x}, \overline{K_y}, \overline{K_z}$). Here $\boldsymbol{\epsilon}$ is the scaling parameter and α is the scaling

exponent of the corresponding variable. Scaling ratio of a variable can be defined as the variable in original domain to the same variable in scaled domain:

$$SR_\theta = \epsilon^{\alpha_\theta} \text{ (water content)}$$
$$SR_t = \epsilon^{\alpha_t} \text{ (time)}$$
$$SR_x = \epsilon^{\alpha_x} \text{ (distance in x-direction)}$$
$$SR_y = \epsilon^{\alpha_y} \text{ (distance in y-direction)}$$
$$SR_z = \epsilon^{\alpha_z} \text{ (distance in z-direction)} \quad \ldots\ldots (4.2)$$
$$SR_\Psi = \epsilon^{\alpha_\Psi} \text{ (Matric potential)}$$
$$SR_{K_x} = \epsilon^{\alpha_{K_x}} \text{ (hydraulic conductivity in x-direction)}$$
$$SR_{K_y} = \epsilon^{\alpha_{K_y}} \text{ (hydraulic conductivity in y-direction)}$$
$$SR_{K_z} = \epsilon^{\alpha_{K_z}} \text{ (hydraulic conductivity in z-direction)}$$

Self-similarity conditions for unsteady flow through porous media can be identified when the initial-boundary value problem (IBVP) governing the flow in the prototype domain remains invariant, i.e., retains its original form, under the Lie group of point scaling transformations applied to the governing variables.

4.2 One Parameter Lie Group Point Scaling Transformations

4.2.1 One-dimensional unsteady flow through porous media

Schematic description of the transformation from the original domain to the scaled domain for one-dimensional flow through unsaturated porous media is depicted in Figure 4.1. Applying the one-parameter Lie scaling transformations on the one-dimensional governing equation of unsteady flow through porous media yields

$$\frac{\partial(\epsilon^{\alpha_\theta}\bar{\theta})}{\partial(\epsilon^{\alpha_t}\bar{t})} = \frac{\partial}{\partial(\epsilon^{\alpha_z}\bar{z})}\left(\epsilon^{\alpha_{K_z}}\overline{K_z}\ \frac{\partial\epsilon^{\alpha_\Psi}\bar{\Psi}}{\partial(\epsilon^{\alpha_z}\bar{z})}\right) + \frac{\partial(\epsilon^{\alpha_{K_z}}\overline{K_z})}{\partial(\epsilon^{\alpha_z}\bar{z})} \ldots\ldots\ldots\ldots (4.3)$$

Then, one can write the one-dimensional governing equation of unsteady flow through porous media in transformed domain as

$$\epsilon^{\alpha_\theta-\alpha_t}\frac{\partial(\bar{\theta})}{\partial(\bar{t})}=\epsilon^{\alpha_{K_z}+\alpha_\Psi-2\alpha_z}\frac{\partial}{\partial(\bar{z})}\left(\overline{K_z}\ \frac{\partial\overline{\Psi}}{\partial(\bar{z})}\ \right)+\epsilon^{\alpha_{K_z}-\alpha_z}\frac{\partial\overline{K_z}}{\partial(\bar{z})}\ldots\ldots\ldots\ldots(4.4)$$

The initial condition in transformed domain can be written as

$$\overline{\Psi}(\bar{z},\bar{t}=0)=\epsilon^{-\alpha_\Psi}\Psi_0(\epsilon^{\alpha_z}\bar{z})\ldots\ldots\ldots(4.5)$$

Dirichlet boundary condition in transformed domain can be written as

$$\overline{\Psi}(\bar{z},\bar{t})=\epsilon^{-\alpha_\Psi}\Psi_D(\epsilon^{\alpha_z}\bar{z},\epsilon^{\alpha_t}\bar{t})\ \ on\ \overline{\Gamma_D}\ldots\ldots\ldots\ldots\ldots\ldots\ldots\ldots(4.6)$$

Neumann boundary condition in transformed domain can be written as

$$\overline{q_N}(\bar{z},\bar{t})\ =-\epsilon^{-\alpha_q}K(\epsilon^{\alpha_z}\bar{z})\big(\nabla h(\epsilon^{\alpha_z}\bar{z},\epsilon^{\alpha_t}\bar{t})\big)\cdot\bar{n}\ \ on\ \overline{\Gamma_N}\ \ldots.(4.7)$$

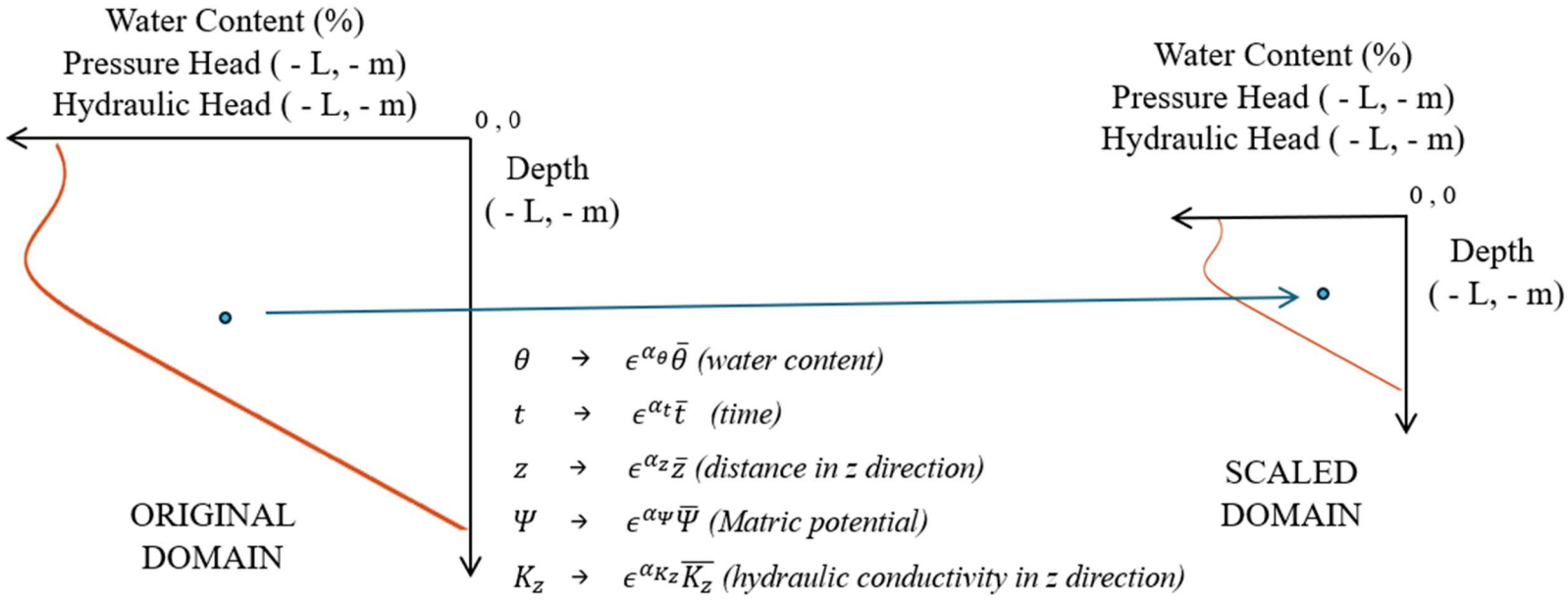

Figure 4.1. Schematic representation of the transformation from the original domain to the scaled domain in one-dimensional flow through unsaturated porous media

4.2.2 Two-dimensional unsteady flow through porous media

Schematic description of the transformation from the original domain to the scaled domain for two-dimensional flow through unsaturated porous media is depicted in Figure 4.2. Applying the one-parameter Lie scaling transformations on the two-dimensional governing equation of unsteady flow through porous media yields

$$\frac{\partial(\epsilon^{\alpha_\theta}\bar{\theta})}{\partial t(\epsilon^{\alpha_t}\bar{t})} = \frac{\partial}{\partial(\epsilon^{\alpha_x}\bar{x})}\left(\epsilon^{\alpha_{K_x}}\overline{K_x}\ \frac{\partial\epsilon^{\alpha_\Psi}\overline{\Psi}}{\partial(\epsilon^{\alpha_x}\bar{x})}\right) + \frac{\partial}{\partial(\epsilon^{\alpha_z}\bar{z})}\left(\epsilon^{\alpha_{K_z}}\overline{K_z}\ \frac{\partial\epsilon^{\alpha_\Psi}\overline{\Psi}}{\partial(\epsilon^{\alpha_z}\bar{z})}\right)$$

$$+\frac{\partial(\epsilon^{\alpha_{K_z}}\overline{K_z})}{\partial(\epsilon^{\alpha_z}\bar{z})} \dots\dots\dots\dots\dots\dots\dots\dots\dots\dots\dots\dots\dots\dots (4.8)$$

Then, one can write the two-dimensional governing equation of unsteady flow through porous media in transformed domain as

$$\epsilon^{\alpha_\theta-\alpha_t}\frac{\partial(\bar{\theta})}{\partial(\bar{t})} = \epsilon^{\alpha_{K_x}+\alpha_\Psi-2\alpha_x}\frac{\partial}{\partial(\bar{x})}\left(\overline{K_x}\ \frac{\partial\overline{\Psi}}{\partial(\bar{x})}\right) + \epsilon^{\alpha_{K_z}+\alpha_\Psi-2\alpha_z}\frac{\partial}{\partial(\bar{z})}\left(\overline{K_z}\ \frac{\partial\overline{\Psi}}{\partial(\bar{z})}\right)$$

$$+\epsilon^{\alpha_{K_z}-\alpha_z}\frac{\partial\overline{K_z}}{\partial(\bar{z})} \dots\dots\dots\dots\dots\dots\dots\dots\dots\dots\dots\dots\dots\dots (4.9)$$

The initial condition in transformed domain can be written as

$$\overline{\Psi}(\bar{x},\bar{z},\bar{t}=0) = \epsilon^{-\alpha_\Psi}\Psi_0(\epsilon^{\alpha_x}\bar{x},\epsilon^{\alpha_z}\bar{z}) \dots\dots\dots (4.10)$$

Dirichlet boundary condition in transformed domain can be written as

$$\overline{\Psi}(\bar{x},\bar{z},\bar{t}) = \epsilon^{-\alpha_\Psi}\Psi_D(\epsilon^{\alpha_x}\bar{x},\epsilon^{\alpha_z}\bar{z},\epsilon^{\alpha_t}\bar{t}) \ \ on\ \overline{\Gamma_D} \dots\dots\dots\dots\dots\dots\dots\dots (4.11)$$

Neumann boundary condition in transformed domain can be written as

$$\overline{q_N}(\bar{x},\bar{z},\bar{t}) = -\epsilon^{-\alpha_q}K(\epsilon^{\alpha_x}\bar{x},\epsilon^{\alpha_z}\bar{z})\left(\nabla h(\epsilon^{\alpha_z}\bar{x},\epsilon^{\alpha_z}\bar{z},\epsilon^{\alpha_t}\bar{t})\right)\cdot\bar{n}\ \ on\ \overline{\Gamma_N} \dots (4.12)$$

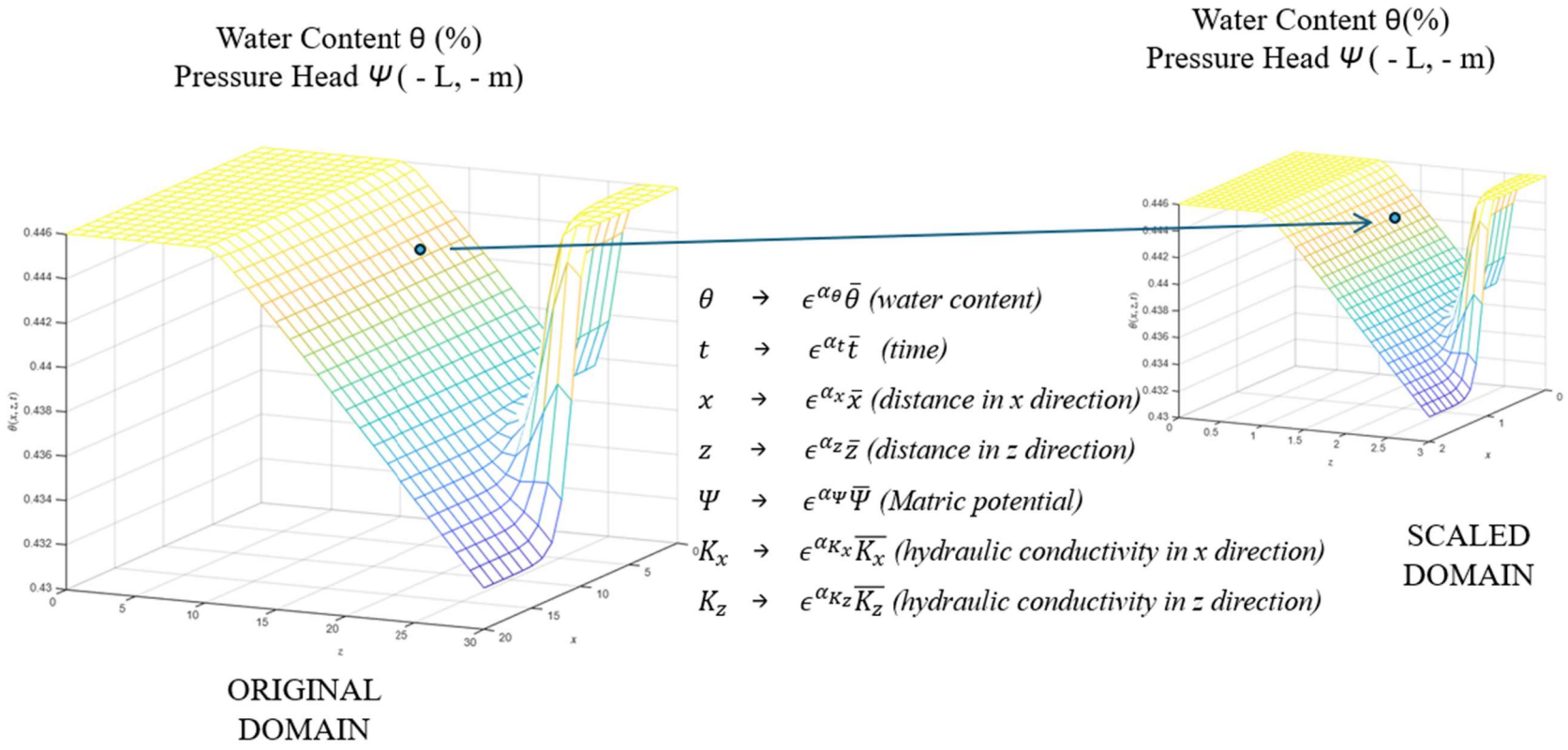

Figure 4.2. Schematic representation of the transformation from the original domain to the scaled domain in two-dimensional flow through unsaturated porous media

4.2.3 Three-dimensional unsteady flow through porous media

Applying the one-parameter Lie scaling transformations on the three-dimensional governing equation of unsteady flow through porous media yields

$$\frac{\partial(\epsilon^{\alpha_\theta}\bar{\theta})}{\partial t(\epsilon^{\alpha_t}\bar{t})} = \frac{\partial}{\partial(\epsilon^{\alpha_x}\bar{x})}\left(\epsilon^{\alpha_{K_x}}\overline{K_x}\ \frac{\partial\epsilon^{\alpha_\Psi}\bar{\Psi}}{\partial(\epsilon^{\alpha_x}\bar{x})}\right) + \frac{\partial}{\partial(\epsilon^{\alpha_y}\bar{y})}\left(\epsilon^{\alpha_{K_y}}\overline{K_y}\ \frac{\partial\epsilon^{\alpha_\Psi}\bar{\Psi}}{\partial(\epsilon^{\alpha_y}\bar{y})}\right)$$
$$+ \frac{\partial}{\partial(\epsilon^{\alpha_z}\bar{z})}\left(\epsilon^{\alpha_{K_z}}\overline{K_z}\ \frac{\partial\epsilon^{\alpha_\Psi}\bar{\Psi}}{\partial(\epsilon^{\alpha_z}\bar{z})}\right) + \frac{\partial(\epsilon^{\alpha_{K_z}}\overline{K_z})}{\partial(\epsilon^{\alpha_z}\bar{z})} \dots\dots\dots\dots\dots\dots (4.13)$$

Then, one can write the three-dimensional governing equation of unsteady flow through porous media in transformed domain as

$$\epsilon^{\alpha_\theta-\alpha_t}\frac{\partial(\bar{\theta})}{\partial(\bar{t})} = \epsilon^{\alpha_{K_x}+\alpha_\Psi-2\alpha_x}\frac{\partial}{\partial(\bar{x})}\left(\overline{K_x}\ \frac{\partial\bar{\Psi}}{\partial(\bar{x})}\right)$$
$$+ \epsilon^{\alpha_{K_y}+\alpha_\Psi-2\alpha_y}\frac{\partial}{\partial(\bar{y})}\left(\overline{K_y}\ \frac{\partial\bar{\Psi}}{\partial(\bar{y})}\right)$$
$$+ \epsilon^{\alpha_{K_z}+\alpha_\Psi-2\alpha_z}\frac{\partial}{\partial(\bar{z})}\left(\overline{K_z}\ \frac{\partial\bar{\Psi}}{\partial(\bar{z})}\right) + \epsilon^{\alpha_{K_z}-\alpha_z}\frac{\partial\overline{K_z}}{\partial(\bar{z})} \dots (4.14)$$

The initial condition in transformed domain can be written as

$$\bar{\Psi}(\bar{x},\bar{y},\bar{z},\bar{t}=0) = \epsilon^{-\alpha_\Psi}\Psi_0(\epsilon^{\alpha_x}\bar{x},\epsilon^{\alpha_y}\bar{y},\epsilon^{\alpha_z}\bar{z}) \dots\dots\dots (4.15)$$

Dirichlet boundary condition in transformed domain can be written as

$$\bar{\Psi}(\bar{x},\bar{y},\bar{z},\bar{t}) = \epsilon^{-\alpha_\Psi}\Psi_D(\epsilon^{\alpha_x}\bar{x},\epsilon^{\alpha_y}\bar{y},\epsilon^{\alpha_z}\bar{z},\epsilon^{\alpha_t}\bar{t}) \ \ on\ \overline{\Gamma_D} \dots\dots\dots\dots\dots\dots\dots\dots (4.16)$$

Neumann boundary condition in transformed domain can be written as

$$\overline{q_N}(\bar{x},\bar{y},\bar{z},\bar{t}) = -\epsilon^{-\alpha_q}K(\epsilon^{\alpha_x}\bar{x},\epsilon^{\alpha_y}\bar{y},\epsilon^{\alpha_z}\bar{z})(\nabla h(\epsilon^{\alpha_z}\bar{x},\epsilon^{\alpha_y}\bar{y},\epsilon^{\alpha_z}\bar{z},\epsilon^{\alpha_t}\bar{t}))\cdot\bar{n}\ on\ \overline{\Gamma_N}$$
$$\dots (4.17)$$

4.3 Novel scaling and self-similarity conditions

4.3.1 One-dimensional unsteady flow through porous media

For one-dimensional governing equation of unsteady flow through porous media in transformed domain (Eqn. 4.4) to be invariant, it must be in the same form as Eq. (3.6). Thus,

$$\epsilon^{\alpha_\theta-\alpha_t} = \epsilon^{\alpha_{K_z}+\alpha_\Psi-2\alpha_z}=\epsilon^{\alpha_{K_z}-\alpha_z} \quad \ldots\ldots\ldots\ldots\ldots\ldots\ldots (4.18)$$

Therefore, the following conditions must be satisfied to ensure self-similarity in one-dimensional flow:

$$\alpha_\theta - \alpha_t = \alpha_{K_z} + \alpha_\Psi - 2\alpha_z=\alpha_{K_z} - \alpha_z \quad \ldots\ldots\ldots\ldots\ldots\ldots\ldots (4.19)$$

Then $\alpha_\Psi = \alpha_z$ and given that $\alpha_\theta = 0$ it follows that $\alpha_{K_z} = \alpha_z - \alpha_t$.

4.3.2 Two-dimensional unsteady flow through porous media

For two-dimensional governing equation of unsteady flow through porous media in transformed domain (Eqn. 4.9) to be invariant, it must be in the same form as Eq. (3.5). Thus,

$$\epsilon^{\alpha_\theta-\alpha_t} = \epsilon^{\alpha_{K_x}+\alpha_\Psi-2\alpha_x}=\epsilon^{\alpha_{K_z}+\alpha_\Psi-2\alpha_z} = \epsilon^{\alpha_{K_z}-\alpha_z} \quad \ldots\ldots\ldots\ldots\ldots\ldots\ldots (4.20)$$

Therefore, the following conditions must be satisfied to ensure self-similarity in two-dimensional flow:

$$\alpha_\theta - \alpha_t = \alpha_{K_x} + \alpha_\Psi - 2\alpha_x = \alpha_{K_z} + \alpha_\Psi - 2\alpha_z=\alpha_{K_z} - \alpha_z \quad \ldots\ldots\ldots (4.21)$$

4.3.3 Three-dimensional unsteady flow through porous media

For three-dimensional governing equation of unsteady flow through porous media in transformed domain (Eqn. 4.14) to be invariant, it must be in the same form as Eq. (3.4). Thus,

$$\epsilon^{\alpha_\theta - \alpha_t} = \epsilon^{\alpha_{K_x} + \alpha_\Psi - 2\alpha_x} = \epsilon^{\alpha_{K_y} + \alpha_\Psi - 2\alpha_y} = \epsilon^{\alpha_{K_z} + \alpha_\Psi - 2\alpha_z} = \epsilon^{\alpha_{K_z} - \alpha_z} \quad \ldots\ldots\ldots (4.22)$$

Therefore, the following conditions must be satisfied to ensure self-similarity in two-dimensional flow:

$$\alpha_\theta - \alpha_t = \alpha_{K_x} + \alpha_\Psi - 2\alpha_x = \alpha_{K_y} + \alpha_\Psi - 2\alpha_y = \alpha_{K_z} + \alpha_\Psi - 2\alpha_z = \alpha_{K_z} - \alpha_z \quad \ldots (4.23)$$

4.4 Usage of Scaling of Richards Equation in Engineering Practice

In engineering practice, the configuration of experimental studies is constrained by factors such as the available laboratory space, accessible materials, and feasible experimental durations. By applying the novel scaling conditions derived in Section 4.3, the corresponding scaling parameters can be determined to accommodate these practical limitations. In this way, the derived scaling relations enhance spatial, temporal, and economic flexibility in the design and implementation of physical models, while providing new insights into unsteady, multi-dimensional flow in unsaturated porous media.

The proposed scaling framework enables the construction of self-similar experimental setups in a scaled domain that can represent field conditions (the prototype domain). The specific characteristics of such experiments are typically determined by the availability of laboratory space, the properties and accessibility of materials, and the duration over which experiments can be performed. Using the derived scaling conditions, appropriate scaling parameters can be calculated so that the scaled experiment reproduces the desired prototype behavior in terms of spatial

dimensions, temporal evolution, and material properties such as hydraulic conductivity.

Typical engineering applications of the proposed scaling relations include the following:

1. Based on the availability of experimental space, determine the required length scaling ratios $SR_x, SR_y, SR_z,$ corresponding scaling parameter ϵ and the scaling exponents $\alpha_x, \alpha_y, \alpha_z$ between the prototype domain (e.g., a 10 m deep field soil profile) and the laboratory model (e.g., a 1 m soil column). Based on practical experimental duration limitations, determine the required time scaling ratio SR_t and the scaling exponents α_t between the prototype domain and the laboratory model. For example, a 10-day prototype event can be compressed into a 1-day laboratory experiment. If the temporal scaling ratio is different from the spatial scaling ratio, velocities of the fluid flow and hydraulic conductivities will be different. Therefore, it should be determined whether the same soil hydraulic conductivity can be used in both domains, or whether a surrogate soil with scaled hydraulic properties is required.

2. The self-similarity conditions derived in section 4.3 can provide a way to reduce computational costs. Rather than independently solving Richards' equation on every spatial and temporal domain of interest, a practitioner can solve the governing equations once on a selected domain. Then, using the scaling conditions presented in Section 4.3, solutions of other self-similar domains can be obtained. As demonstrated in Chapters 5 and 5, the numerical verification examples confirm that the self-similar solutions of the scaled domains are in excellent agreement with solutions of the prototype domains.

CHAPTER 5

NUMERICAL VERIFICATION OF SCALING ONE-DIMENSIONAL UNSTEADY FLOW THROUGH POROUS MEDIA

In this chapter, numerical simulations for one-dimensional flow through unsaturated porous media problems are presented, with a detailed explanation of the applied scaling methodology. The results obtained from the original domain, are systematically compared with those from the scaled domains to verify the accuracy and effectiveness of the scaling approach. Numbering and identification of original and scaled domains are listed in table 5.1.

To numerically solve the one-dimensional Richards equation, this study employs an example problem and open-source MATLAB code developed by Holzbecher (2012) which is a one-dimensional infiltration problem in a soil column with a disturbed upper layer and constant boundary conditions. The soil column's profile is mostly linear, except for the top 10 cm where a high-pressure head and water content layer disrupt it. Constant inflow is applied at the top, with a zero-pressure head set 2 meters down to represent the groundwater table. The simulation indicates movement toward steady-state infiltration, with volumetric water content rising from 38% to a maximum of 52%. All measurements use cm for length and hours for time.

The soil hydraulic parameters are adopted from Hornberger and Wiberg (2005), ensuring consistency with established literature. The original MATLAB implementation has been modified to incorporate scaling parameters and associated exponents for each variable. These modifications enable automated generation of self-similar domains and their solutions by adjusting the scaling inputs.

Two different cases are studied. In the first case, hydraulic conductivity is held constant. Identical hydraulic conductivity values are applied to both the original and scaled domains. This condition is achieved by assigning equal scaling exponents to the spatial and temporal dimensions, $\alpha_x - \alpha_t = 0$. Using same hydraulic conductivity in original and scaled domains has practical implications. In many laboratory experiments it is easier to use the same soil hydraulic conductivity. However, it should be noted that this does not imply that the same soil is used in both the prototype and the scaled domains. Although the saturated hydraulic conductivity may remain unchanged, the soil hydraulic functions (e.g., the van Genuchten parameters) scale with the length scaling ratio.

On the other hand, for the second case, different hydraulic conductivity values are applied. This condition is achieved by assigning unequal scaling exponents to the spatial and temporal dimensions, $\alpha_x - \alpha_t \neq 0$. In both cases, the example problem in Holzbecher (2012) is used as the basis of comparison, i.e., as the original domain. Table 5.1 summarizes both cases.

Table 5.1 Identification of original and scaled domains used for 1-dimensional flow through unsaturated porous media

	Domain 1D-0		**Original/Prototype**
1D	Case1: Scaling Using Identical Hydraulics Conductivities	Domain 1D-1	scaled by $\varepsilon = 10$, $\alpha_x = 1$ and $\alpha_t = 1$
		Domain 1D-2	scaled by $\varepsilon = 10$, $\alpha_x = 2$ and $\alpha_t = 2$
		Domain 1D-3	scaled by $\varepsilon = 10$, $\alpha_x = -1$ and $\alpha_t = -1$
	Case2: Scaling Using Different Hydraulics Conductivities	Domain 1D-4	scaled by $\varepsilon = 2$, $\alpha_x = 1$ and $\alpha_t = 2$
		Domain 1D-5	scaled by $\varepsilon = 0.5$, $\alpha_x = 1$ and $\alpha_t = 2$
		Domain 1D-6	scaled by $\varepsilon = 2$, $\alpha_x = 2$ and $\alpha_t = 1$

4.5 Scaling Using Identical Hydraulics Conductivities in One-Dimensional Flow

Identical hydraulic conductivities in the original and scaled domains are obtained by adopting equal scaling exponents for distance and time, $\alpha_x = \alpha_t$. Under this

condition, the hydraulic conductivity remains unchanged between the two domains because $\alpha_x - \alpha_t = 0$. Therefore, the scaling ratio of hydraulic conductivity is unity ($SR_K = \epsilon^{\alpha_K} = \epsilon^{\alpha_x - \alpha_t} = 1$).

Table 5.1 shows the numbering and identification of original and scaled domains and Table 5.2 tabulates the scaling conditions used to obtain scaled domains from the original domain by keeping constant hydraulic conductivities for 1-dimensional flow through unsaturated porous media for case 1. Original (prototype domain) is named as Domain 1D-0. "0" (zero) is used to be able to separately identify the original domain from scaled domains. All other scaled domains are numbered sequentially after 1D suffix as Domain 1D-1, 1D-2 and 1D-3. Domain 1D-1 is obtained by scaling spatial coordinate by $SR_x = \epsilon^{\alpha_x} = 10$ and time coordinate by $SR_t = \epsilon^{\alpha_t} = 10$. Domain 1D-2 is generated by applying a larger scaling ratio: $SR_x = \epsilon^{\alpha_x} = 100$ for space and $SR_t = \epsilon^{\alpha_t} = 100$ for time. Domain 1D-3, on the other hand, is obtained by downscaling the original domain with $SR_x = \epsilon^{\alpha_x} = 0.1$ and $SR_t = \epsilon^{\alpha_t} = 0.1$. Thus, Domain 1D-3 represents an upscaled version of Domain 1D-0 by a factor of 10 in both space and time. The scaling exponents and ratios of the other variables are then obtained as described above for all domains. Problem descriptions for the original and scaled domains for case 1 are tabulated in Table 5.2.

Pressure head values between Domain 1D-0 and scaled domains (Domains 1D-1, 1D-2, and 1D-3) at times t = 0 to 4 hours in Domain 1D-0 and corresponding scaled times in scaled domains (Domains 1D-1, 1D-2, and 1D-3) are compared in Figure 5.1.

Hydraulic head values between Domain 1D-0 and scaled domains (Domains 1D-1, 1D-2, and 1D-3) at times t = 0 to 4 hours in Domain 1D-0 and corresponding scaled times in scaled domains (Domains 1D-1, 1D-2, and 1D-3) are compared in Figure 5.2.

Water content values between Domain 1D-0 and scaled domains (Domains 1D-1, 1D-2, and 1D-3) at times t = 0 to 4 hours in Domain 1D-0 and corresponding

scaled times in scaled domains (Domains 1D-1, 1D-2, and 1D-3) are compared in Figure 5.3.

The same color is used for the original domain and corresponding scaled times in scaled domains (Domains 1D-1, 1D-2, and 1D-3). For example, orange color in Domain 1D-0 shows t =1 hour in original domain, t = 0.1 hour in Domain 1D-1, t = 0.01 hour in Domain 1D-2, and t =10 hour in Domain 1D-3. The vertical axis in each figure shows the soil depth in z-direction and it is scaled by the scaling ratio of the space in each domain with respect to original domain. Figures 5.1-5.3 shows self-similar behavior for a pressure head, hydraulic head, and water content, respectively.

To quantitatively demonstrate self-similarity, scatter plots of pressure head values in Domain 1D-0 (original) and in scaled domains (Domains 1D-1, 1D-2, and 1D-3), and 4 are shown in Figures 5.4 - 5.6, respectively. These plots compare data at times t = 1 to 4 hours in Domain 1D-0 with the corresponding scaled times in each respective domain. R2, NRMSE and NSE values are also calculated between the pressure head values of the original domain and their corresponding scaled domain values multiplied with pressure head scaling ratio. Across all comparisons, the R^2 and NSE values remain ~1.000, and RMSE value remain ~0.000, indicating perfect self-similarity between the original and scaled domains. The slope of each scatter plot where the vertical axis represents the scaled domain and the horizontal axis represents original Domain 1D-0, is equal to the pressure head scaling ratio:

- In Figure 5.4 (Domain 1D-1), the slope is 1 / 10 = 0.1
- In Figure 5.5 (Domain 1D-2), the slope is 1 / 100 = 0.01
- In Figure 5.6 (Domain 1D-3), the slope is 1 / 0.1 = 10

Similarly, scatter plots of water content values in Domain 1D-0 (original) and scaled domains (Domains 1D-1, 1D-2, and 1D-3) are shown in Figures 5.7 - 5.9. These plots compare data at times t = 1 to 4 hours in original Domain 1D-0 with the corresponding scaled times in each respective domain. R2, NRMSE and NSE values are also calculated between the water content values of the original domain

and their corresponding scaled domain values. Across all comparisons, the R^2 and NSE values remain ~1.000, and RMSE value remain ~0.000, indicating perfect self-similarity between the original and scaled domains. The slope of each scatter plot where the vertical axis represents the scaled domain and the horizontal axis represents original Domain 1D-0, is equal to the water content scaling ratio:

- In Figure 5.7 (Domain 1D-1), the slope is 1
- In Figure 5.8 (Domain 1D-2), the slope is 1
- In Figure 5.9 (Domain 1D-3), the slope is 1

These slopes directly reflect the scaling ratios of pressure head and water content between each scaled domain and the original domain.

Table 5.2 Scaling conditions used to obtain scaled domains from the original domain while maintaining constant hydraulic conductivity for 1-dimensional flow through unsaturated porous media

Description	**Symbol / scaling condition**	**Domain 1D-1**	**Domain 1D-2**	**Domain 1D-3**
Scaling parameter	ε	10	10	10
Scaling exponent of length	α_x	1	2	-1
Scaling exponent of time	α_t	1	2	-1
Scaling exponent of hydraulic conductivity	$\alpha_K = \alpha_x - \alpha_t$	0	0	0
Scaling exponent of infiltration velocity	$\alpha_V = \alpha_x - \alpha_t$	0	0	0
Scaling exponent of pressure head	$\alpha_h = \alpha_x$	1	2	-1
Scaling ratio of length	$SR_x = \epsilon^{\alpha_x}$	10	100	0.1
Scaling ratio of time	$SR_t = \epsilon^{\alpha_t}$	10	100	0.1
Scaling ratio of hydraulic conductivity	$SR_K = \epsilon^{\alpha_K}$	1	1	1
Scaling ratio of velocity	$SR_V = \epsilon^{\alpha_V}$	1	1	1
Scaling ratio of pressure head	$SR_h = \epsilon^{\alpha_h}$	10	100	0.1

Table 5.3 Problem descriptions for the original and scaled domains with identical hydraulic conductivities for 1-dimensional flow through unsaturated porous media

Symbol	Variable	Dimension	Domain 1D-0 (Original)	Domain 1D-1	Domain 1D-2	Domain 1D-3
L	length	[L] (cm)	200	20	2	2000
V	infiltration velocity	[L/T] (m)	0.5	0.5	0.5	0.5
S_2	bottom suction head	[L] (m)	0	0	0	0
T	maximum time	[T] (hours)	4	0.4	0.04	40
q_r	residual water content		0.218	0.218	0.218	0.218
f	porosity		0.52	0.52	0.52	0.52
a	van Genuchten parameter	[1/L] (1/m)	0.0115	0.115	1.15	0.00115
n	van Genuchten parameter		2.03	2.03	2.03	2.03
K_s	saturated conductivity	[L/T] (m/hr)	31.6	31.6	31.6	31.6

Domain1D-0 (Original/Prototype Domain)

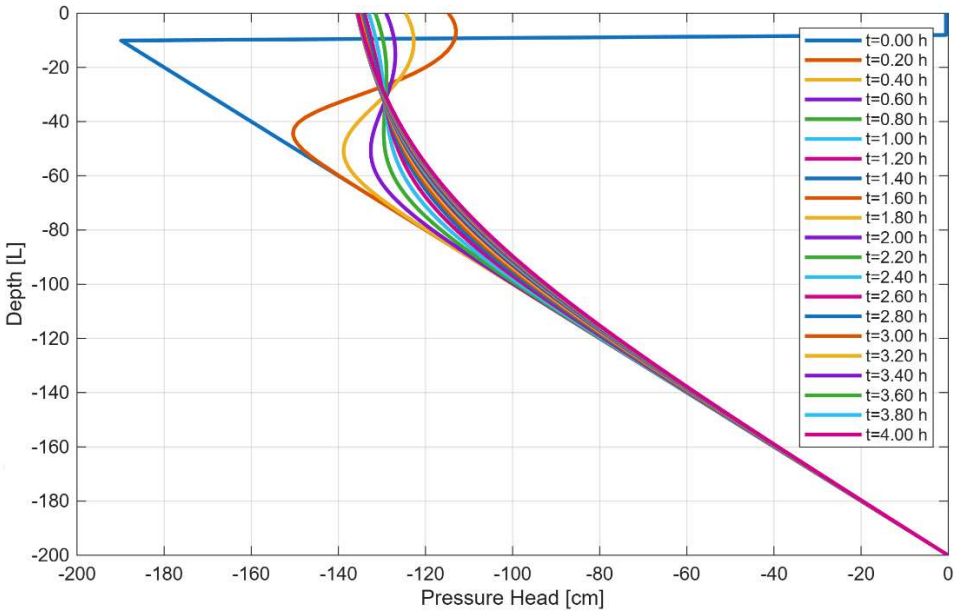

Domain 1D-1 (scaled by $\varepsilon = 10$, with $\alpha_x = 1$ and $\alpha_t = 1$)

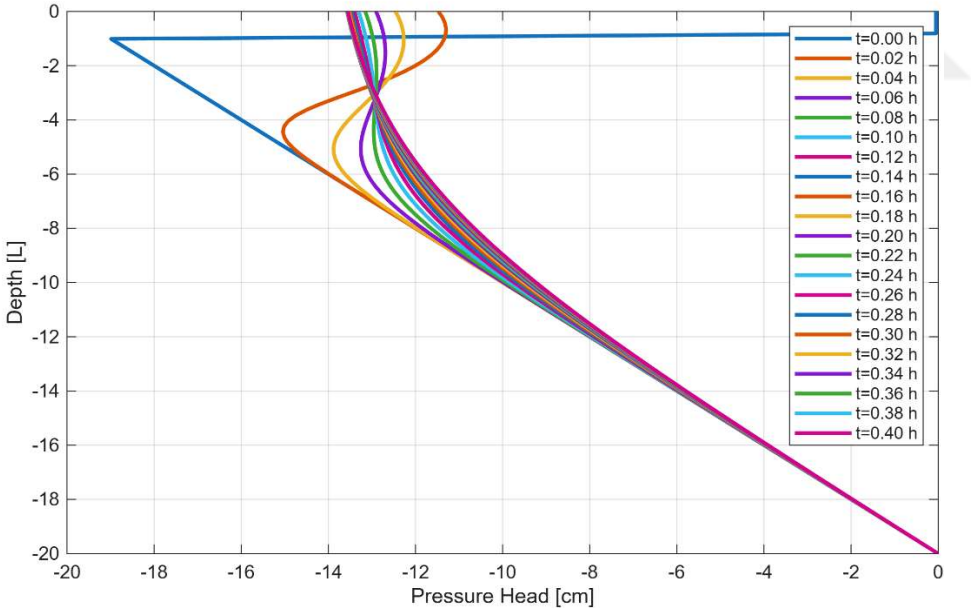

Figure 5.1. Comparison of pressure head between original domain (1D-0) and scaled domains (1D-1, 1D-2, and 1D-3) at Times t = 0 to 4 Hours in original domain and corresponding scaled times in scaled domains for 1D flow with constant hydraulic conductivity (continued)

Domain 1D-2 (scaled by $\varepsilon = 10$, with $\alpha_x = 2$ and $\alpha_t = 2$)

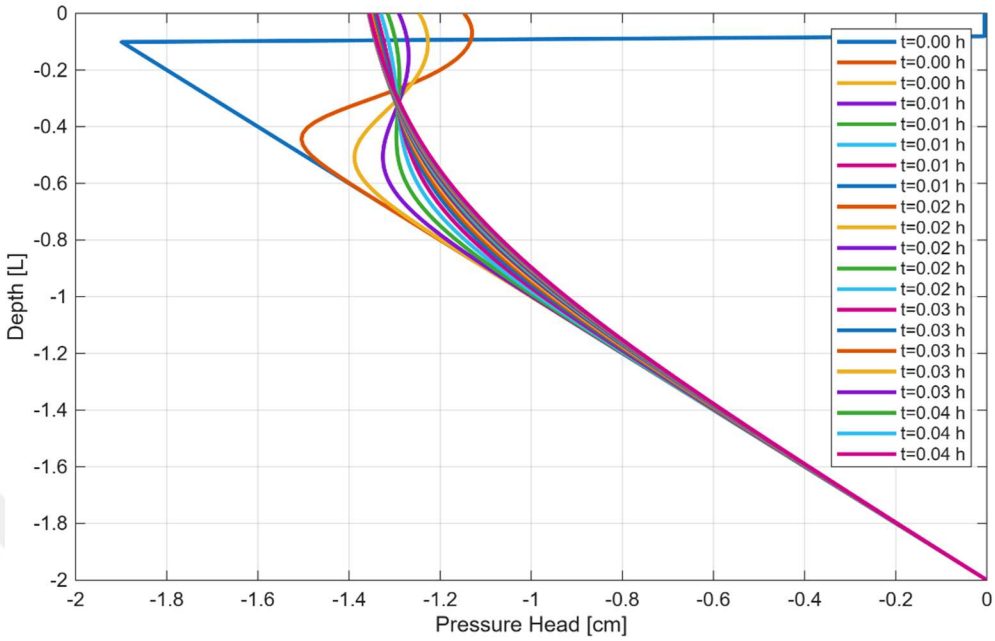

Domain 1D-3 (scaled by $\varepsilon = 10$, with $\alpha_x = -1$ and $\alpha_t = -1$)

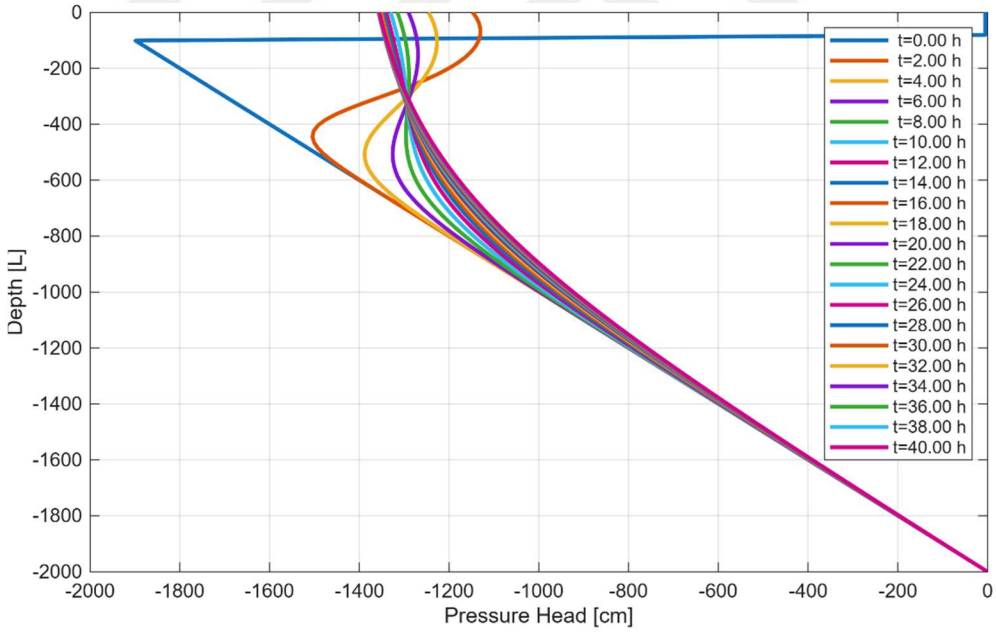

Figure 5.1. Comparison of pressure head between original domain (1D-0) and scaled domains (1D-1, 1D-2, and 1D-3) at Times t = 0 to 4 Hours in original domain and corresponding scaled times in scaled domains for 1D flow with constant hydraulic conductivity.

Domain 1D-0 (Original/Prototype Domain)

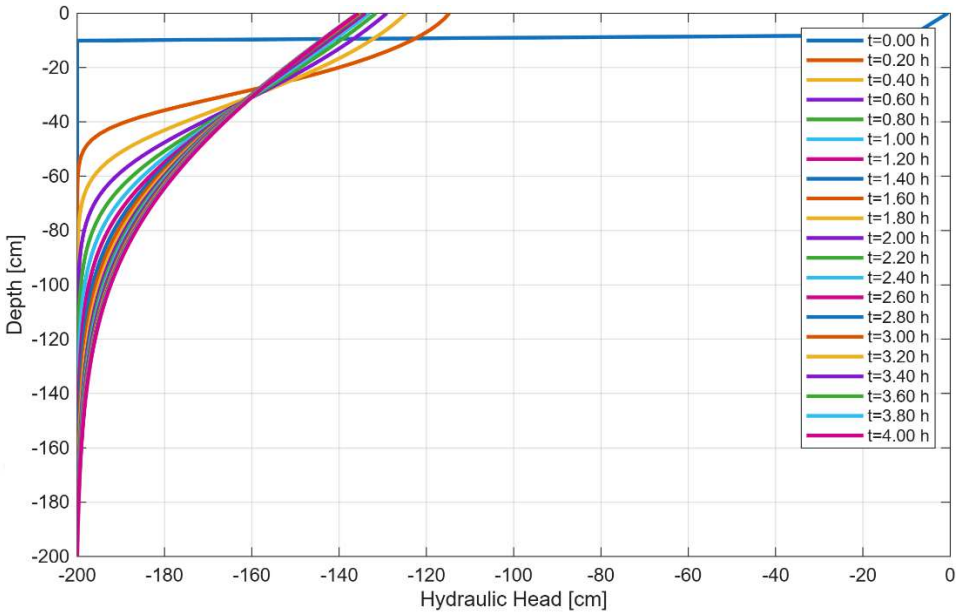

Domain 1D-2 (scaled by $\varepsilon = 10$, with $\alpha_x = 1$ and $\alpha_t = 1$)

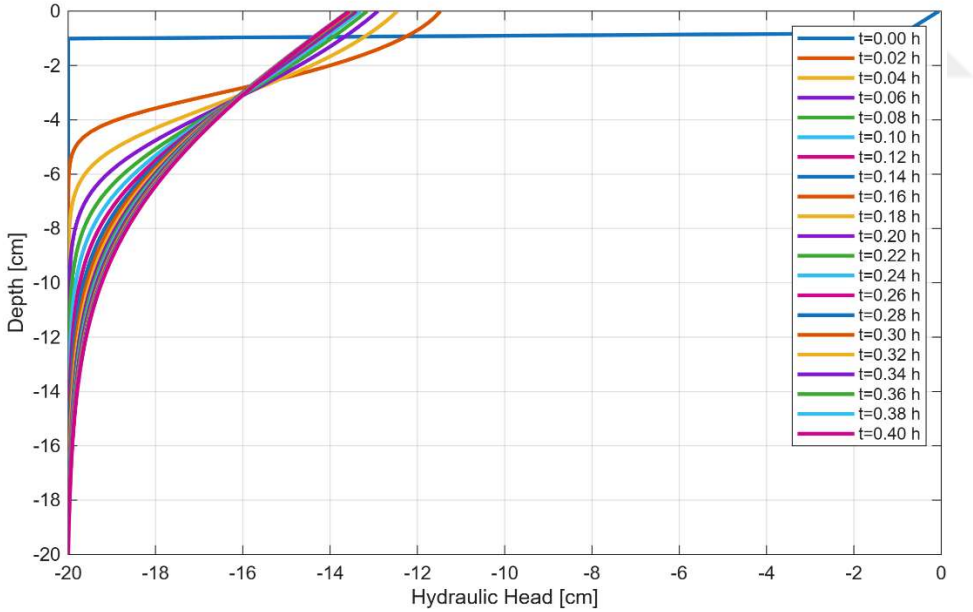

Figure 5.2. Comparison of hydraulic head between original domain (1D-0) and scaled domains (1D-1, 1D-2, and 1D-3) at Times t = 0 to 4 Hours in original domain and corresponding scaled times in scaled domains for 1D flow with constant hydraulic conductivity (continued)

Domain 1D-2 (scaled by $\varepsilon = 10$, with $\alpha_x = 2$ and $\alpha_t = 2$)

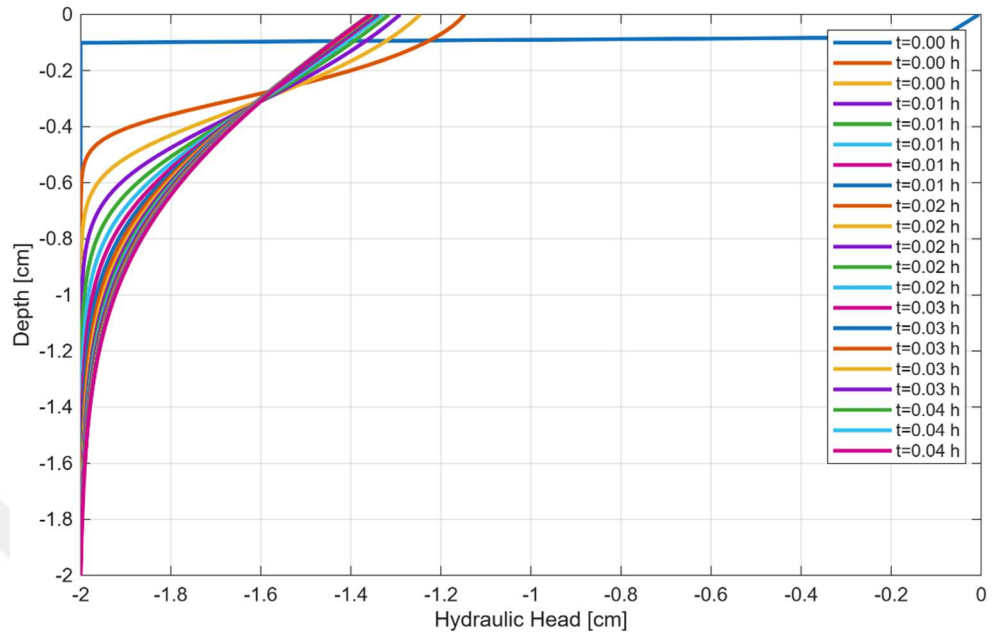

Domain 1D-3 (scaled by $\varepsilon = 10$, with $\alpha_x = -1$ and $\alpha_t = -1$)

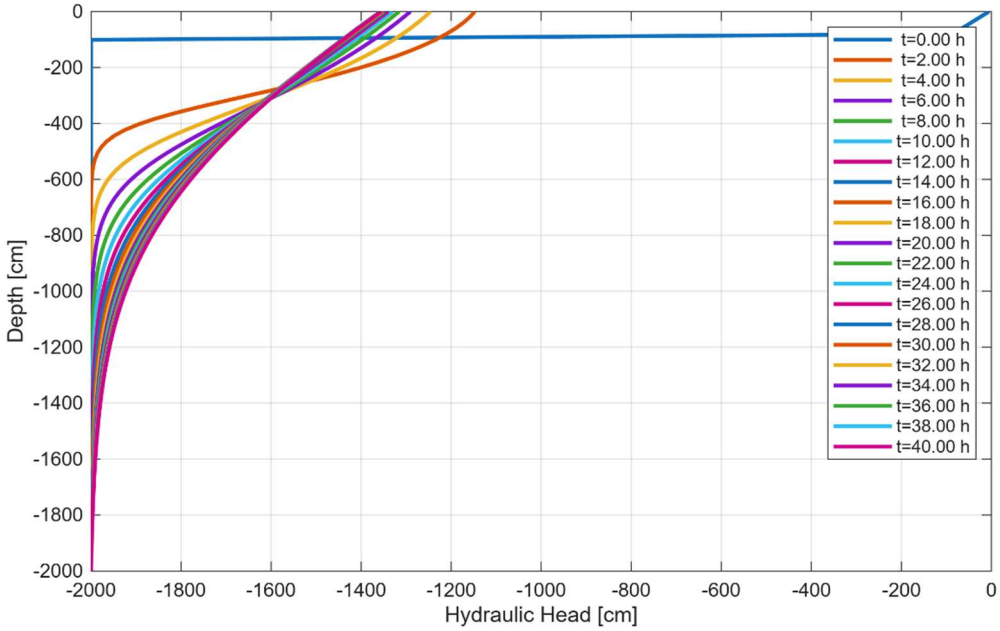

Figure 5.2. Comparison of hydraulic head between original domain (1D-0) and scaled domains (1D-1, 1D-2, and 1D-3) at Times t = 0 to 4 Hours in original domain and corresponding scaled times in scaled domains for 1D flow with constant hydraulic conductivity.

Domain 1D-0 (Original/Prototype Domain)

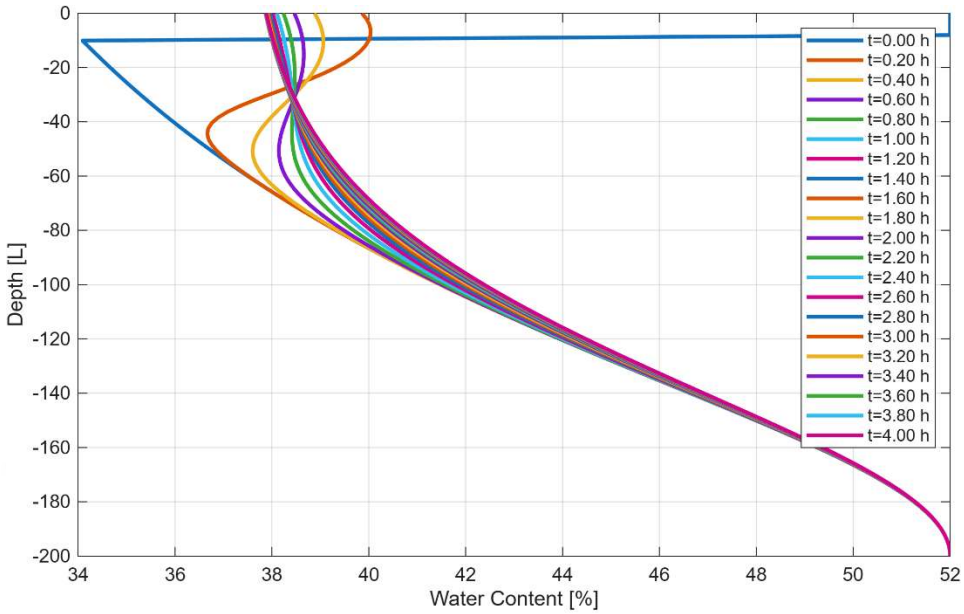

Domain 1D-1 (scaled by $\varepsilon = 10$, with $\alpha_x = 1$ and $\alpha_t = 1$)

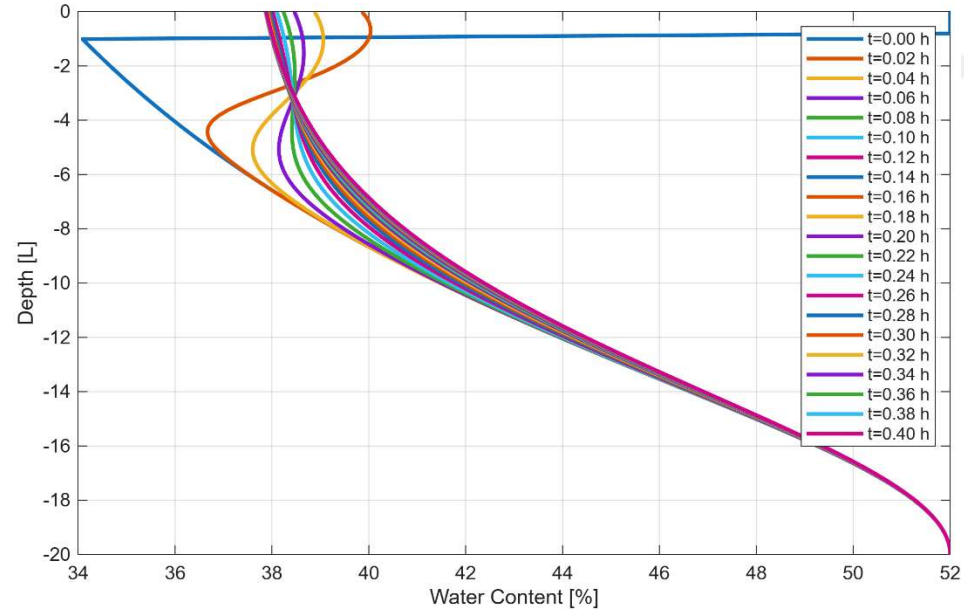

Figure 5.3. Comparison of water content between original domain (1D-0) and scaled domains (1D-1, 1D-2, and 1D-3) at Times t = 0 to 4 Hours in original domain and corresponding scaled times in scaled domains for 1D flow with constant hydraulic conductivity. (continued)

Domain 1D-3 (scaled by $\varepsilon = 10$, with $\alpha_x = 2$ and $\alpha_t = 2$)

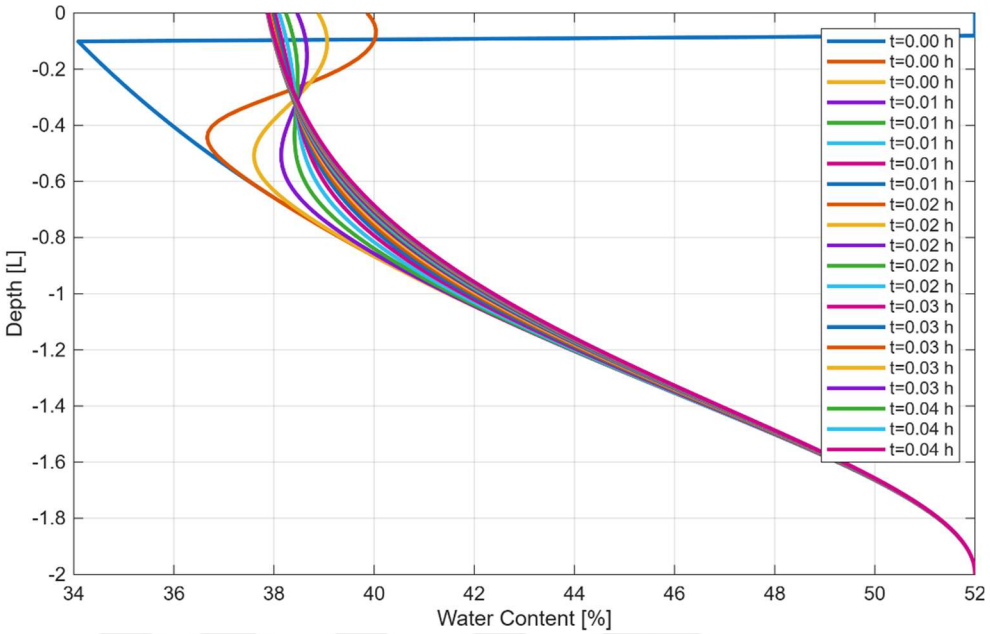

Domain 1D-3 (scaled by $\varepsilon = 10$, with $\alpha_x = -1$ and $\alpha_t = -1$)

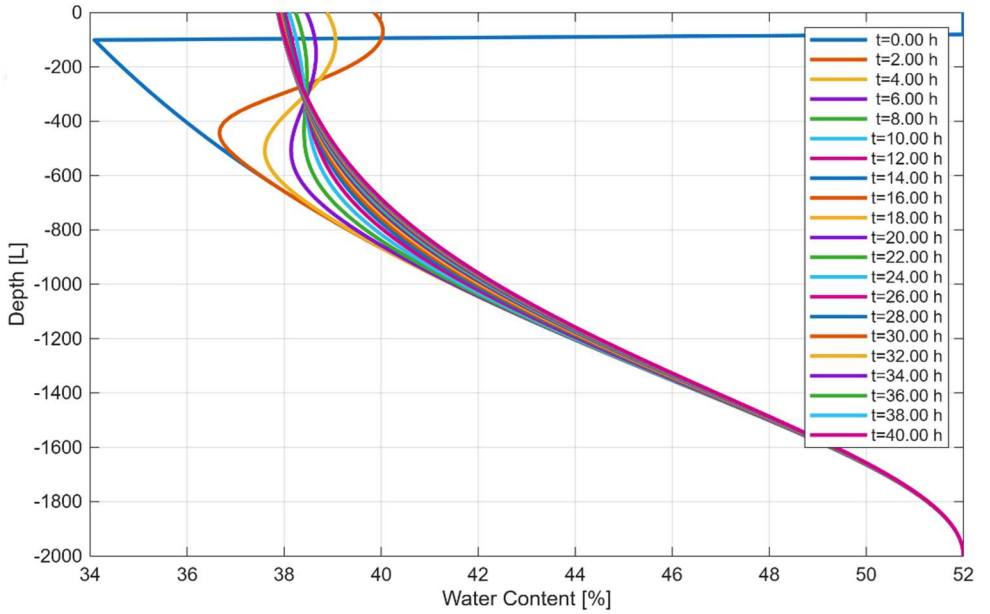

Figure 5.3. Comparison of water content between original domain (1D-0) and scaled domains (1D-1, 1D-2, and 1D-3) at Times t = 0 to 4 Hours in original domain and corresponding scaled times in scaled domains for 1D flow with constant hydraulic conductivity.

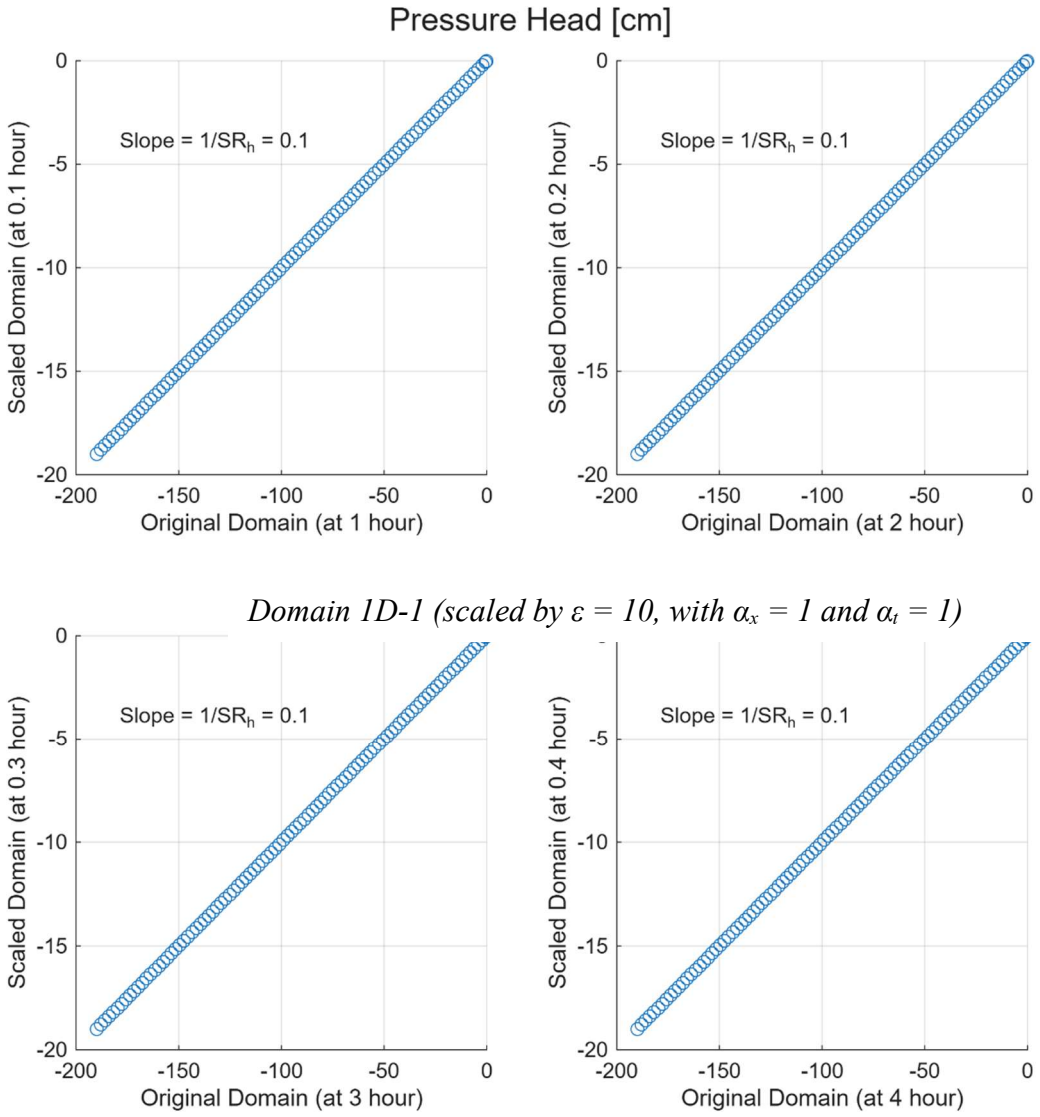

Figure 5.4. Scatter plots comparing pressure head values in Original Domain (1D-0) and scaled domains (1D-1, 1D-2, 1D-3) at Times t = 1 to 4 hours in original domain and corresponding scaled times in scaled domains for 1D flow with constant hydraulic conductivity. The slope of the regression line reflects the pressure head scaling ratio between scaled and original domain. (continued)

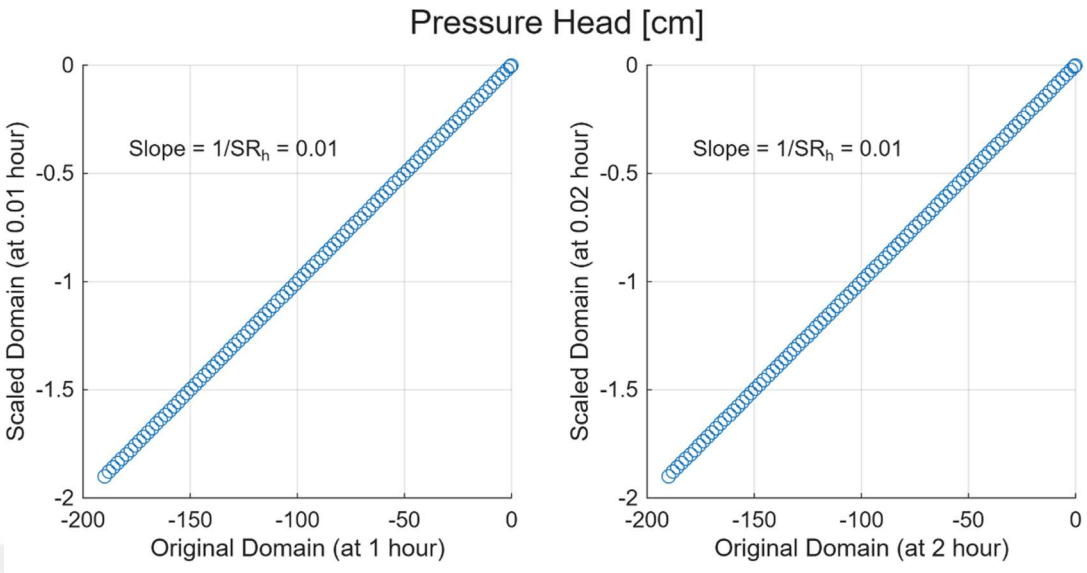

Domain 1D-2 (scaled by ε = 10, with α_x = 2 and α_t = 2)

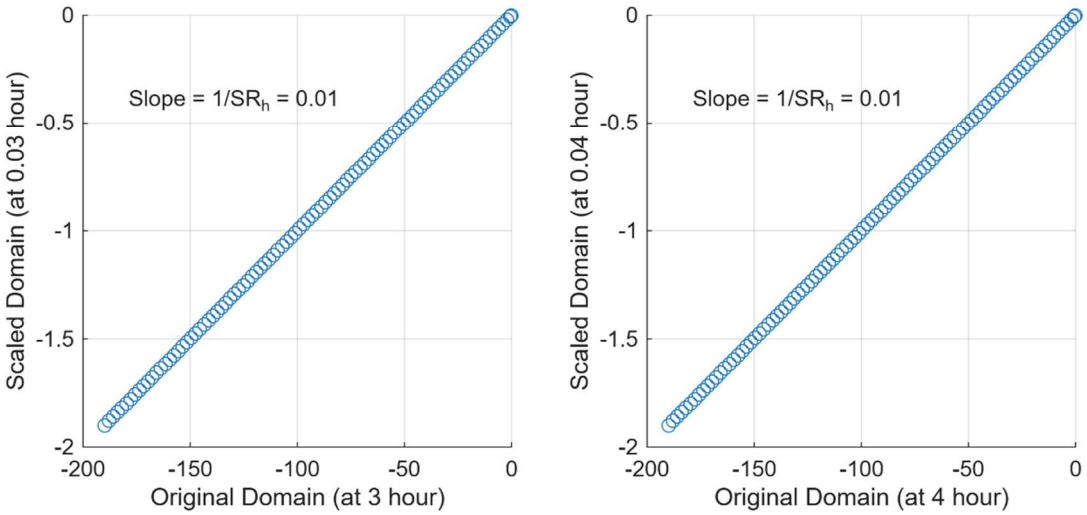

Figure 5.4. (continued) Scatter plots comparing pressure head values in Original Domain (1D-0) and scaled domains (1D-1, 1D-2, 1D-3) at Times t = 1 to 4 hours in original domain and corresponding scaled times in scaled domains for 1D flow with constant hydraulic conductivity. The slope of the regression line reflects the pressure head scaling ratio between scaled and original domain. (continued)

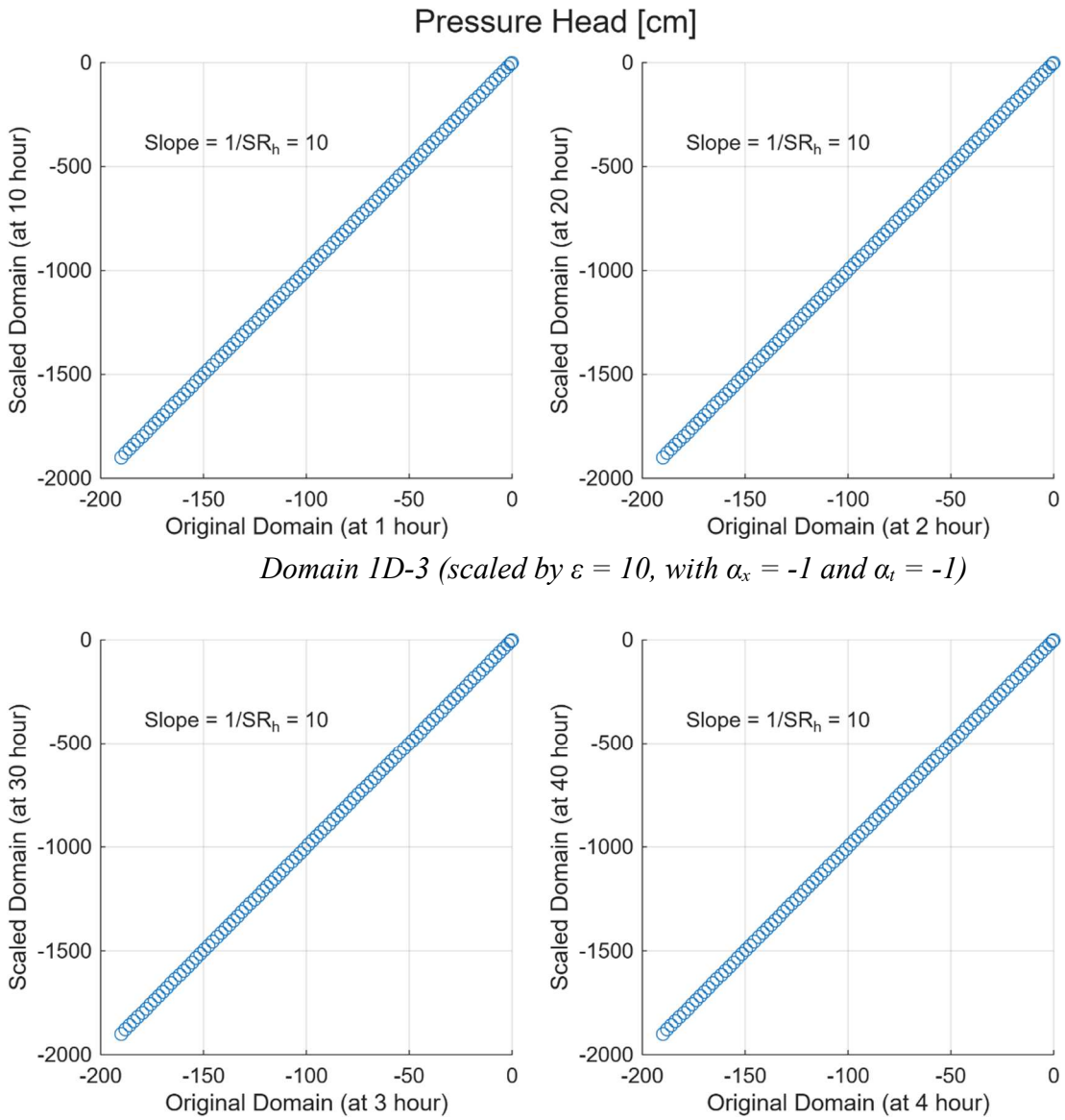

Domain 1D-3 (scaled by ε = 10, with α_x = -1 and α_t = -1)

Original domain at 4 hour	R2	RMSE	NSE	NRMSE
Domain 1D-1 vs 1D-0	1.00000000	0.00000000	1.00000000	0.00000000
Domain 1D-2 vs 1D-0	1.00000000	0.00000000	1.00000000	0.00000000
Domain 1D-3 vs 1D-0	1.00000000	0.00000000	1.00000000	0.00000000

Figure 5.4. Scatter plots comparing pressure head values in Original Domain (1D-0) and scaled domains (1D-1, 1D-2, 1D-3) at Times t = 1 to 4 hours in original domain and corresponding scaled times in scaled domains for 1D flow with constant hydraulic conductivity. The slope of the regression line reflects the pressure head scaling ratio between scaled and original domain.

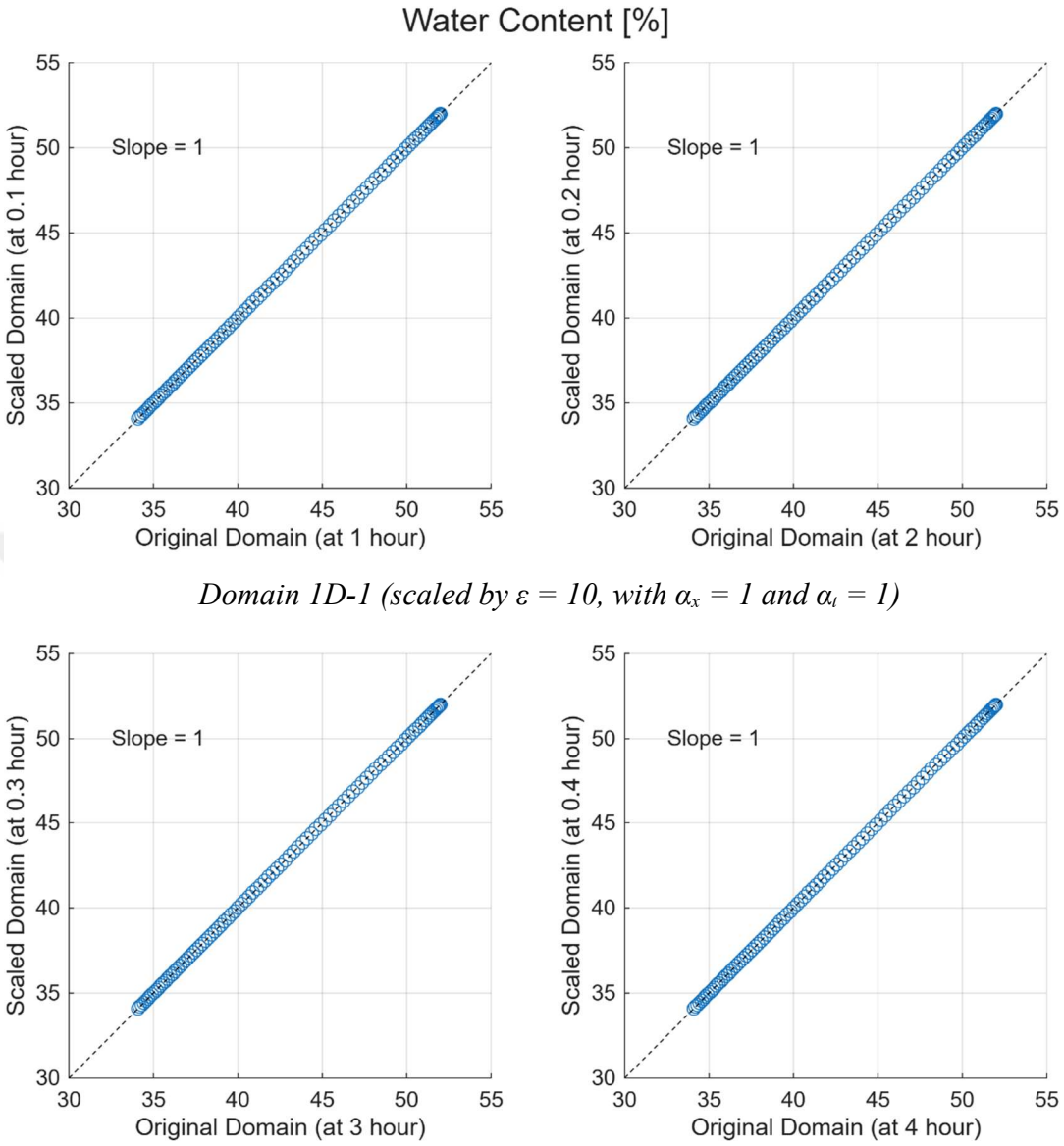

Domain 1D-1 (scaled by $\varepsilon = 10$, with $\alpha_x = 1$ and $\alpha_t = 1$)

Figure 5.5. Scatter plots comparing water content values in Original Domain (1D-0) and scaled domains (1D-1, 1D-2, 1D-3) at Times t = 1 to 4 hours in original domain and corresponding scaled times in scaled domains for 1D flow with constant hydraulic conductivity. The slope of the regression line reflects the pressure head scaling ratio between scaled and original domain. (continued)

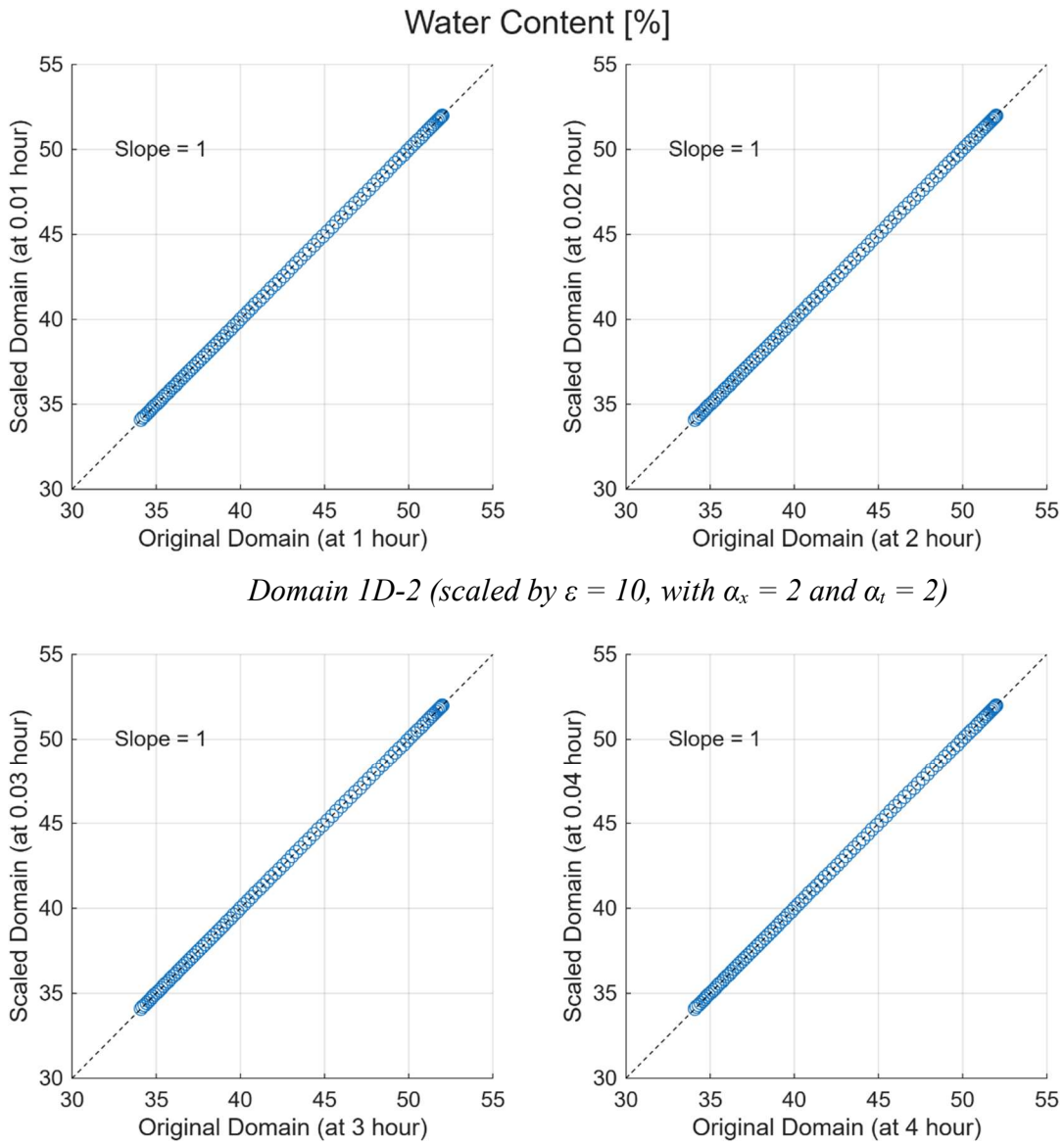

Figure 5.5. Scatter plots comparing water content values in Original Domain (1D-0) and scaled domains (1D-1, 1D-2, 1D-3) at Times t = 1 to 4 hours in original domain and corresponding scaled times in scaled domains for 1D flow with constant hydraulic conductivity. The slope of the regression line reflects the pressure head scaling ratio between scaled and original domain. (continued)

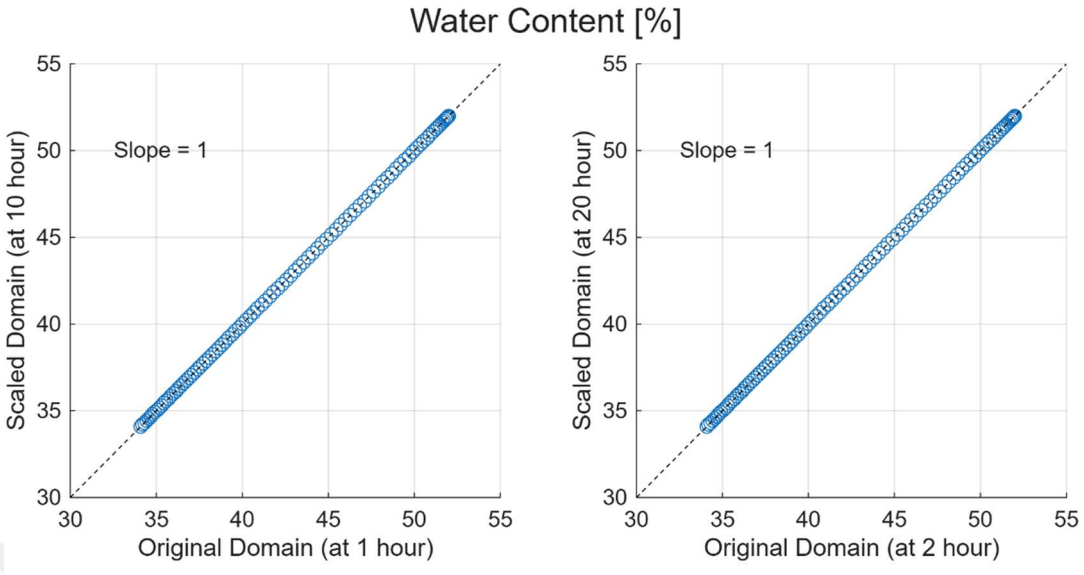

Domain 1D-3 (scaled by ε = 10, with α_x = -1 and α_t = -1)

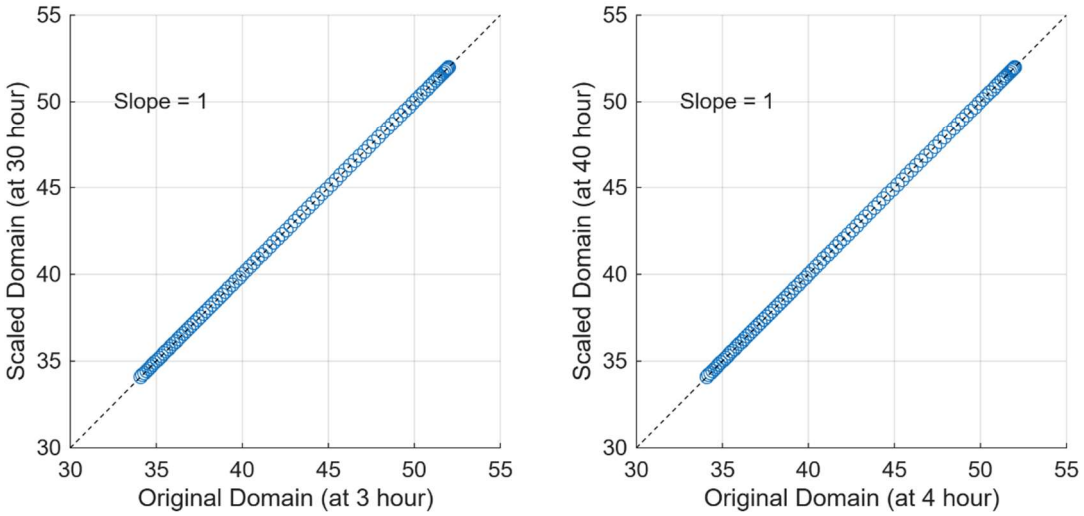

Original domain at 4 hour	R2	RMSE	NSE	NRMSE
Domain 1D-1 vs 1D-0	1.00000000	0.00000000	1.00000000	0.00000000
Domain 1D-2 vs 1D-0	1.00000000	0.00000000	1.00000000	0.00000000
Domain 1D-3 vs 1D-0	1.00000000	0.00000000	1.00000000	0.00000000

Figure 5.5. Scatter plots comparing water content values in Original Domain (1D-0) and scaled domains (1D-1, 1D-2, 1D-3) at Times t = 1 to 4 hours in original domain and corresponding scaled times in scaled domains for 1D flow with constant hydraulic conductivity. The slope of the regression line reflects the pressure head scaling ratio between scaled and original domain.

4.6 Scaling Using Different Hydraulic Conductivities in One-Dimensional Flow

In this case, scaling and self-similarity are achieved by employing different hydraulic conductivities in the original and scaled domains. This is achieved by using varying scaling exponents for distance and time, $\alpha_x \neq \alpha_t$. As such, hydraulic conductivity is not kept constant as $\alpha_x - \alpha_t \neq 0$ and, therefore, the scaling ratio of hydraulic conductivity will not be unity ($SR_K = \epsilon^{\alpha_K} = \epsilon^{\alpha_x - \alpha_t} \neq 1$).

Table 5.4 tabulates Scaling conditions used to obtain scaled domains from the original domain with different hydraulic conductivities for 2-dimensional flow through unsaturated porous media for case 2. Same original domain (Domain 1D-0) is used for scaling. "0" is used to be able to separately identify the original domain from scaled domains. First 3 scaled domains (Domain D-1, 1D-2 and 1D-3) is for case 1 and the next 3 domains (Domain 1D-4, 1D-5 and 1D-6) will be for case 2. Domain 1D-4 is obtained by scaling spatial coordinate by $SR_x = \epsilon^{\alpha_x} = 2$ and time coordinate by $SR_t = \epsilon^{\alpha_t} = 4$. Domain 1D-5 is generated by scaling ratio: $SR_x = \epsilon^{\alpha_x} = 0.5$ for space and $SR_t = \epsilon^{\alpha_t} = 0.25$ for time. Domain 1D-6 is obtained by scaling the original domain with $SR_x = \epsilon^{\alpha_x} = 4$ and $SR_t = \epsilon^{\alpha_t} = 2$. Thus, Domain 1D-5 represents an upscaled version of original/prototype Domain 1 D-0 by a factor of 2 in in space, and 4 in time. The scaling exponents and ratios of the other variables are then obtained as described above for all domains. Problem descriptions for the original and scaled domains for case 2 are tabulated in Table 5.5.

Pressure head values between Domain 1D-0 and scaled domains (Domains 1D-4, 1D-5, and 1D-6) at times t = 0 to 4.0 hours in Domain 1D-0 and corresponding scaled times in scaled domains (Domains 1D-4, 1D-5, and 1D-6) are compared in Figure 5.10.

Hydraulic head values between Domain 1D-0 and scaled domains (Domains 1D-4, 1D-5, and 1D-6) at times t = 0 to 4.0 hours in Domain 1D-0 and corresponding

scaled times in scaled domains (Domains 1D-4, 1D-5, and 1D-6) are compared in Figure 5.9.

Water content values between Domain 1D-0 and scaled domains (Domains 1D-4, 1D-5, and 1D-6) at times t = 0 to 4.0 hours in Domain 1D-0 and corresponding scaled times in scaled domains (Domains 1D-4, 1D-5, and 1D-6) are compared in Figure 5.10.

The same color is used for the original domain and corresponding scaled times in scaled domains. For example, orange color in Domain 1D-0 shows t=1.00 hour in original domain, t = 0.25 hour in Domain 1D-4, t = 4 hour in Domain 1D-5, and t = 0.5 hour in Domain 1D-6. The vertical axis in each figure shows the soil depth in z-direction and it is scaled by the scaling ratio of the space in each domain with respect to original domain.

To quantitatively demonstrate self-similarity, scatter plots of pressure head values in Domain 1D-0 (original) and scaled Domains (Domain 1D-4, 1D-5 and 1D-6) are shown in Figures 5.13-5.15, respectively. These plots compare data at times t = 1 to 4 hours in original Domain 1D-0 with the corresponding scaled times in each respective domain. R2, NRMSE and NSE values are also calculated between the pressure head values of the original domain and their corresponding scaled domain values multiplied with pressure head scaling ratio. Across all comparisons, the R^2 and NSE values remain 1.000, and RMSE value remain 0.000, indicating perfect self-similarity between the original and scaled domains. The slope of each scatter plot where the vertical axis represents the scaled domain and the horizontal axis represents original Domain 1D-0, is equal to the pressure head scaling ratio:

- In Figure 5.13 (Domain 1D-4), the slope is 1 / 2 = 0.5
- In Figure 5.14 (Domain 1D-5), the slope is 1 / 0.5 = 2
- In Figure 5.15 (Domain 1D-6), the slope is 1 / 4 = 0.25

Similarly, scatter plots of water content values in Domain 1D-0 (original) and Domains 1D-4, 1D-5, and 1D-6 are shown in Figures 5.16-5.18. These plots

compare data at times t = 1 to 4 hours in original Domain 1D-0 with the corresponding scaled times in each respective domain. R2, NRMSE and NSE values are also calculated between the water content values of the original domain and their corresponding scaled domain values. Across all comparisons, the R^2 and NSE values remain 1.000, and RMSE value remain 0.000, indicating perfect self-similarity between the original and scaled domains. The slope of each scatter plot where the vertical axis represents the scaled domain and the horizontal axis represents original Domain 1D-0, is equal to the water content scaling ratio:

- In Figure 5.16 (Domain 1D-4), the slope is 1
- In Figure 5.17 (Domain 1D-5), the slope is 1
- In Figure 5.18 (Domain 1D-6), the slope is 1

These slopes directly reflect the scaling ratios of pressure head and water content between each scaled domain and the original domain.

Table 5.4 Scaling conditions used to obtain scaled domains from the original domain with different hydraulic conductivities for 1-dimensional flow through unsaturated porous media

Description	**Symbol / scaling condition**	**Domain 1D-4**	**Domain 1D-5**	**Domain 1D-6**
Scaling parameter	ε	2	0.5	2
Scaling exponent of length	α_x	1	1	2
Scaling exponent of time	α_t	2	2	1
scaling exponent of hydraulic conductivity	$\alpha_K = \alpha_x - \alpha_t$	-1	-1	1
scaling exponent of infiltration velocity	$\alpha_V = \alpha_x - \alpha_t$	-1	-1	1
scaling exponent of pressure head	$\alpha_h = \alpha_x$	1	1	2
scaling ratio of length	$SR_x = \epsilon^{\alpha_x}$	2	0.5	4
scaling ratio of time	$SR_t = \epsilon^{\alpha_t}$	4	0.25	2
scaling ratio of hydraulic conductivity	$SR_K = \epsilon^{\alpha_K}$	0.5	2	2
scaling ratio of velocity	$SR_V = \epsilon^{\alpha_V}$	0.5	2	2
scaling ratio of pressure head	$SR_h = \epsilon^{\alpha_h}$	2	0.5	4

Table 5.5 Problem descriptions for the original and scaled domains with different hydraulic conductivities for 1-dimensional flow through unsaturated porous media

Symbol	Variable	Dimension	Domain 1D-0 (Original)	Domain 1D-4	Domain 1D-5	Domain 1D-6
L	length	[L] (cm)	200	100	400	50
s_1	infiltration velocity	[L/T] (m)	0.5	1.0	0.25	0.25
s_2	bottom suction head	[L] (m)	0	0	0	0
T	maximum time	[T] (hours)	4	1.0	16.00	2.00
q_r	residual water content		0.218	0.218	0.218	0.218
f	porosity		0.52	0.52	0.52	0.52
a	van Genuchten parameter	[1/L] (1/m)	0.0115	0.023	0.01	0.046
n	van Genuchten parameter		2.03	2.03	2.03	2.03
K_s	saturated conductivity	[L/T] (m/hr)	31.6	63.2	15.8	15.8

Domain 1D-0 (Original/Prototype Domain)

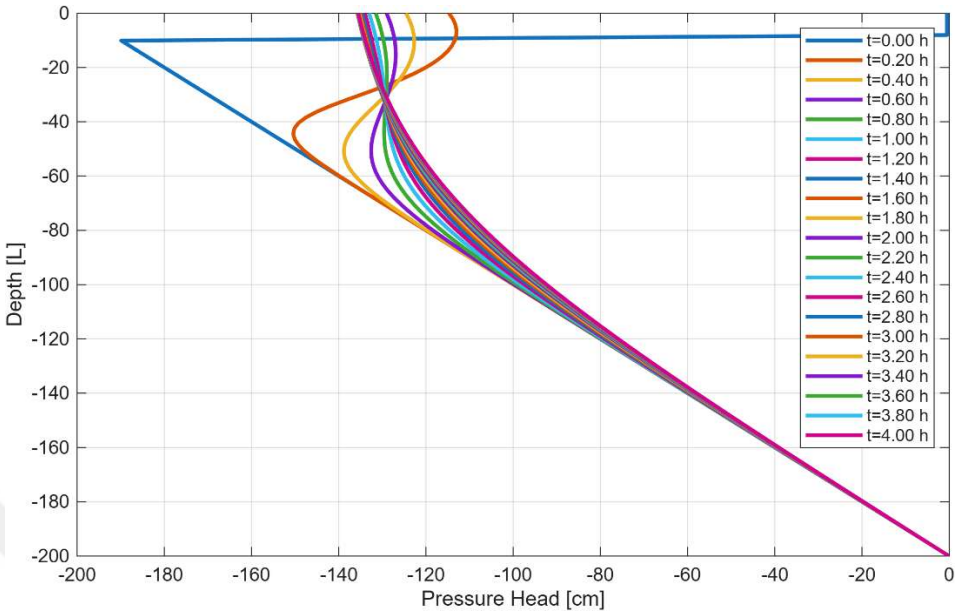

Domain 1D-4 (scaled by $\varepsilon = 2$, with $\alpha_x = 1$ and $\alpha_t = 2$)

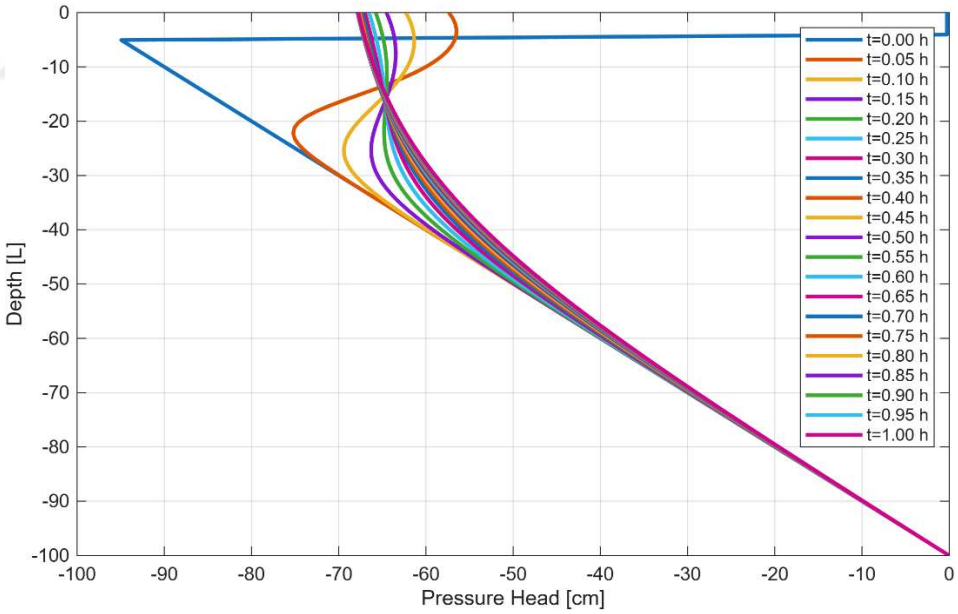

Figure 5.6. Comparison of pressure head between original domain (1D-0) and scaled domains (1D-4, 1D-5, and 1D-6) at Times t = 0 to 4 Hours in original domain and corresponding scaled times in scaled domains for 1D flow with distinct hydraulic conductivity (continued)

Domain 1D-5 (scaled by $\varepsilon = 0.5$, with $\alpha_x = 1$ and $\alpha_t = 2$)

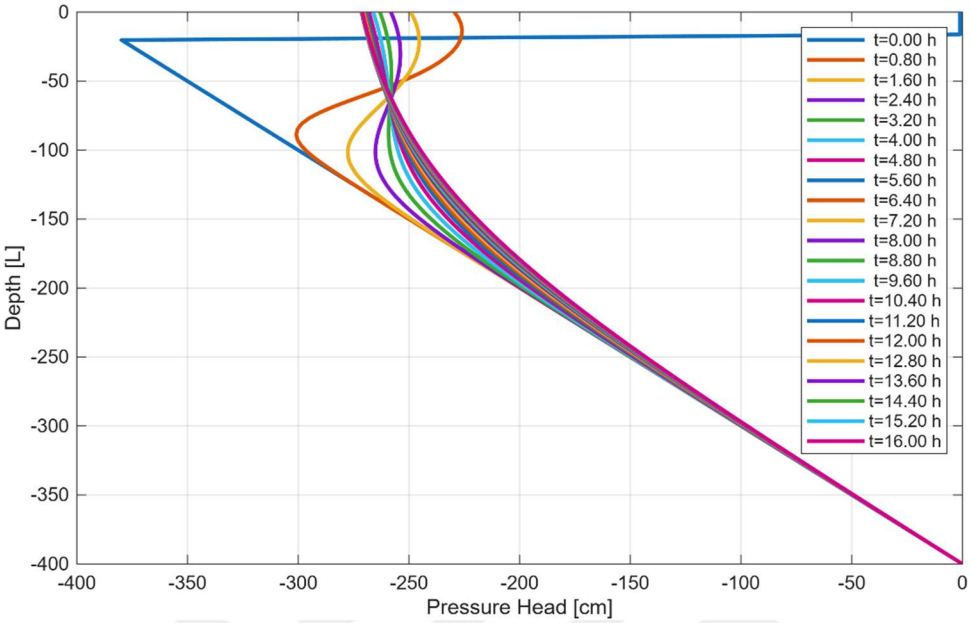

Domain 1D-6 (scaled by $\varepsilon = 2$, with $\alpha_x = 2$ and $\alpha_t = 1$)

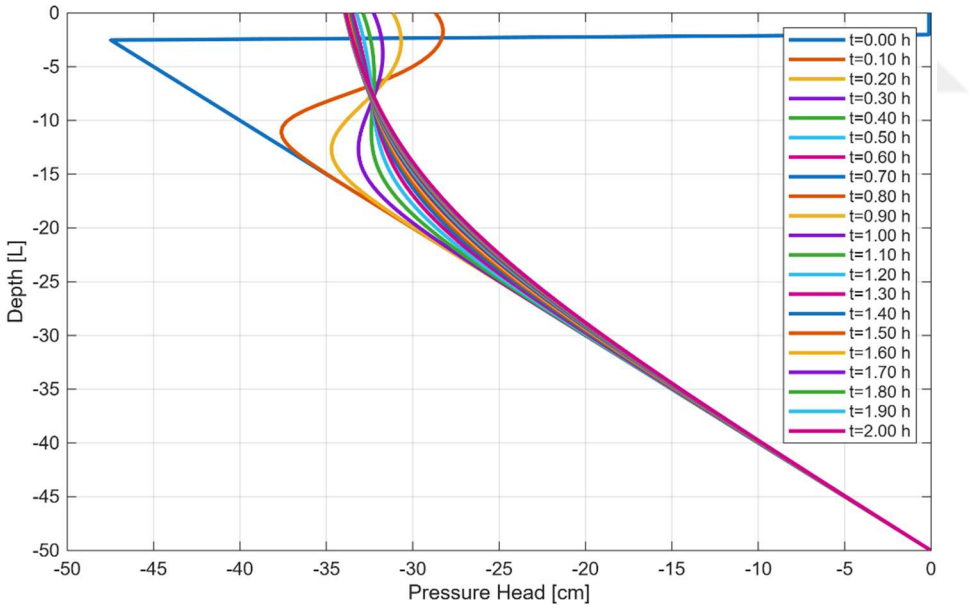

Figure 5.6. Comparison of pressure head between original domain (1D-0) and scaled domains (1D-4, 1D-5, and 1D-6) at Times t = 0 to 4 Hours in original domain and corresponding scaled times in scaled domains for 1D flow with distinct hydraulic conductivity.

Domain1D-0 (Original/Prototype Domain)

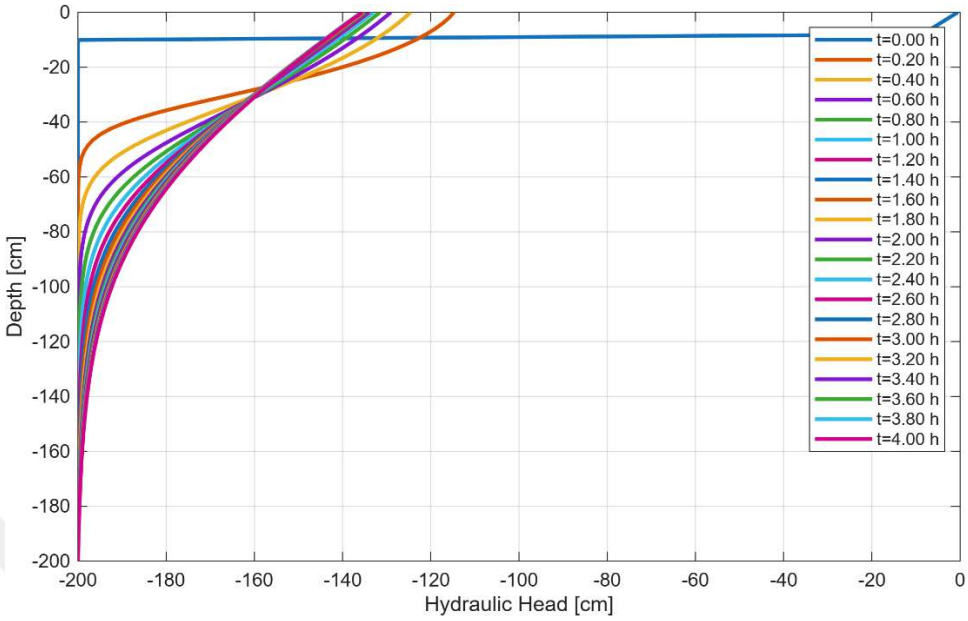

Domain 1D-4 (scaled by $\varepsilon = 2$, with $\alpha_x = 1$ and $\alpha_t = 2$)

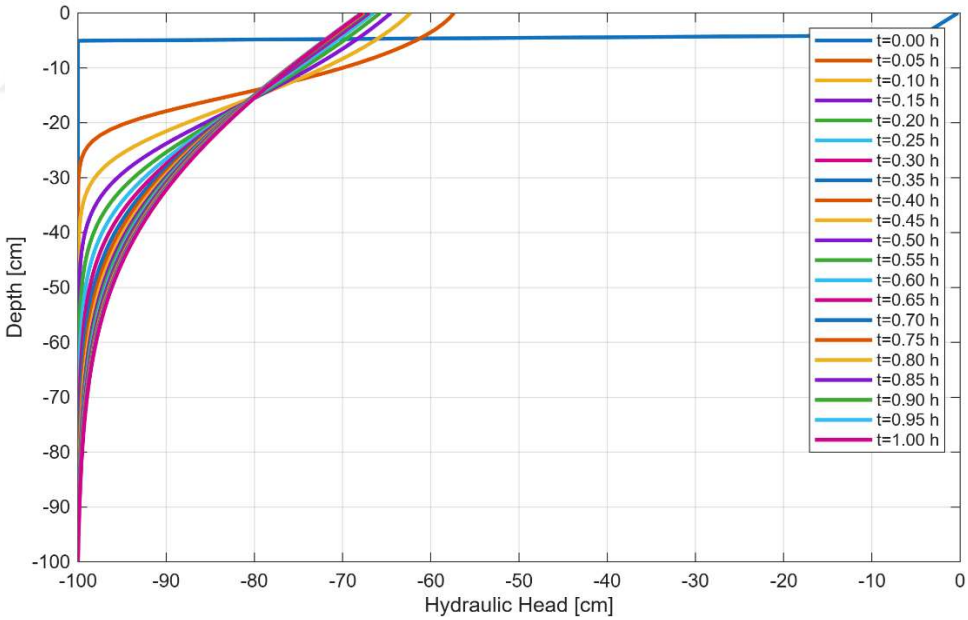

Figure 5.7. Comparison of hydraulic head between original domain (1D-0) and scaled domains (1D-4, 1D-5, and 1D-6) at Times t = 0 to 4 Hours in original domain and corresponding scaled times in scaled domains for 1D flow with constant hydraulic conductivity. (continued)

Domain 1D-5 (scaled by $\varepsilon = 0.5$, with $\alpha_x = 1$ and $\alpha_t = 2$)

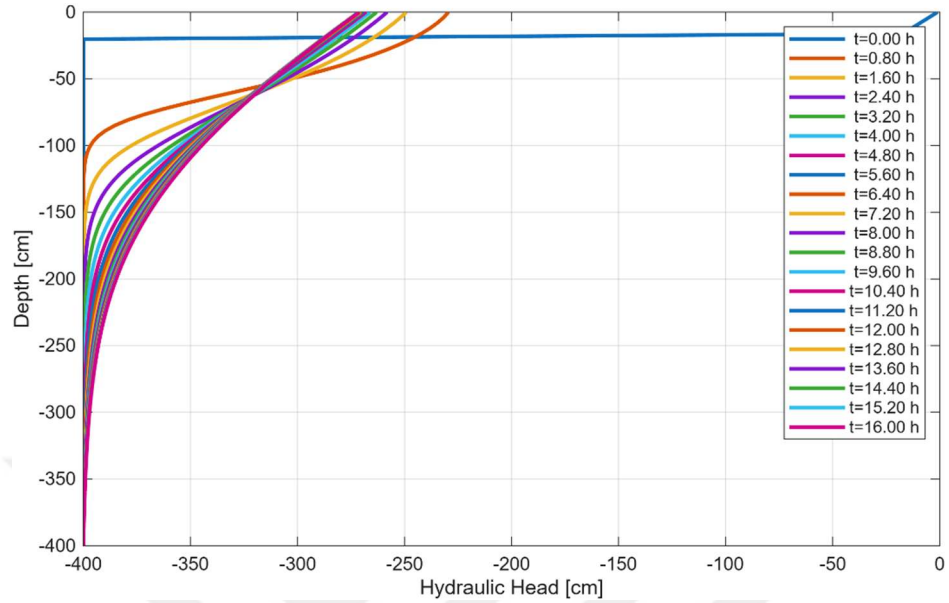

Domain 1D-6 (scaled by $\varepsilon = 2$, with $\alpha_x = 2$ and $\alpha_t = 1$)

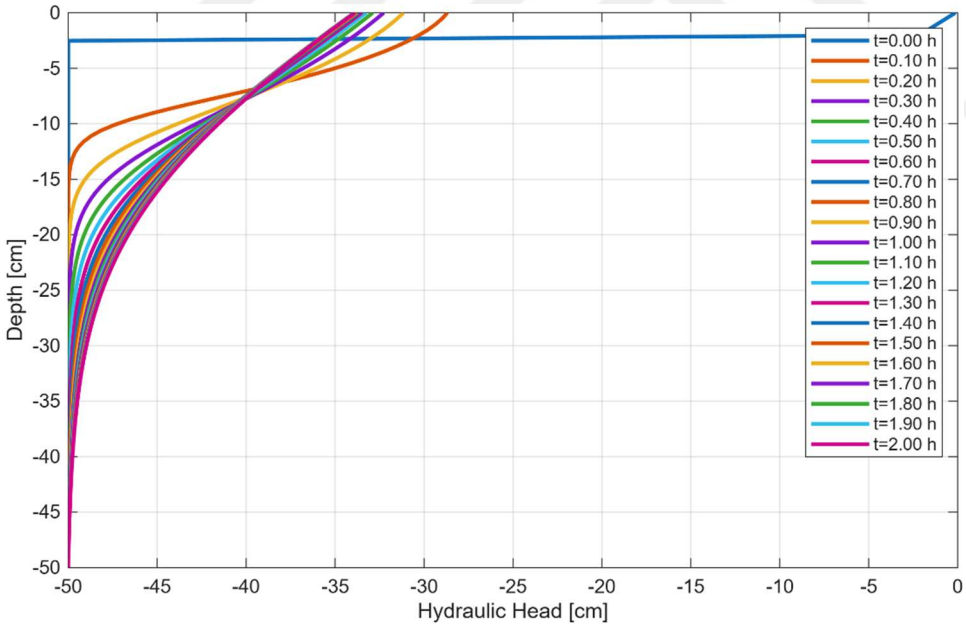

Figure 5.7. Comparison of hydraulic head between original domain (1D-0) and scaled domains (1D-4, 1D-5, and 1D-6) at Times t = 0 to 4 Hours in original domain and corresponding scaled times in scaled domains for 1D flow with distinct hydraulic conductivity.

Domain1D-0 (Original Domain)

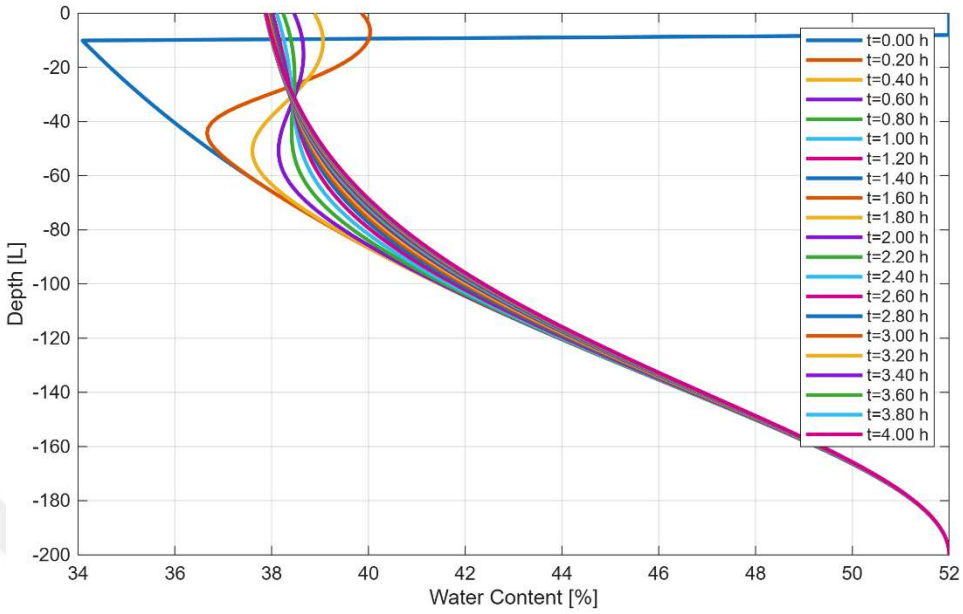

Domain 1D-4 (scaled by $\varepsilon = 2$, with $\alpha_x = 1$ and $\alpha_t = 2$)

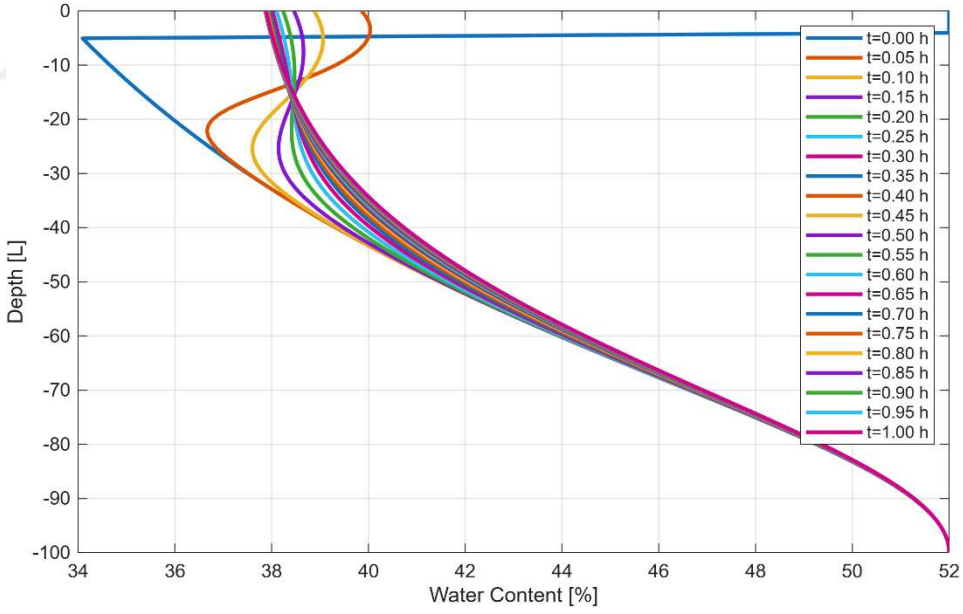

Figure 5.8. Comparison of water content between original domain (1D-0) and scaled domains (1D-4, 1D-5, and 1D-6) at Times t = 0 to 4 Hours in original domain and corresponding scaled times in scaled domains for 1D flow with district hydraulic conductivity (continued)

Domain 1D-5 (scaled by $\varepsilon = 0.5$, with $\alpha_x = 1$ and $\alpha_t = 2$)

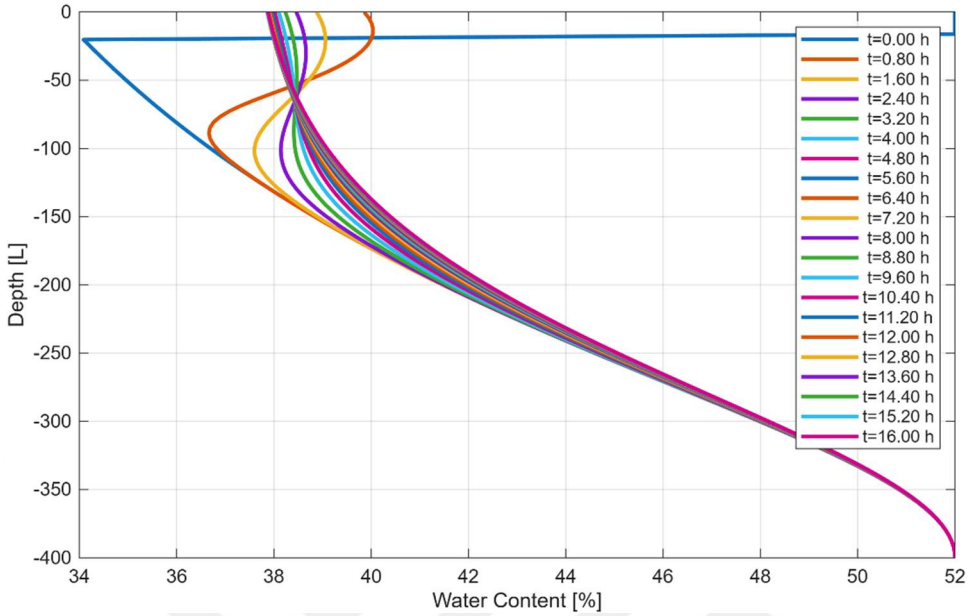

Domain 1D-6 (scaled by $\varepsilon = 2$, with $\alpha_x = 2$ and $\alpha_t = 1$)

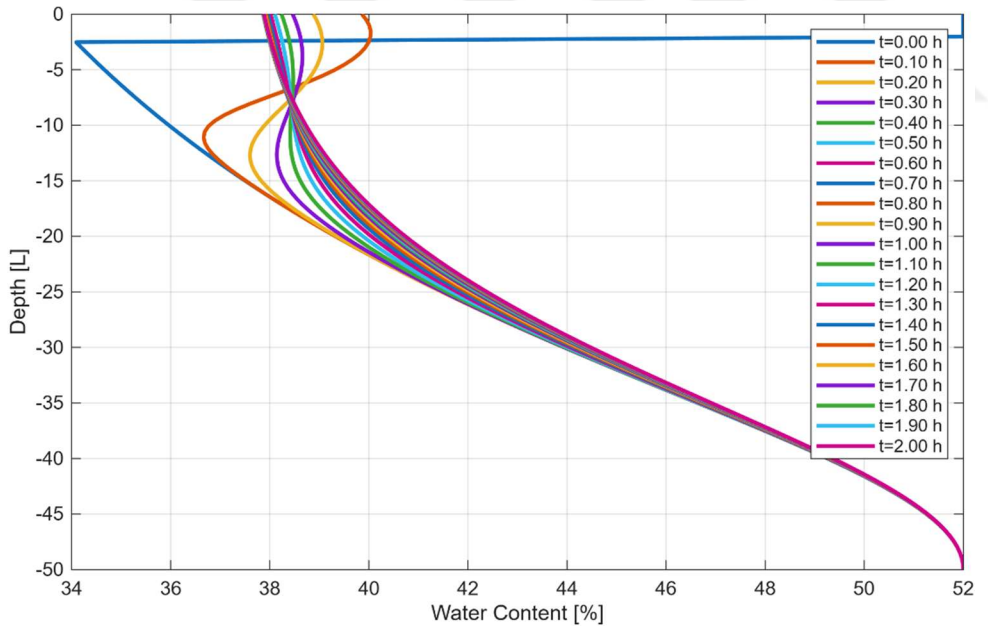

Figure 5.8. Comparison of water content between original domain (1D-0) and scaled domains (1D-4, 1D-5, and 1D-6) at Times t = 0 to 4 Hours in original domain and corresponding scaled times in scaled domains for 1D flow with district hydraulic conductivity.

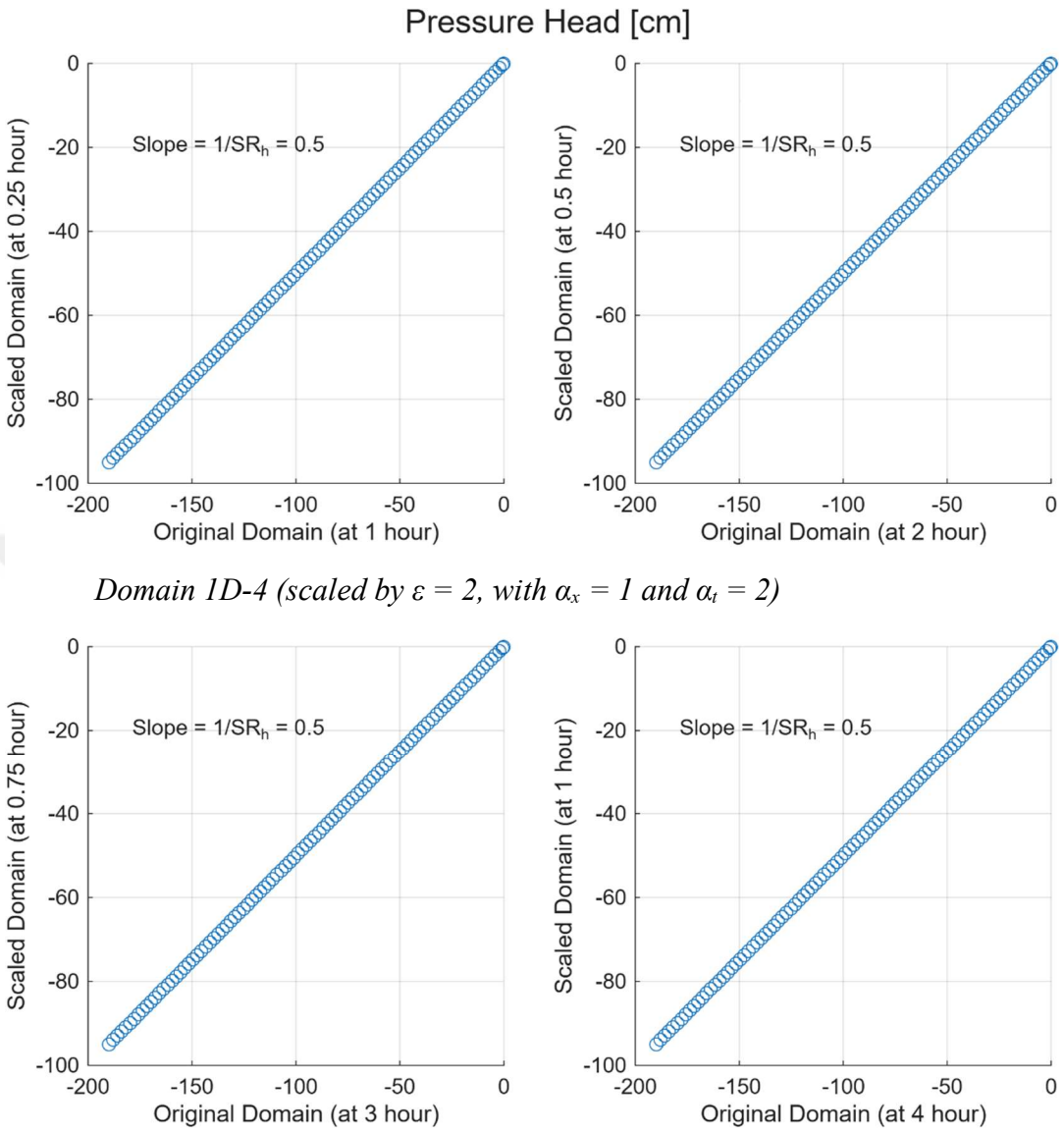

Domain 1D-4 (scaled by $\varepsilon = 2$, with $\alpha_x = 1$ and $\alpha_t = 2$)

Figure 5.9. Scatter plots comparing pressure head values in Original Domain (1D-0) and scaled domains (1D-4, 1D-5, 1D-6) at Times t = 1 to 4 hours in original domain and corresponding scaled times in scaled domains for 1D flow with distinct hydraulic conductivity. The slope of the regression line reflects the pressure head scaling ratio between scaled and original domain (continued)

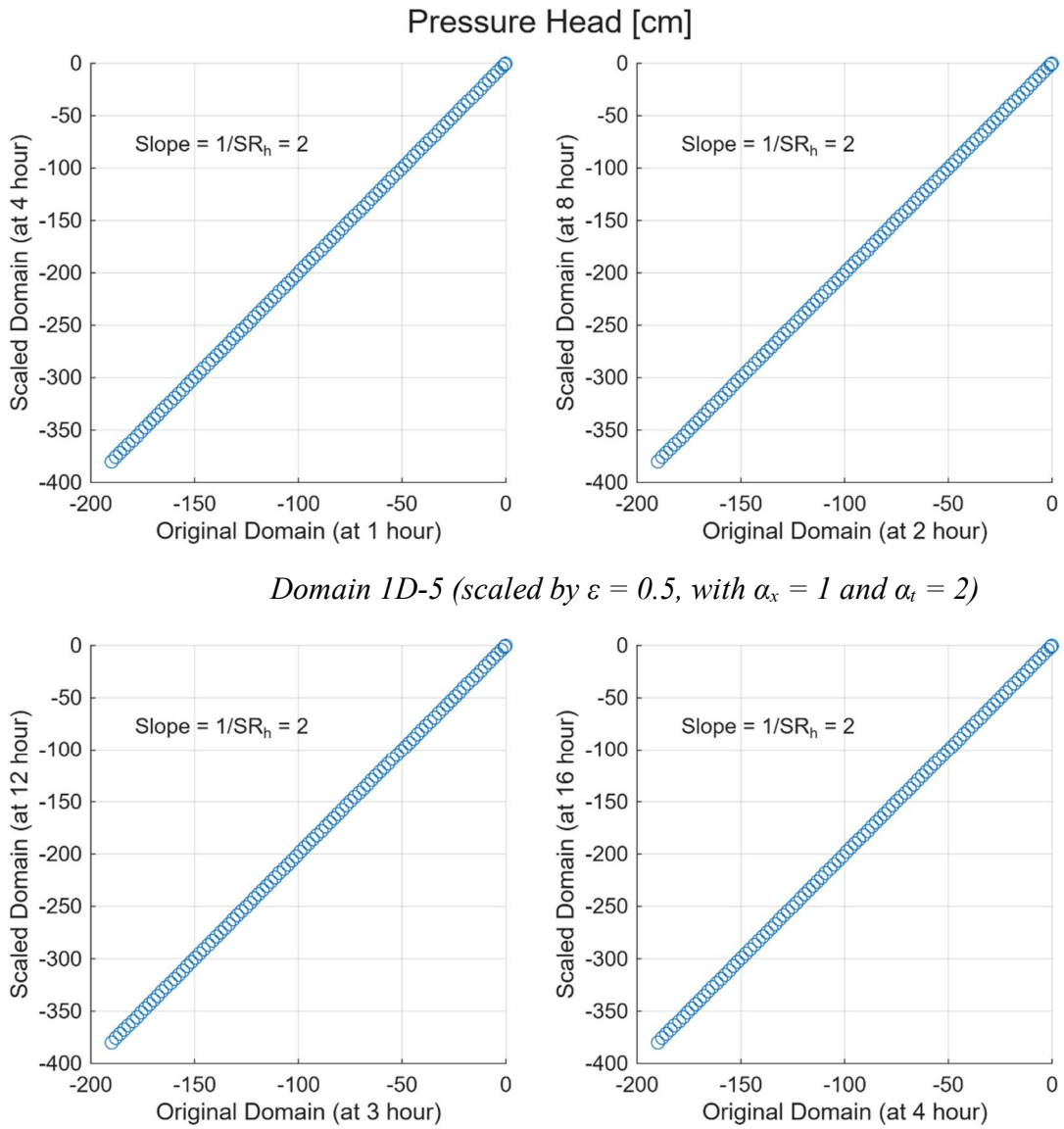

Domain 1D-5 (scaled by $\varepsilon = 0.5$, with $\alpha_x = 1$ and $\alpha_t = 2$)

Figure 5.9. Scatter plots comparing pressure head values in Original Domain (1D-0) and scaled domains (1D-4, 1D-5, 1D-6) at Times t = 1 to 4 hours in original domain and corresponding scaled times in scaled domains for 1D flow with distinct hydraulic conductivity. The slope of the regression line reflects the pressure head scaling ratio between scaled and original domain (continued)

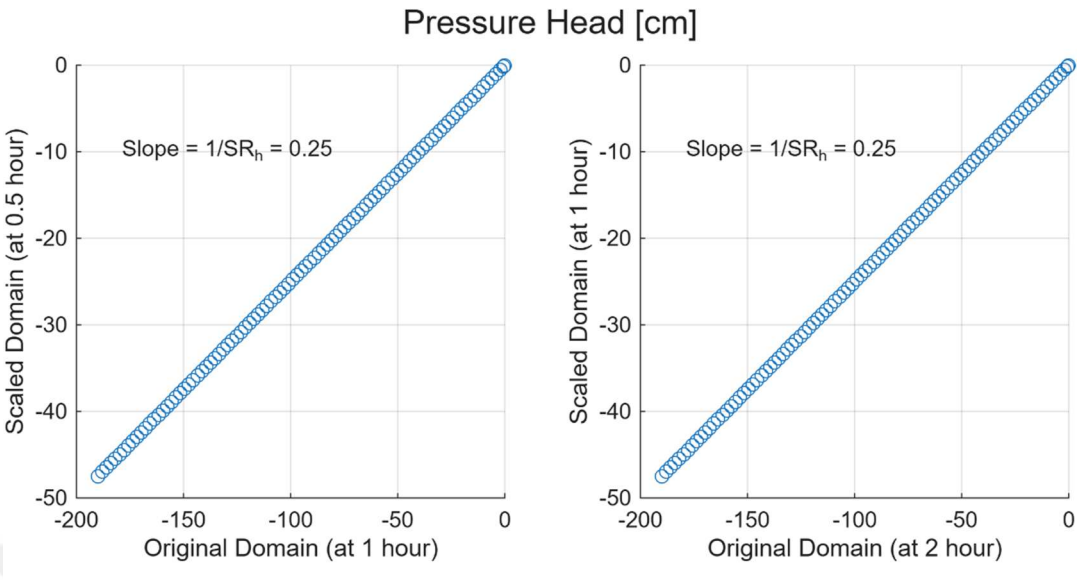

Domain 1D-6 (scaled by $\varepsilon = 2$, with $\alpha_x = 2$ and $\alpha_t = 1$)

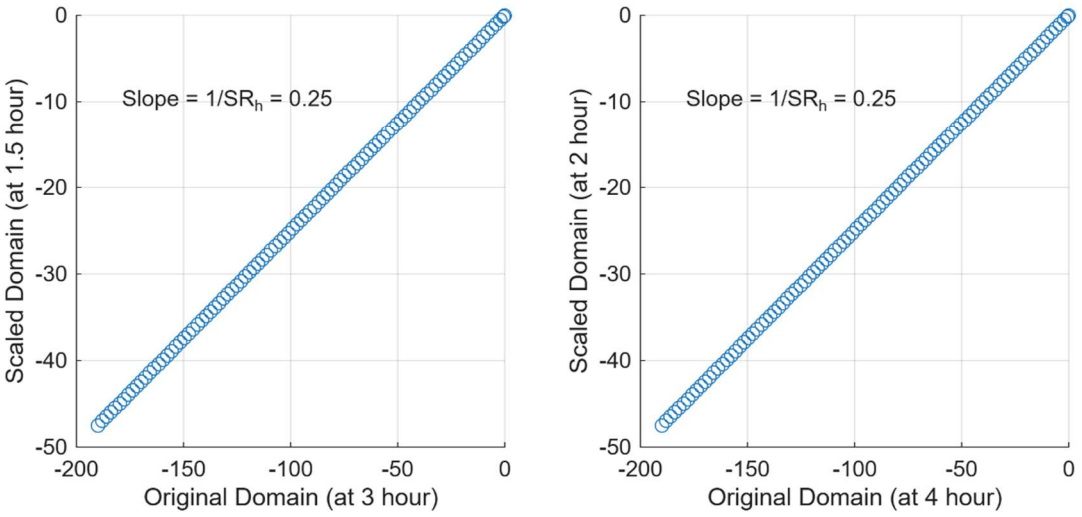

Original domain at 4 hour	R2	RMSE	NSE	NRMSE
Domain 1D-1 vs 1D-0	1.00000000	0.00000000	1.00000000	0.00000000
Domain 1D-2 vs 1D-0	1.00000000	0.00000000	1.00000000	0.00000000
Domain 1D-3 vs 1D-0	1.00000000	0.00000000	1.00000000	0.00000000

Figure 5.9. Scatter plots comparing pressure head values in Original Domain (1D-0) and scaled domains (1D-4, 1D-5, 1D-6) at Times t = 1 to 4 hours in original domain and corresponding scaled times in scaled domains for 1D flow with distinct hydraulic conductivity. The slope of the regression line reflects the pressure head scaling ratio between scaled and original domain.

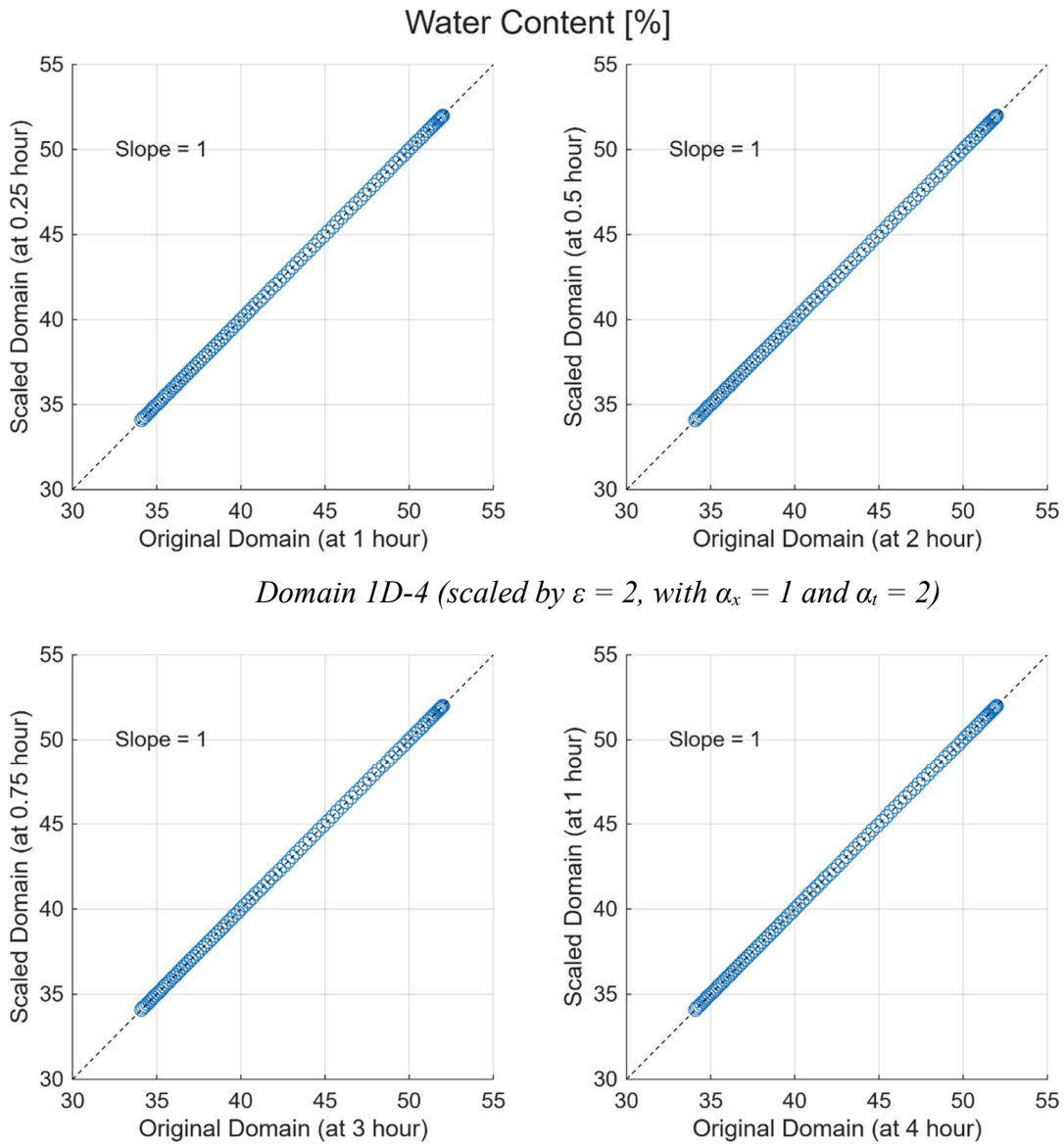

Domain 1D-4 (scaled by $\varepsilon = 2$, with $\alpha_x = 1$ and $\alpha_t = 2$)

Figure 5.10. Scatter plots comparing water content values in Original Domain (1D-0) and scaled domains (1D-4, 1D-5, 1D-6) at Times t = 1 to 4 hours in original domain and corresponding scaled times in scaled domains for 1D flow with distinct hydraulic conductivity. The slope of the regression line reflects the pressure head scaling ratio between scaled and original domain (continued)

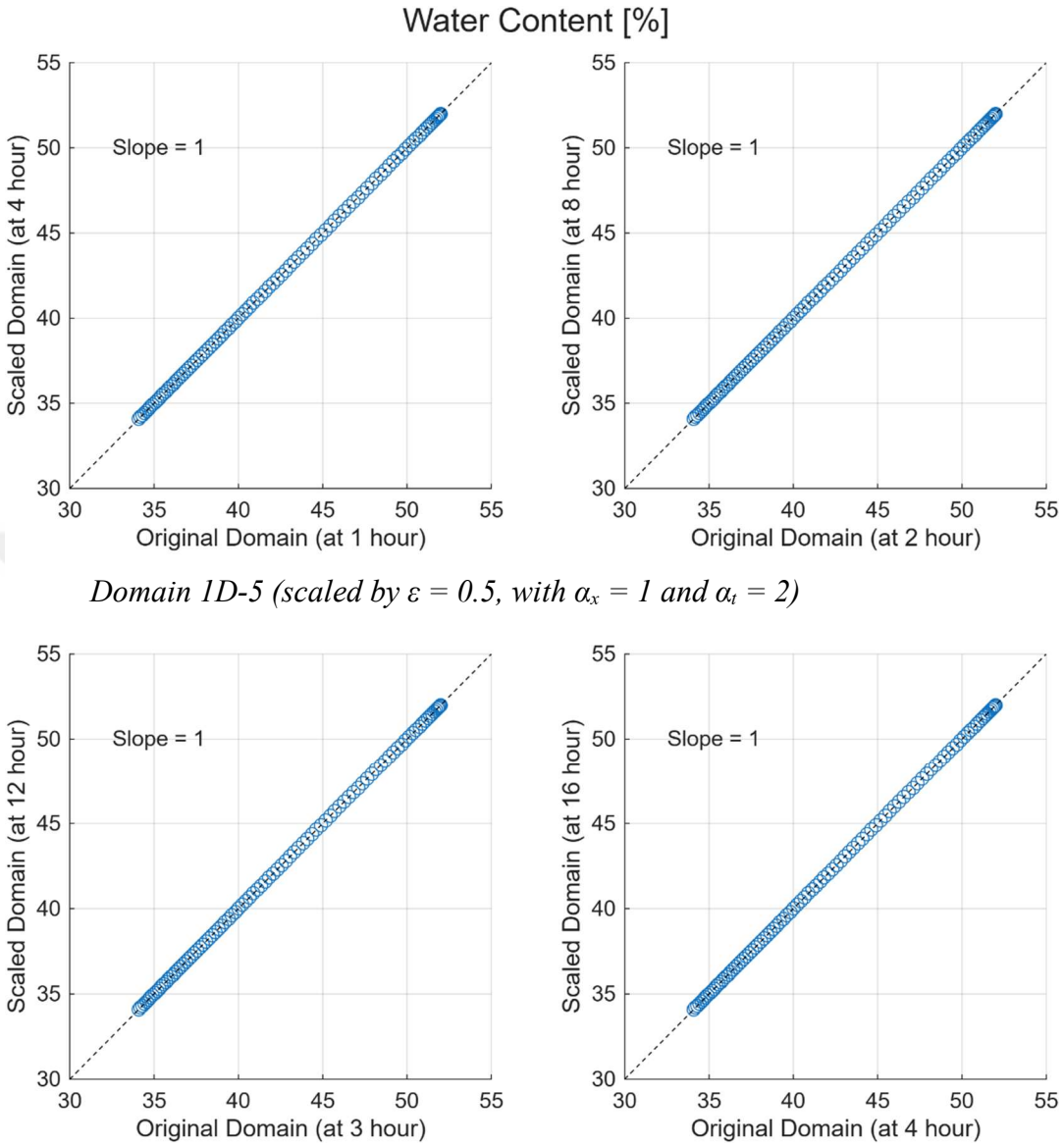

Domain 1D-5 (scaled by $\varepsilon = 0.5$, with $\alpha_x = 1$ and $\alpha_t = 2$)

Figure 5.10. Scatter plots comparing water content values in Original Domain (1D-0) and scaled domains (1D-4, 1D-5, 1D-6) at Times t = 1 to 4 hours in original domain and corresponding scaled times in scaled domains for 1D flow with distinct hydraulic conductivity. The slope of the regression line reflects the pressure head scaling ratio between scaled and original domain (continued)

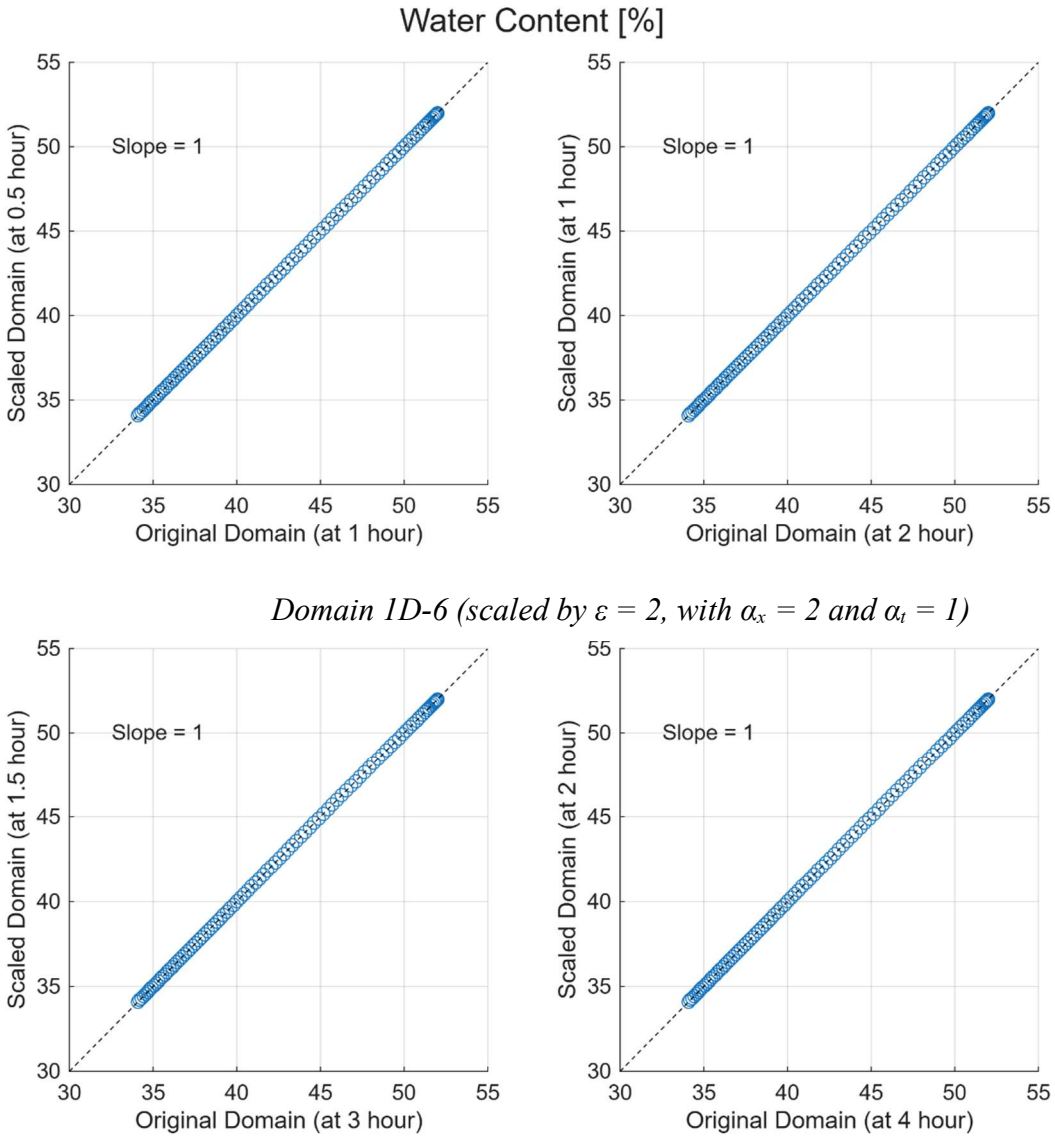

Original domain at 4 hour	R2	RMSE	NSE	NRMSE
Domain 1D-1 vs 1D-0	1.00000000	0.00000000	1.00000000	0.00000000
Domain 1D-2 vs 1D-0	1.00000000	0.00000000	1.00000000	0.00000000
Domain 1D-3 vs 1D-0	1.00000000	0.00000000	1.00000000	0.00000000

Figure 5.10. Scatter plots comparing water content values in Original Domain (1D-0) and scaled domains (1D-4, 1D-5, 1D-6) at Times t = 1 to 4 hours in original domain and corresponding scaled times in scaled domains for 1D flow with distinct hydraulic conductivity. The slope of the regression line reflects the pressure head scaling ratio between scaled and original domain.

CHAPTER 6

NUMERICAL VERIFICATION OF SCALING TWO-DIMENSIONAL UNSTEADY FLOW THROUGH POROUS MEDIA

In this chapter, numerical simulations for two-dimensional flow through unsaturated porous media problems are presented, with a detailed explanation of the applied scaling methodology. The results obtained from the original domain are systematically compared with those from the scaled domains to verify the accuracy and effectiveness of the scaling approach.

To numerically solve the two-dimensional Richards equation, this study employs an already verified example problem as seen in Figure 6.1 below and the open-source MATLAB code developed by Suciuet al. (2021) which solves the example problem described introduced by List and Radu (2016). The problem concerns groundwater reservoir recharge from a drainage trench in a two-dimensional domain. Following the procedure used for the one-dimensional case, the existing MATLAB code was modified by introducing scaling parameters and exponents for each variable. This modification automates the generation of self-similar domains by adjusting the scaling parameters and exponents to achieve the desired level of scaling.

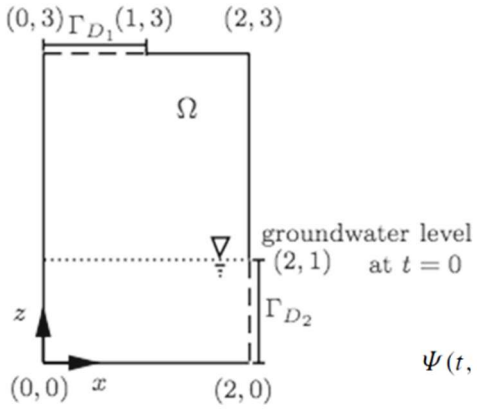

Geometry:

$$\Omega = (0, 2) \times (0, 3),$$
$$\Gamma_{D_1} = \{(x, z) \in \partial\Omega \mid x \in [0, 1] \wedge z = 3\},$$
$$\Gamma_{D_2} = \{(x, z) \in \partial\Omega \mid x = 2 \wedge z \in [0, 1]\},$$
$$\Gamma_D = \Gamma_{D_1} \cup \Gamma_{D_2},$$
$$\Gamma_N = \partial\Omega \setminus \Gamma_D.$$

Initial and Boundary Conditions:

$$\Psi(t, x, z) = \begin{cases} -2 + 2.2\, t/\Delta t_D, & \text{on } \Gamma_{D_1}, t \le \Delta t_D, \\ 0.2, & \text{on } \Gamma_{D_1}, t > \Delta t_D, \\ 1 - z, & \text{on } \Gamma_{D_2}, \end{cases}$$
$$-K(\Psi(t, x, z))(\nabla\Psi(t, x, z) + \mathbf{e_z}) \cdot \mathbf{n} = 0 \quad \text{on } \Gamma_N,$$
$$\Psi^0(x, z) = 1 - z \qquad \text{on } \Omega,$$

Figure 6.1. Sample 2D domain which represents the groundwater reservoir recharge from a drainage trench (List and Radu, 2016).

Same as in 1D, for 2D case, again two different scenarios are studied. In the first case, hydraulic conductivity is held constant. Identical hydraulic conductivity values are applied to both the original and scaled domains. This condition is achieved by assigning equal scaling exponents to the spatial and temporal dimensions, $\alpha_x = \alpha_z = \alpha_t$ ($or\ \alpha_x - \alpha_t = 0$ and $\alpha_z - \alpha_t = 0$). Using the same hydraulic conductivity in both the original and scaled domains has practical advantages. In many laboratory experiments, it is easier to work with a soil having the same saturated hydraulic conductivity. However, it should be emphasized that this does not necessarily imply that the same soil is used in both the prototype and the scaled domains. Although the saturated hydraulic conductivity may remain unchanged, the soil hydraulic functions (e.g., the van Genuchten parameters) scale with the length scaling ratio.

On the other hand, for the second case, different hydraulic conductivity values are applied. This is achieved by assigning unequal scaling exponents to the spatial and temporal dimensions, $\alpha_x = \alpha_z \neq \alpha_t$ (or $\alpha_x - \alpha_t \neq 0$ and $\alpha_z - \alpha_t \neq 0$). In both cases, the example problem in List and Radu (2016) is used as the basis of comparison, i.e., as the original domain. Numbering and identification of original and scaled domains are listed in Table 6.1.

Table 6.1 Identification of original and scaled domains used for 2-dimensional flow through unsaturated porous media

	Domain 2D-0		Original/Prototype
2D	Case1: Scaling Using Identical Hydraulics Conductivities	Domain 2D-1	scaled by ε = 2, $\alpha_x = \alpha_z$ = -1 and α_t = -1
		Domain 2D-2	scaled by ε = 2, $\alpha_x = \alpha_z$ = 1 and α_t = 1
		Domain 2D-3	scaled by ε = 2, $\alpha_x = \alpha_z$ = 2 and α_t = 2
	Case2: Scaling Using Different Hydraulics Conductivities	Domain 2D-4	scaled by ε = 2, $\alpha_x = \alpha_z$ = -1 and α_t = 2
		Domain 2D-5	scaled by ε = 2, $\alpha_x = \alpha_z$ = 1 and α_t = 2
		Domain 2D-6	scaled by ε = 2, $\alpha_x = \alpha_z$ = 2 and α_t = -1

5.1 Scaling Using Identical Hydraulics Conductivities in Two-Dimensional Flow

Identical hydraulic conductivities in the original and scaled domains are obtained by adopting equal scaling exponents for distance and time, $\alpha_x = \alpha_z = \alpha_t$. Under this condition, the hydraulic conductivity remains unchanged between the two domains because $\alpha_x = \alpha_z$, $\alpha_x - \alpha_t = 0$ and $\alpha_z - \alpha_t = 0$, therefore, the scaling ratio of hydraulic conductivity will be unity ($SR_K = \epsilon^{\alpha_K} = \epsilon^{\alpha_{x,z} - \alpha_t} = 1$).

Table 6.2 tabulates the scaling conditions used to obtain scaled domains from the original domain by keeping constant hydraulic conductivities for 2-dimensional flow through unsaturated porous media. Original (prototype domain) is named as Domain 2D-0. "0" is used to be able to separately identify the original domain from scaled domains. All other scaled domains are numbered sequentially after 2D suffix as Domain 2D-1, 2D-2 and 2D-3. Domain 2D-1 is obtained by scaling spatial coordinates by $SR_x = \epsilon^{\alpha_x}$ and $\epsilon^{\alpha_z} = 0.5$, thus upscaling the original domain and scaling the time by $SR_t = \epsilon^{\alpha_t} = 0.5$. Domain 2D-2 is generated by applying scaling spatial coordinates by $SR_x = \epsilon^{\alpha_x}$ and $\epsilon^{\alpha_z} = 2$, thus downscaling the original domain, and scaling the time by $SR_t = \epsilon^{\alpha_t} = 2$. Domain 2D-3, on the other hand, is obtained by downscaling the original domain with $SR_x = \epsilon^{\alpha_x} = 4$ and $SR_t = \epsilon^{\alpha_t} = 4$. Problem descriptions for the original and scaled domains for case 1 are tabulated in Table 6.3.

Temporal evolution of pressure head from t = 0 to 3 days in Domain 2D-0 (prototype domain), and at the corresponding scaled times in Domains 2D-1, 2D-2, and 2D-3 for two-dimensional flow under identical hydraulic conductivity values are plotted in Figure 6.2. This figure demonstrates the visual self-similarity of progression of unsteady flow regime between original (prototype) domain and scaled domains (Domains 2D-1, 2D-2, and 2D-3).

Temporal evolution of water content from t = 0 to 3 days in Domain 2D-0 (prototype domain), and at the corresponding scaled times in Domains 2D-1, 2D-2, and 2D-3 for two-dimensional flow under identical hydraulic conductivity values are plotted in Figure 6.3. This figure visually demonstrates and compares the scaling and self-similarity concept between original and scaled domains. These figures are used to visually demonstrate and compare the scaling and self-similarity concept between original and scaled domains.

To quantitatively demonstrate self-similarity, scatter plots comparing pressure head values in Domain 2D-0 (prototype domain) with those in scaled Domains 2D-1, 2D-2, and 2D-3 at time steps from t = 0 to 3 days in the original domain and at the corresponding scaled times in the scaled domains are plotted in Figure 6.4. R2, NRMSE and NSE values are also calculated between the pressure head values of the original domain and their corresponding scaled domain values multiplied with pressure head scaling ratio. Across all comparisons, the R^2 and NSE values remain 1.000, and RMSE value remain 0.000, indicating perfect self-similarity between the original and scaled domains. The slope of each scatter plot where the vertical axis represents the scaled domain and the horizontal axis represents Domain 2D-0, is equal to the inverse of the pressure head scaling ratio:

In Figure 6.4:

- (Domain 2D-1), the slope is 2 which is $1/SR_\psi$ as expected
- (Domain 2D-2), the slope is 0.5 which is $1/SR_\psi$ as expected
- (Domain 2D-3), the slope is 0.25 which is $1/SR_\psi$ as expected

Similarly, scatter plots of water content values in Domain 2D-0 (original) and Domains 2D-1, 2D-2, and 2D-3 are shown in Figure 6.5. These plots compare data at times t = 0 to 3 days in Domain 2D-0 with the corresponding scaled times in each respective domain. R2, NRMSE and NSE values are also calculated between the water content values of the original domain and their corresponding scaled domain values. Across all comparisons, the R2 and NSE values remain 1.000, and RMSE value remain 0.000, indicating perfect self-similarity between the original and scaled domains. The slope of each scatter plot where the vertical axis represents the scaled domain and the horizontal axis represents Domain 2D-0 (original domain), is equal to unity, which shows water content is scale invariant:

In Figure 6.5:

- (Domain 2D-1), the slope is 1 where water content is scale invariant as expected
- (Domain 2D-2), the slope is 1 where water content is scale invariant as expected
- (Domain 2D-3), the slope is 1 where water content is scale invariant as expected

These slopes directly reflect the scaling ratios of pressure head and water content between each scaled domain and the original domain.

Table 6.2 Scaling conditions used to obtain scaled domains from the original domain while maintaining constant hydraulic conductivity for 2-dimensional flow through unsaturated porous media

Description	**Symbol / scaling condition**	**Domain 2D-1**	**Domain 2D-2**	**Domain 2D-3**
Scaling parameter	ε	2	2	2
Scaling exponent of x	α_x	-1	1	2
Scaling exponent of z	α_z	-1	1	2
Scaling exponent of time	α_t	-1	1	2
scaling exponent of hydraulic conductivity	$\alpha_K = \alpha_x - \alpha_t$	0	0	0
scaling exponent of infiltration velocity	$\alpha_V = \alpha_x - \alpha_t$	0	0	0
scaling exponent of pressure head	$\alpha_h = \alpha_x$	-1	1	2
scaling ratio of x	$SR_x = \epsilon^{\alpha_x}$	0.5	2	4
scaling ratio of z	$SR_z = \epsilon^{\alpha_z}$	0.5	2	4
scaling ratio of time	$SR_t = \epsilon^{\alpha_t}$	0.5	2	4
scaling ratio of hydraulic conductivity	$SR_K = \epsilon^{\alpha_K}$	1	1	1
scaling ratio of velocity	$SR_V = \epsilon^{\alpha_V}$	1	1	1
scaling ratio of pressure head	$SR_h = \epsilon^{\alpha_h}$	0.5	1	4

Table 6.3 Problem descriptions for the original and scaled domains with identical hydraulic conductivities for 2-dimensional flow through unsaturated porous media

Symbol	Variable	Dimension	Domain 2D-0 Original	Domain 2D-1	Domain 2D-2	Domain 2D-3
Lx	length in X direction	[L] (m)	2	4	1	0.5
Lz	length in Z direction	[L] (m)	3	6	1.5	0.75
T	maximum time	[T] (days)	3	6	1.5	0.75
Δx	Grid size in x direction	[L] (m)	0.2	0.4	0.1	0.05
Δz	Grid size in z direction	[L] (m)	0.3	0.6	0.15	0.075
Δt	Time step	[T] (days)	0.3333	0.6667	0.1667	0.0833
α	van Genuchten parameter	[1/L] (m)	0.152	0.076	0.304	0.608
n	van Genuchten parameter	-	1.17	1.17	1.17	1.17
K_s	saturated conductivity	[L/T] (m)	0.00082	0.00082	0.00082	0.00082
θ_S	Theta (Water Content) saturated	-	0.446	0.446	0.446	0.446
θ_R	Theta (Water Content) residual	-	0	0	0	0

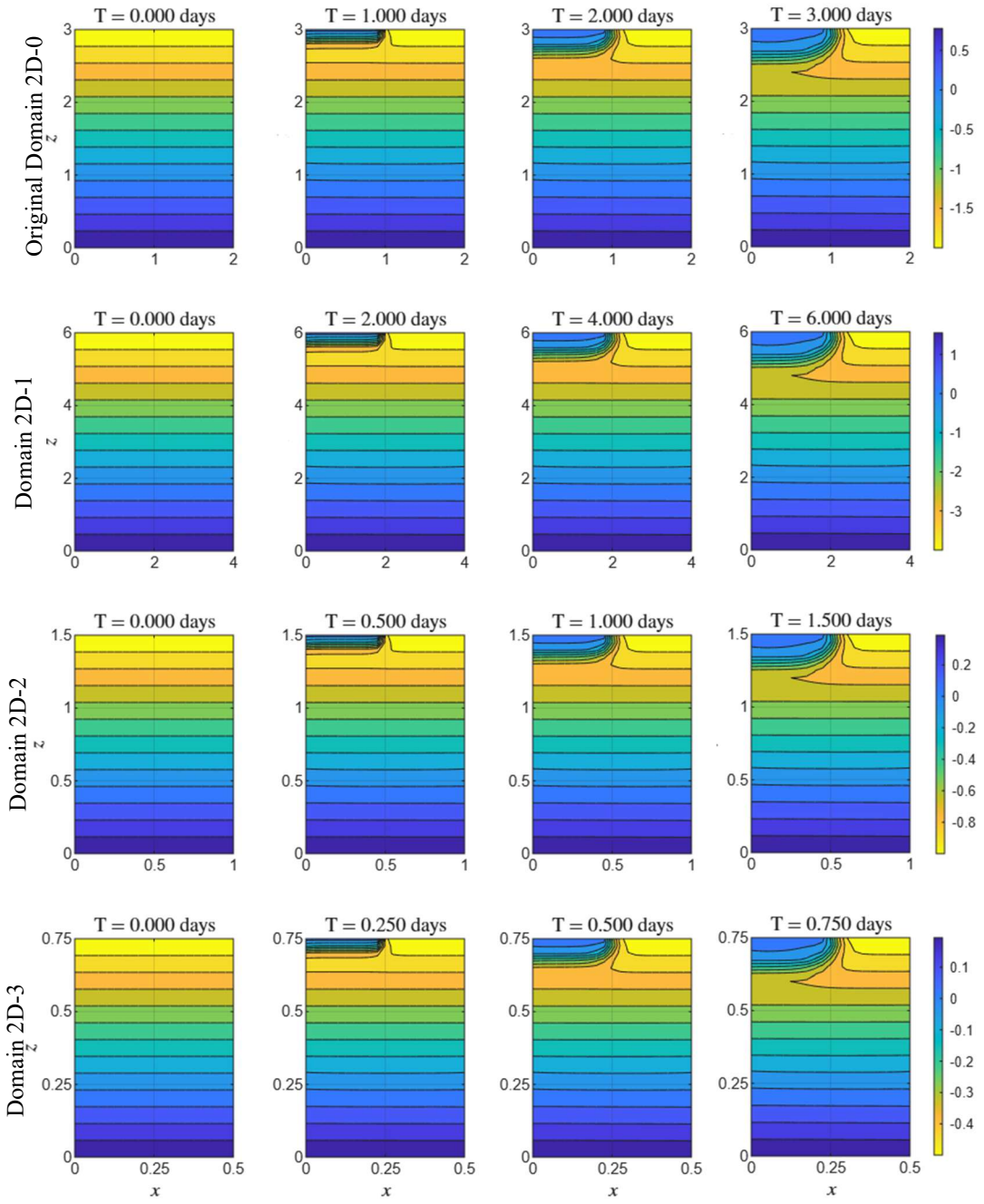

Figure 6.2. Temporal evolution of pressure head (m) from t = 0 to 3 days in Domain 2D-0 (prototype domain), and at the corresponding scaled times in Domains 2D-1, 2D-2, and 2D-3 for two-dimensional flow under identical hydraulic conductivity values (Case 1)

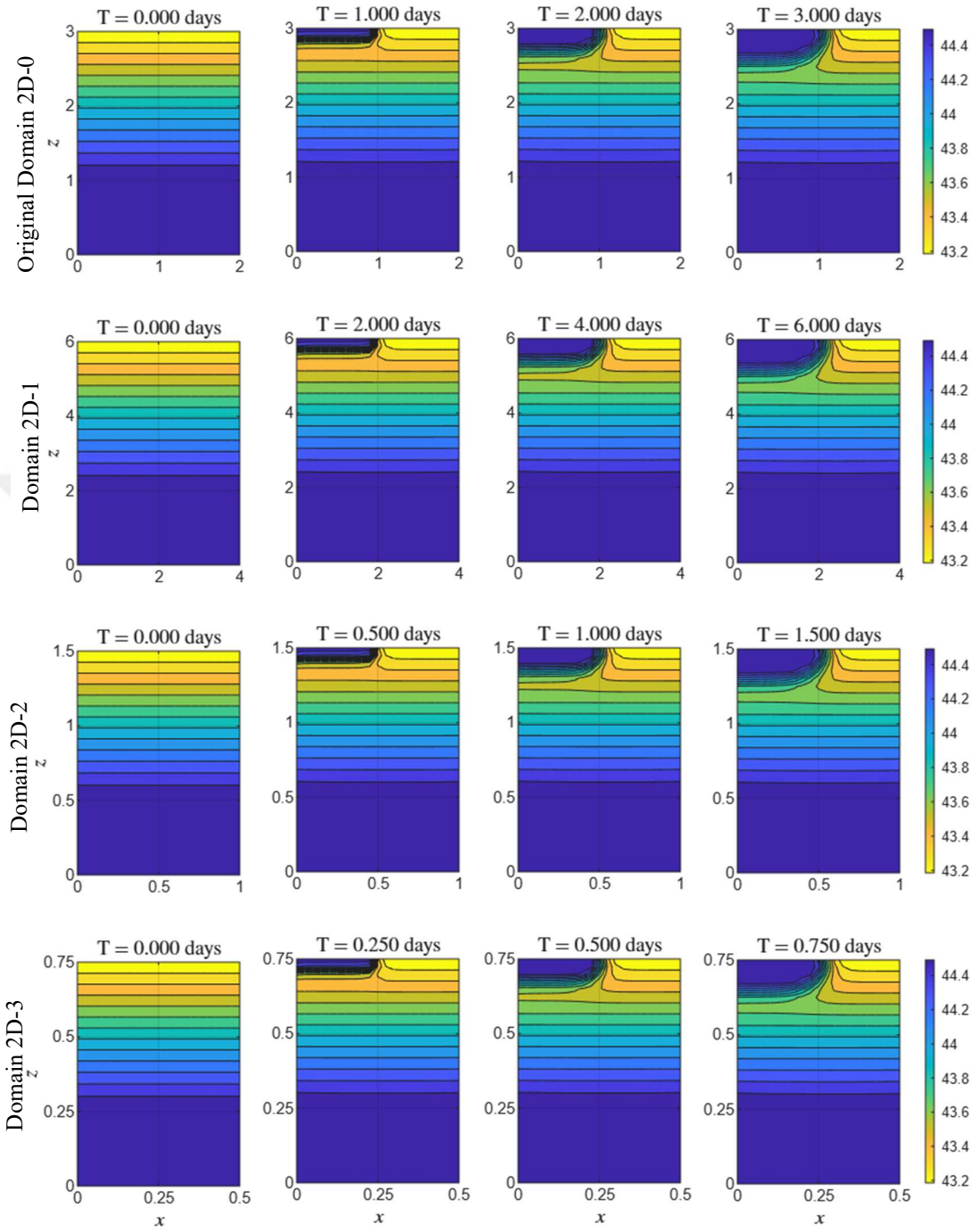

Figure 6.3. Temporal evolution of water content (%) from t = 0 to 3 days in Domain 2D-0 (prototype domain), and at the corresponding scaled times in Domains 2D-1, 2D-2, and 2D-3 for two-dimensional flow under identical hydraulic conductivity values (Case 1)

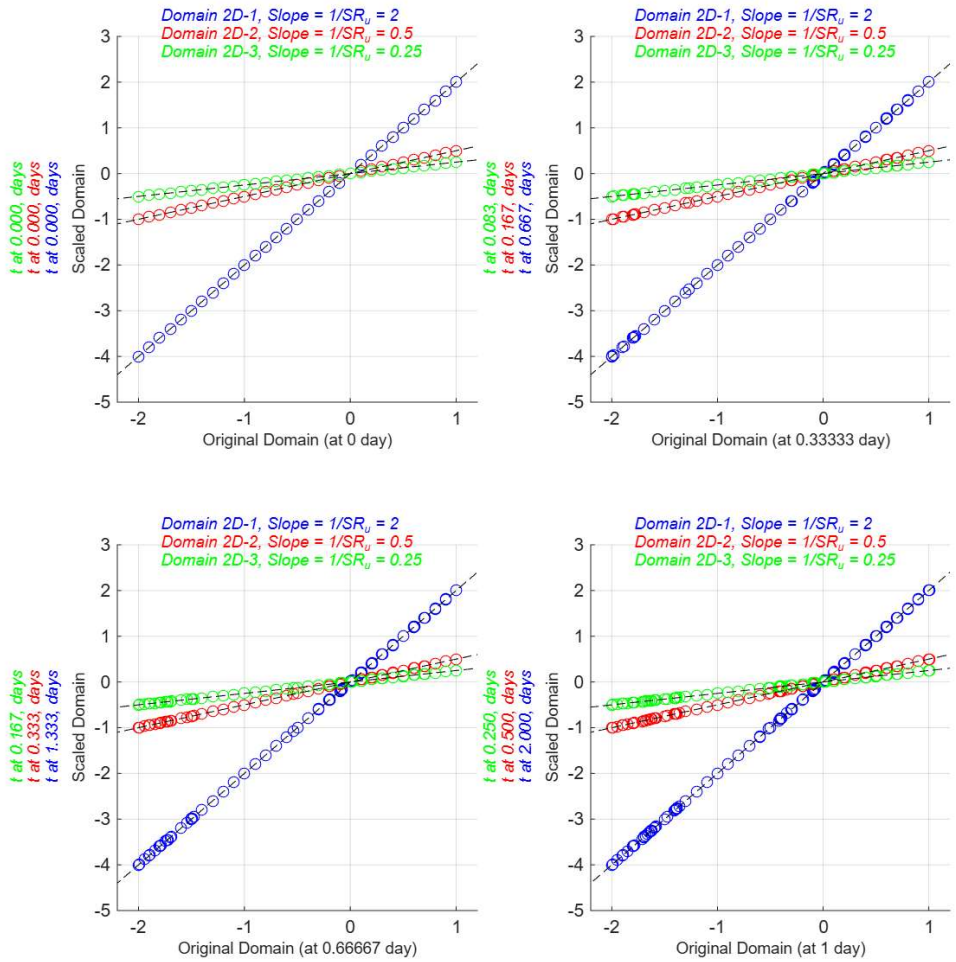

Figure 6.4. Scatter plots comparing pressure head (m) values in Domain 2D-0 (prototype domain) with those in scaled Domains 2D-1,2D-2, and 2D-3 at time steps from t = 0 to 3 days in the original domain and at the corresponding scaled times in the scaled domains for two-dimensional flow under identical hydraulic conductivity values (Case 1). The slope of the regression line represents the inverse of the pressure head scaling ratio (SR_ψ). (continued)

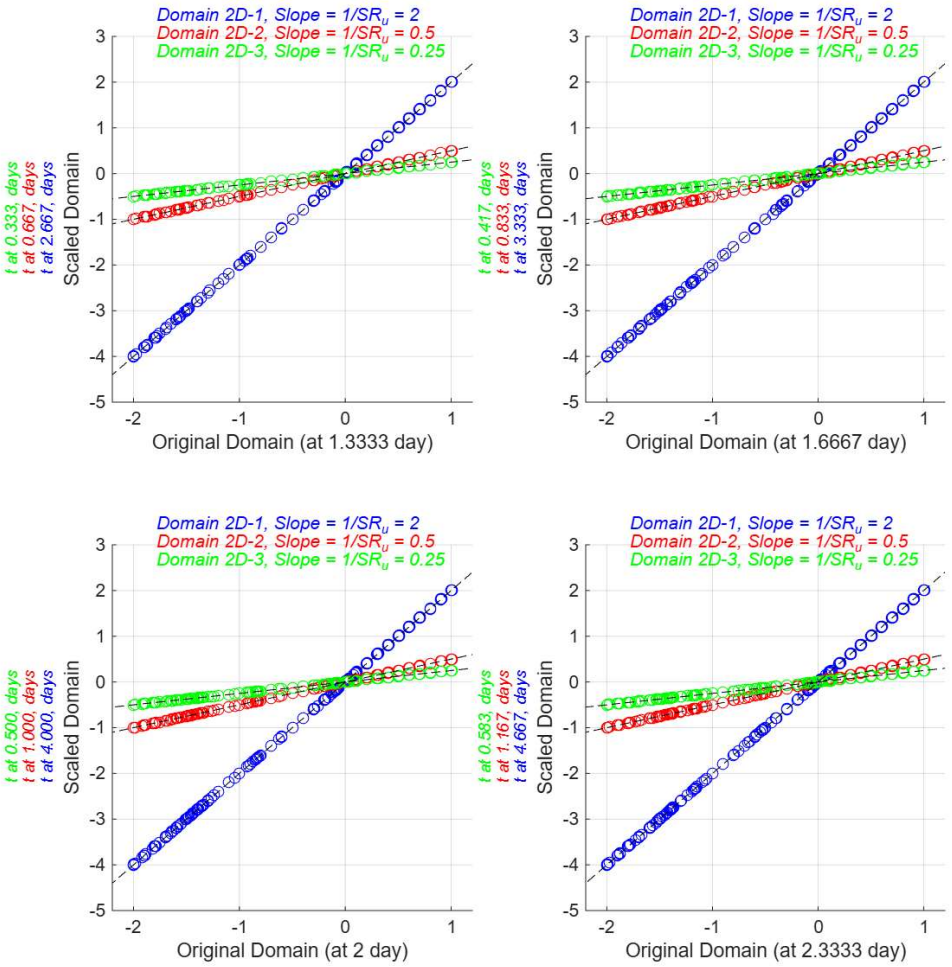

Figure 6.4. Scatter plots comparing pressure head (m) values in Domain 2D-0 (prototype domain) with those in scaled Domains 2D-1,2D-2, and 2D-3 at time steps from t = 0 to 3 days in the original domain and at the corresponding scaled times in the scaled domains for two-dimensional flow under identical hydraulic conductivity values (Case 1). The slope of the regression line represents the inverse of the pressure head scaling ratio (SR_Ψ). (continued)

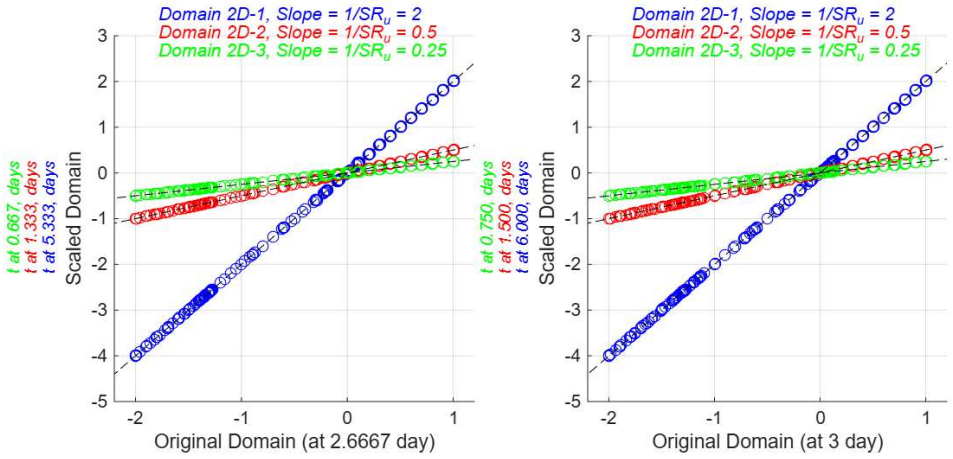

Original Domain at 3 days	R2	RMSE	NSE	NRMSE
Domain 2D-1 vs 2D-0	0.99999958	0.00055117	0.9999958	0.00018349
Domain 2D-2 vs 2D-0	0.99999964	0.00050874	0.9999964	0.00016936
Domain 2D-3 vs 2D-0	0.99999946	0.00062336	0.9999946	0.00020752

Figure 6.4. Scatter plots comparing pressure head (m) values in Domain 2D-0 (prototype domain) with those in scaled Domains 2D-1,2D-2, and 2D-3 at time steps from t = 0 to 3 days in the original domain and at the corresponding scaled times in the scaled domains for two-dimensional flow under identical hydraulic conductivity values (Case 1). The slope of the regression line represents the inverse of the pressure head scaling ratio (SR_Ψ).

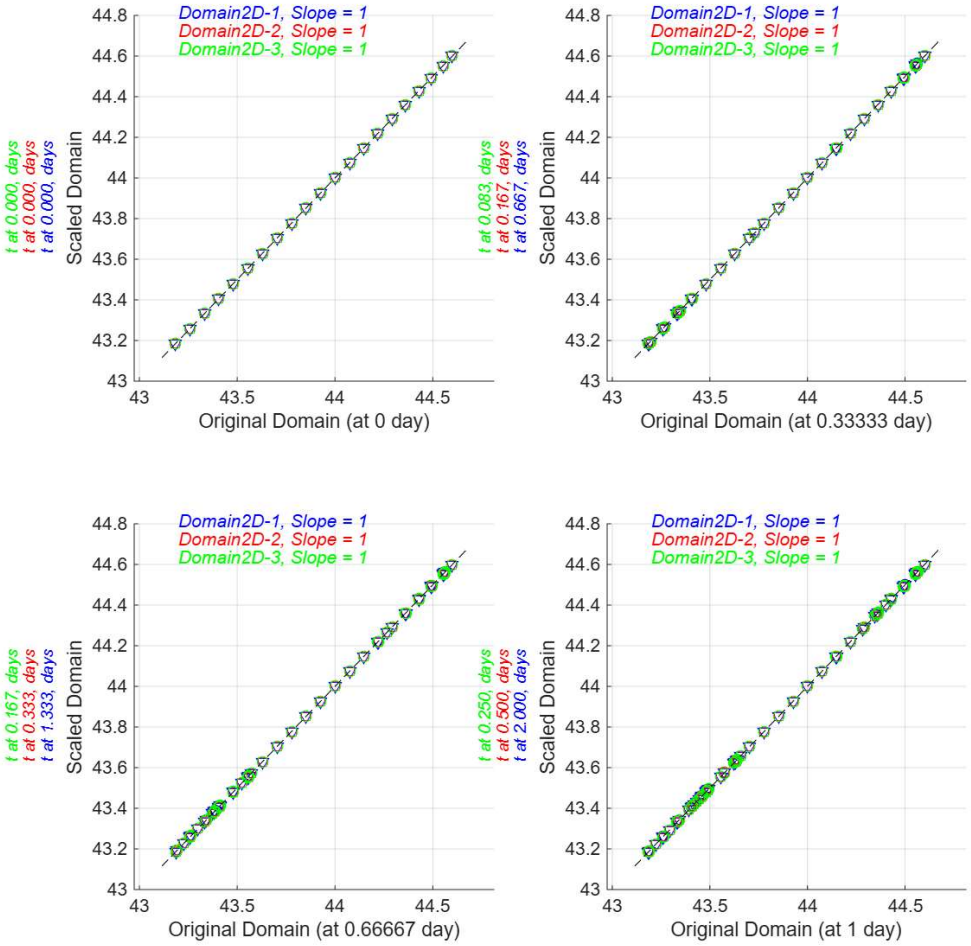

Figure 6.5. Scatter plots comparing water content (%) values in Domain 2D-0 (prototype domain) with those in scaled Domains 2D-1, 2D-2, and 2D-3 at time steps from t = 0 to 3 days in the original domain and at the corresponding scaled times in the scaled domains for two-dimensional flow under identical hydraulic conductivity values (Case 1). The slope of the regression line is 1, reflecting the water content scaling ratio. (continued)

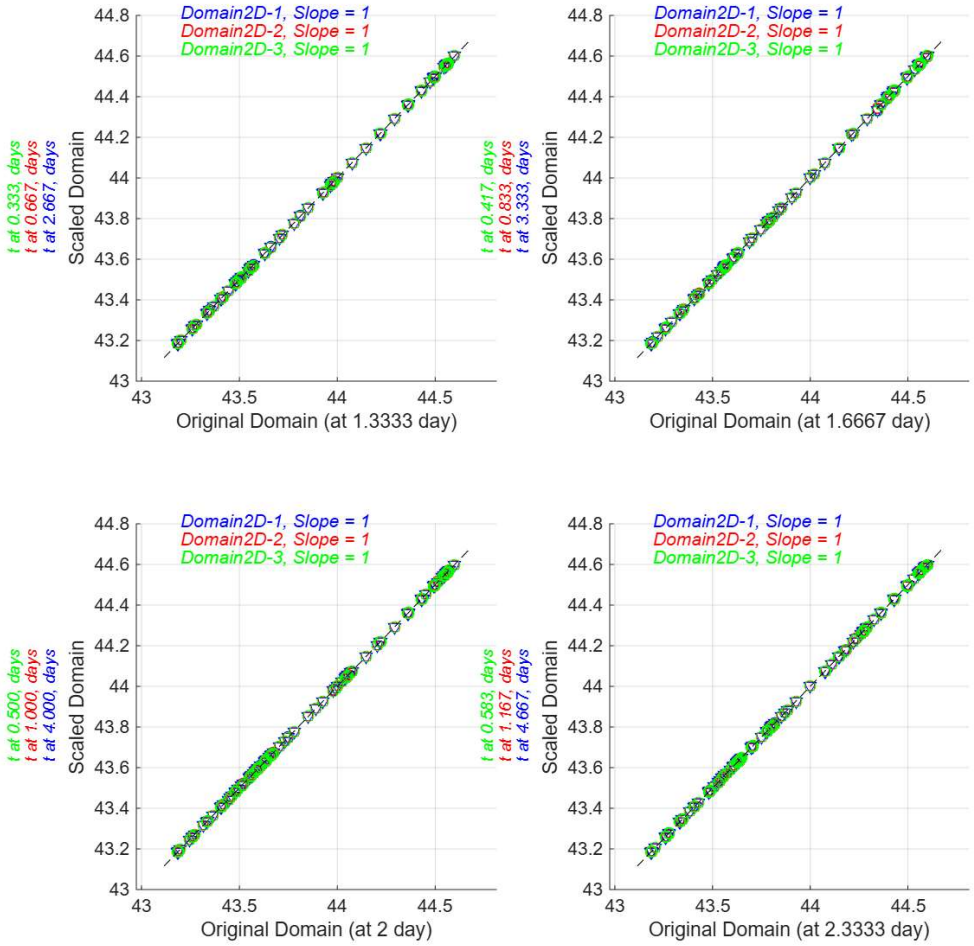

Figure 6.5. Scatter plots comparing water content (%) values in Domain 2D-0 (prototype domain) with those in scaled Domains 2D-1, 2D-2, and 2D-3 at time steps from t = 0 to 3 days in the original domain and at the corresponding scaled times in the scaled domains for two-dimensional flow under identical hydraulic conductivity values (Case 1). The slope of the regression line is 1, reflecting the water content scaling ratio. (continued)

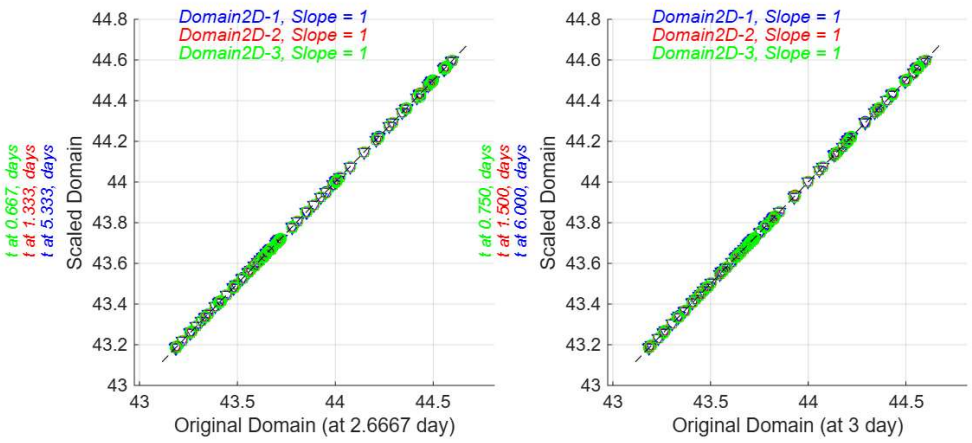

Original Domain at 3 days	R2	RMSE	NSE	NRMSE
Domain 2D-1 vs 2D-0	1.00000000	0.00000000	1.00000000	0.00000000
Domain 2D-2 vs 2D-0	1.00000000	0.00000000	1.00000000	0.00000000
Domain 2D-3 vs 2D-0	1.00000000	0.00000000	1.00000000	0.00000000

Figure 6.5. Scatter plots comparing water content (%) values in Domain 2D-0 (prototype domain) with those in scaled Domains 2D-1, 2D-2, and 2D-3 at time steps from t = 0 to 3 days in the original domain and at the corresponding scaled times in the scaled domains for two-dimensional flow under identical hydraulic conductivity values (Case 1). The slope of the regression line is 1, reflecting the water content scaling ratio.

5.2 Scaling Using Different Hydraulics Conductivities in Two-Dimensional Flow

In this case, scaling and self-similarity are achieved by employing different hydraulic conductivities in the original and scaled domains. This is achieved by using varying scaling exponents for distance and time, $\alpha_x = \alpha_z \neq \alpha_t$. As such, hydraulic conductivity is not kept constant because $\alpha_x - \alpha_t \neq 0$ and $\alpha_z - \alpha_t \neq 0$. Therefore, the scaling ratio of hydraulic conductivity will not be unity ($SR_K = \epsilon^{\alpha_K} = \epsilon^{\alpha_x - \alpha_t} = \epsilon^{\alpha_z - \alpha_t} \neq 1$).

Table 6.4 tabulates the scaling conditions used to obtain scaled domains from the original domain with different hydraulic conductivities for 2-dimensional flow through unsaturated porous media. The same Original (prototype) domain is used as Domain 2D-0 as in section 6.1. First three scaled domains (Domain 2D-1, 2D-2 and 2D-3) are for case 1, as shown above, and the next three domains (Domain 2D-4, 2D-5 and 2D-6) are for case 2. Domain 2D-4 is obtained by scaling spatial coordinates by $SR_x = \epsilon^{\alpha_x}$ and $\epsilon^{\alpha_z} = 0.5$, thus upscaling the original domain and scaling the time by $SR_t = \epsilon^{\alpha_t} = 4$. Domain 2D-5 is generated by applying scaling spatial coordinates by $SR_x = \epsilon^{\alpha_x}$ and $\epsilon^{\alpha_z} = 2$, thus downscaling the original domain, and scaling the time by $SR_t = \epsilon^{\alpha_t} = 4$. Domain 2D-6, on the other hand, is obtained by downscaling the original domain with $SR_x = \epsilon^{\alpha_x} = 4$ and $SR_t = \epsilon^{\alpha_t} = 0.5$. Thus, for domains 2D-4 and 2D-5 maximum simulation time is same. The scaling exponents and ratios of the other variables are then obtained as described above for all domains. Problem descriptions for the original and scaled domains for case 2 are tabulated in Table 6.5.

Temporal evolution of pressure head from t = 0 to 3 days in Domain 2D-0 (prototype domain), and at the corresponding scaled times in Domains 2D-4, 2D-5, and 2D-6 for two-dimensional flow under different hydraulic conductivity values are plotted in Figure 6.6. This figure demonstrates the visual self-similarity of

progression of unsteady flow regime between original (prototype) domain and scaled domains (Domains 2D-4, 2D-5, and 2D-6).

Temporal evolution of water content from t = 0 to 3 days in Domain 2D-0 (prototype domain), and at the corresponding scaled times in Domains 2D-4, 2D-5, and 2D-6 for two-dimensional flow under different hydraulic conductivity values are plotted in Figure 6.7. This figure visually demonstrates and compares the scaling and self-similarity concept between original and scaled domains.

To quantitatively demonstrate self-similarity, scatter plots comparing pressure head values in Domain 2D-0 (prototype domain) with those in scaled Domains 2D-4, 2D-5, and 2D-6 at time steps from t = 0 to 3 days in the original domain and at the corresponding scaled times in the scaled domains are plotted in Figure 6.8. R2, NRMSE and NSE values are also calculated between the pressure head values of the original domain and their corresponding scaled domain values multiplied with pressure head scaling ratio. Across all comparisons, the R2 and NSE values remain 1.000, and RMSE value remain 0.000, indicating perfect self-similarity between the original and scaled domains. The slope of each scatter plot where the vertical axis represents the scaled domain and the horizontal axis represents Domain 2D-0, is equal to the inverse of the pressure head scaling ratio:

In Figure 6.8:

- (Domain 2D-4), the slope is 2 which is $1/SR_\psi$ as expected
- (Domain 2D-5), the slope is 0.5 which is $1/SR_\psi$ as expected
- (Domain 2D-6), the slope is 0.25 which is $1/SR_\psi$ as expected

Similarly, scatter plots of water content values in Domain 2D-0 (original) and Domains 2D-4, 2D-5, and 2D-6 are shown in Figure 6.9. These plots compare data at times t = 0 to 3 days in Domain 2D-0 with the corresponding scaled times in each respective domain. R2, NRMSE and NSE values are also calculated between the water content values of the original domain and their corresponding scaled domain values. Across all comparisons, the R2 and NSE values remain 1.000, and

RMSE value remain 0.000, indicating perfect self-similarity between the original and scaled domains. The slope of each scatter plot where the vertical axis represents the scaled domain and the horizontal axis represents Domain 2D-0 (original domain), is equal to unity, which shows water content is scale invariant:

In Figure 6.9:

- (Domain 2D-4), the slope is 1 where water content is scale invariant as expected
- (Domain 2D-5), the slope is 1 where water content is scale invariant as expected
- (Domain 2D-6), the slope is 1 where water content is scale invariant as expected

These slopes directly reflect the scaling ratios of pressure head and water content between each scaled domain and the original domain.

Table 6.4 Scaling conditions used to obtain scaled domains from the original domain with different hydraulic conductivities for 2-dimensional flow through unsaturated porous media

Description	Symbol / scaling condition	Domain 2D-4	Domain 2D-5	Domain 2D-6
Scaling parameter	ε	2	2	2
Scaling exponent of x	α_x	-1	1	2
Scaling exponent of z	α_z	-1	1	2
Scaling exponent of time	α_t	2	2	-1
scaling exponent of hydraulic conductivity	$\alpha_K = \alpha_x - \alpha_t$	-3	-1	3
scaling exponent of infiltration velocity	$\alpha_V = \alpha_x - \alpha_t$	-3	-1	3
scaling exponent of pressure head	$\alpha_h = \alpha_x$	-1	1	2
scaling ratio of x	$SR_x = \epsilon^{\alpha_x}$	0.5	2	4
scaling ratio of z	$SR_z = \epsilon^{\alpha_z}$	0.5	2	4
scaling ratio of time	$SR_t = \epsilon^{\alpha_t}$	4	4	0.5
scaling ratio of hydraulic conductivity	$SR_K = \epsilon^{\alpha_K}$	0.125	0.5	8
scaling ratio of velocity	$SR_V = \epsilon^{\alpha_V}$	0.125	0.5	8
scaling ratio of pressure head	$SR_h = \epsilon^{\alpha_h}$	0.5	2	4

Table 6.5 Problem descriptions for the original and scaled domains with different hydraulic conductivities for 2-dimensional flow through unsaturated porous media

Symbol	Variable	Dimension	Domain 2D-0 Original	Domain 2D-4	Domain 2D-5	Domain 2D-6
Lx	length in X direction	[L] (m)	2	4	1	0.5
Lz	length in Z direction	[L] (m)	3	6	1.5	0.75
Δx	Grid size in x direction	[L] (m)	0.2	0.4	0.1	0.05
Δz	Grid size in z direction	[L] (m)	0.3	0.6	0.15	0.075
T	maximum time	[T] (days)	3	0.75	0.75	6
Δt	Time step	[T] (days)	0.333	0.083	0.083	0.667
α	van Genuchten parameter	[1/L] (m)	0.152	0.076	0.304	0.608
n	van Genuchten parameter	-	1.17	1.17	1.17	1.17
Ks	saturated conductivity	[L/T] (m)	0.00082	0.00656	0.00164	0.0001025
θ_S	Theta (Water Content) saturated	-	0.446	0.446	0.446	0.446
θ_R	Theta (Water Content) residual	-	0	0	0	0

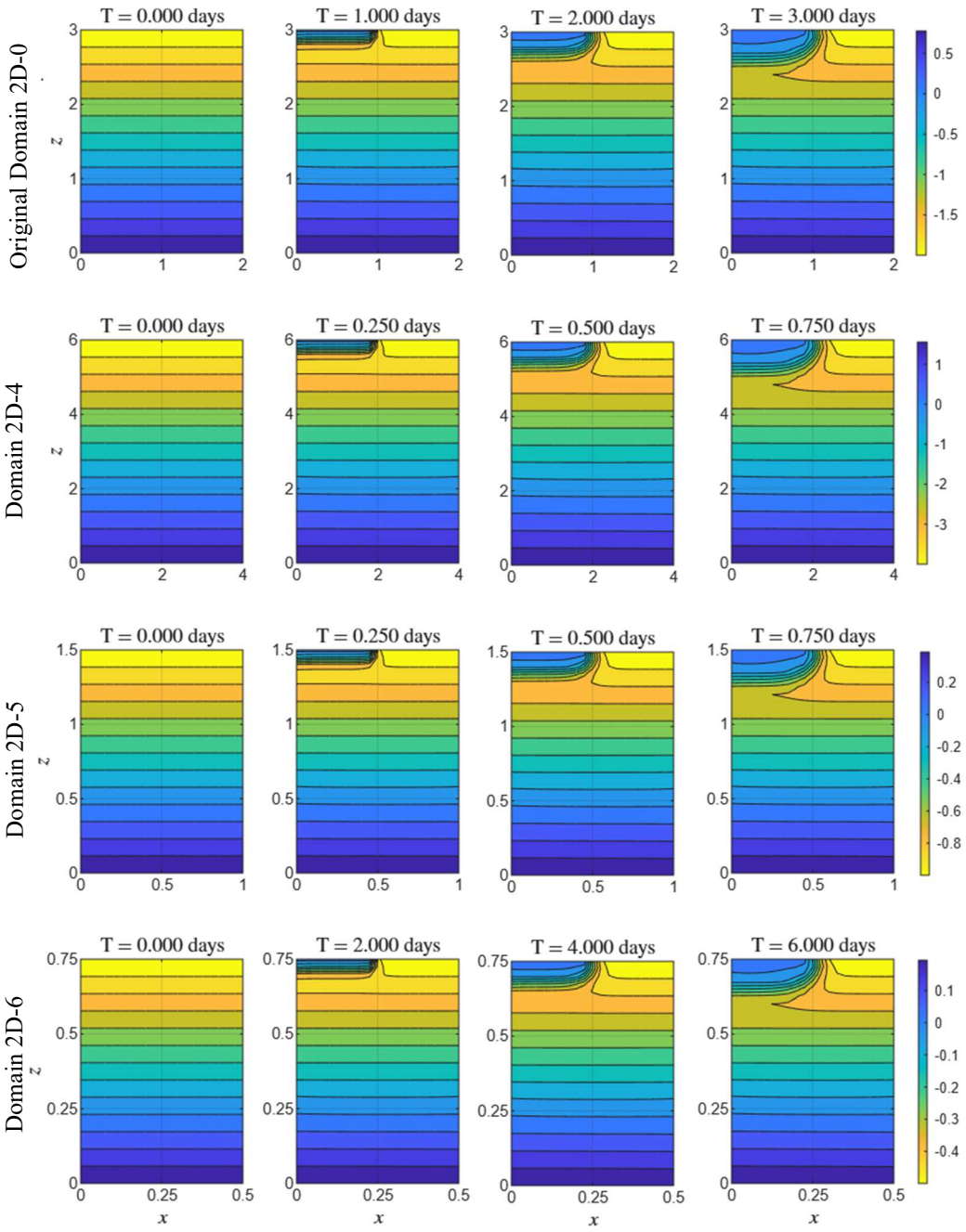

Figure 6.6. Temporal evolution of pressure head (m) from t = 0 to 3 days in Domain 2D-0 (prototype domain), and at the corresponding scaled times in Domains 2D-4, 2D-5, and 2D-6 for two-dimensional flow under different hydraulic conductivity values (Case 2).

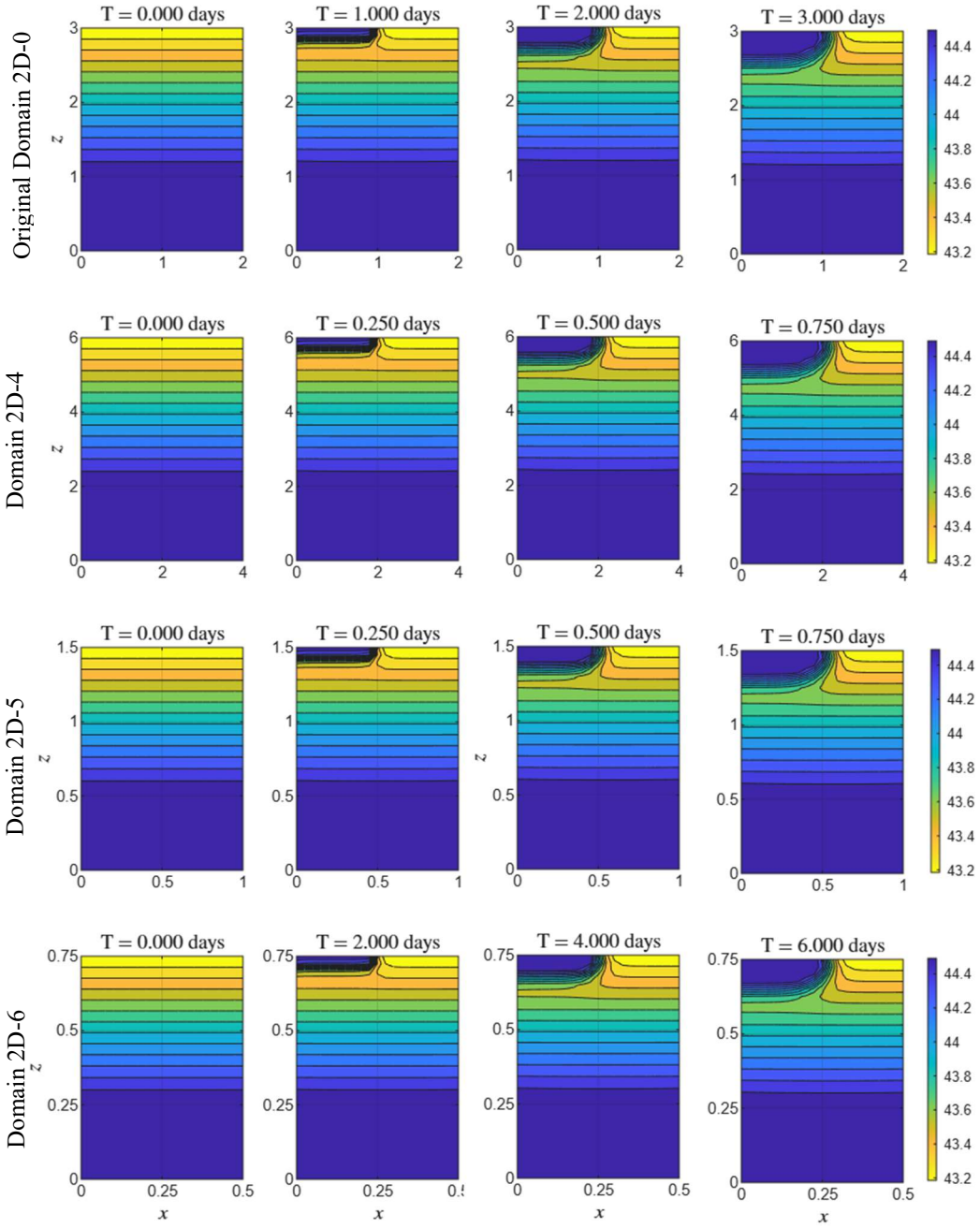

Figure 6.7. Temporal evolution of water content (%) from t = 0 to 3 days in Domain 2D-0 (prototype domain), and at the corresponding scaled times in Domains 2D-4, 2D-5, and 2D-6 for two-dimensional flow under different hydraulic conductivity values (Case 2).

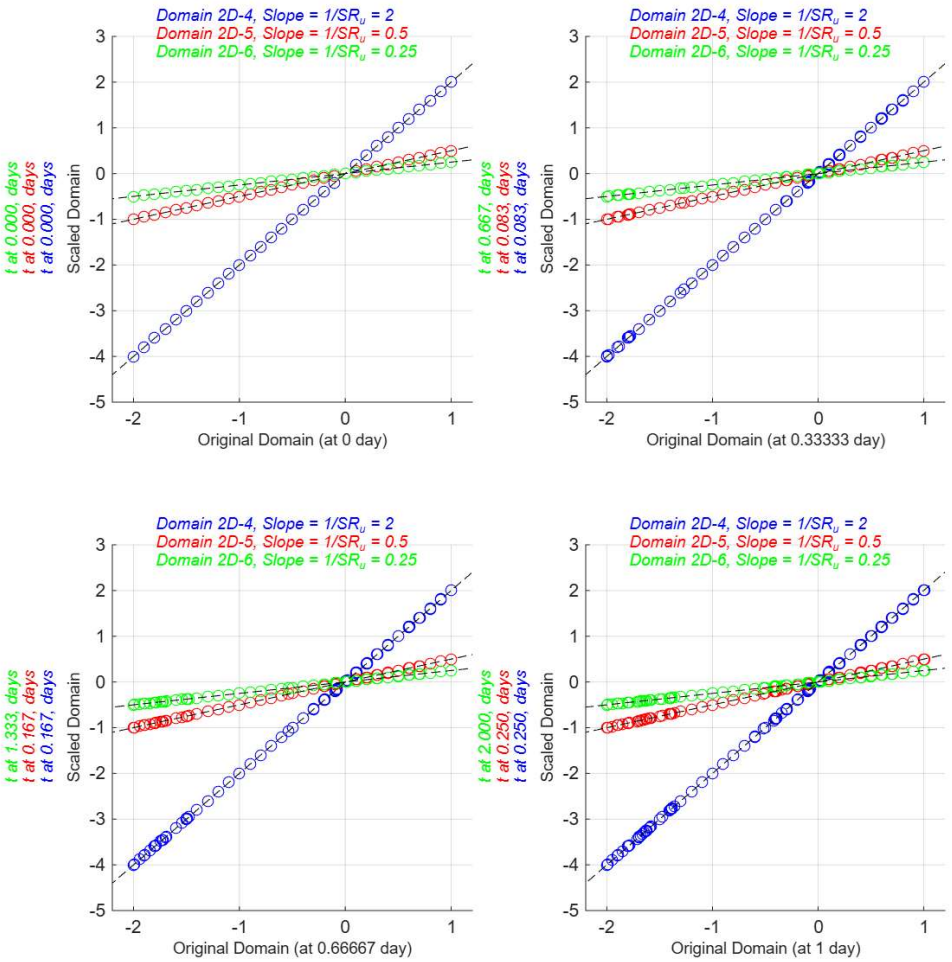

Figure 6.8. Scatter plots comparing pressure head (m) values in Domain 2D-0 (prototype domain) with those in scaled Domains 2D-4, 2D-5, and 2D-6 at time steps from t = 0 to 3 days in the original domain and at the corresponding scaled times in the scaled domains for two-dimensional flow with different hydraulic conductivity values (Case 2). The slope of the regression line represents the inverse of the pressure head scaling ratio ($1/SR_\psi$). (continued)

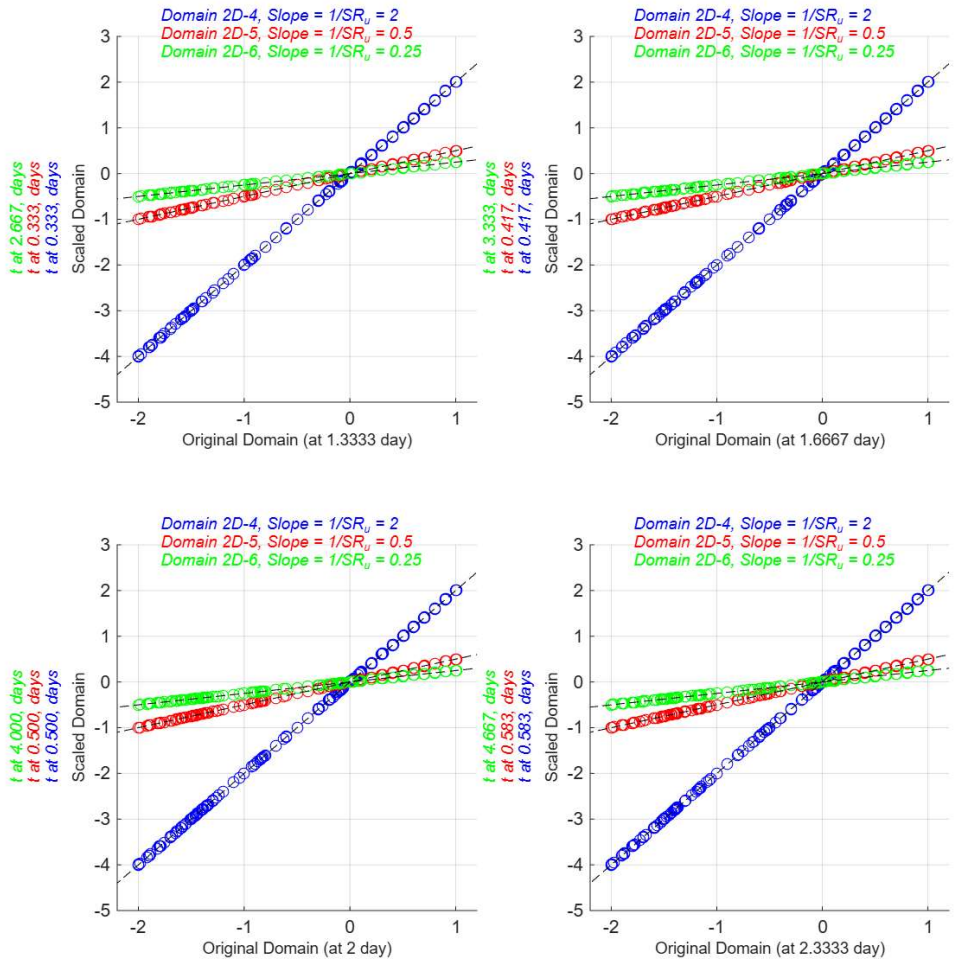

Figure 6.8. Scatter plots comparing pressure head (m) values in Domain 2D-0 (prototype domain) with those in scaled Domains 2D-4, 2D-5, and 2D-6 at time steps from t = 0 to 3 days in the original domain and at the corresponding scaled times in the scaled domains for two-dimensional flow with different hydraulic conductivity values (Case 2). The slope of the regression line represents the inverse of the pressure head scaling ratio ($1/SR_\Psi$). (continued)

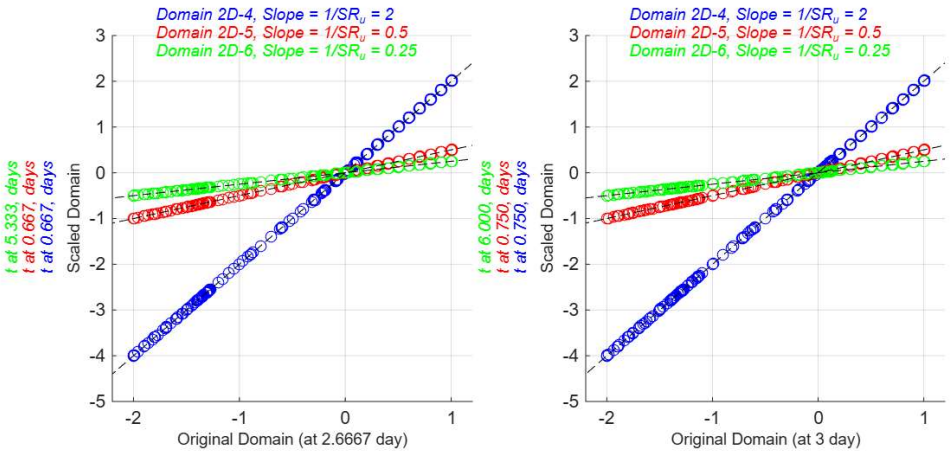

Original Domain at 3 days	R2	RMSE	NSE	NRMSE
Domain 2D-1 vs 2D-0	0.99999958	0.00055117	0.9999958	0.00018349
Domain 2D-2 vs 2D-0	0.99999964	0.00050874	0.9999964	0.00016936
Domain 2D-3 vs 2D-0	0.99999946	0.00062336	0.9999946	0.00020752

Figure 6.8. Scatter plots comparing pressure head (m) values in Domain 2D-0 (prototype domain) with those in scaled Domains 2D-4, 2D-5, and 2D-6 at time steps from t = 0 to 3 days in the original domain and at the corresponding scaled times in the scaled domains for two-dimensional flow with different hydraulic conductivity values (Case 2). The slope of the regression line represents the inverse of the pressure head scaling ratio ($1/SR_\Psi$).

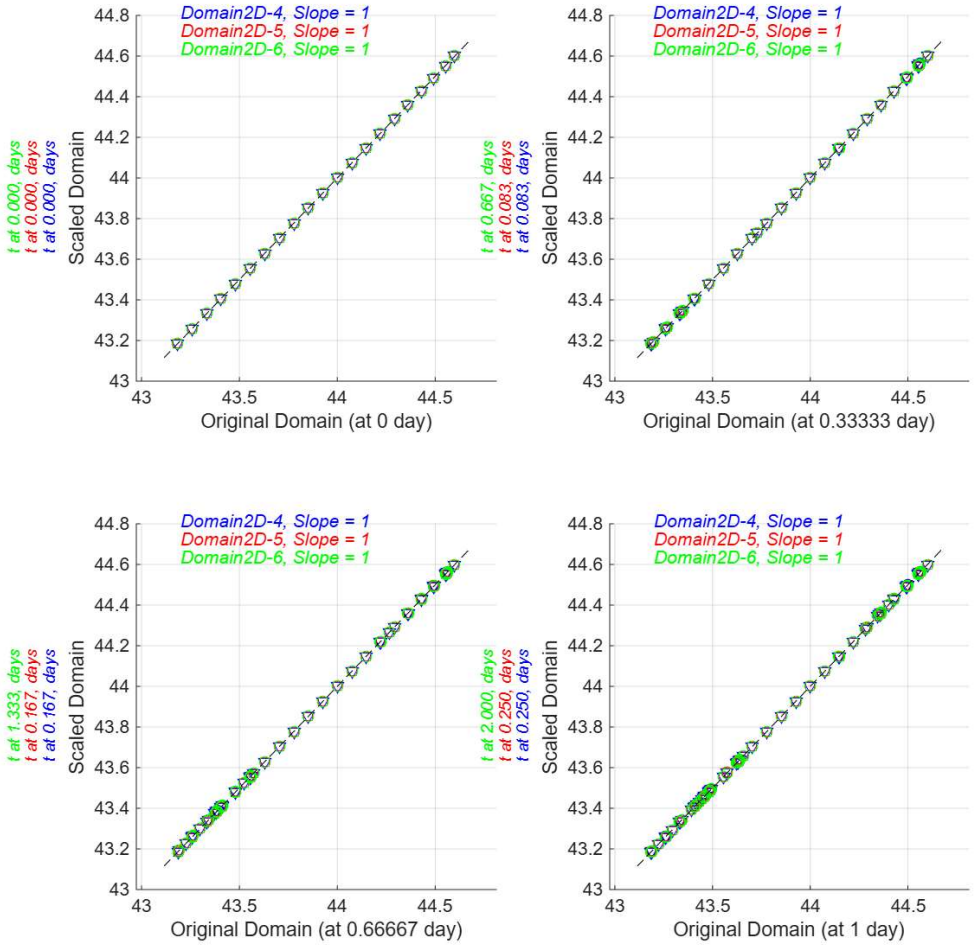

Figure 6.9. Scatter plots comparing water content (%) values in Domain 2D-0 (prototype domain) with those in scaled Domains 2D-4, 2D-5, and 2D-6 at time steps from t = 0 to 3 days in the original domain and at the corresponding scaled times in the scaled domains for two-dimensional flow with different hydraulic conductivity values (Case 2). The slope of the regression line is 1, reflecting the water content scaling ratio. (continued)

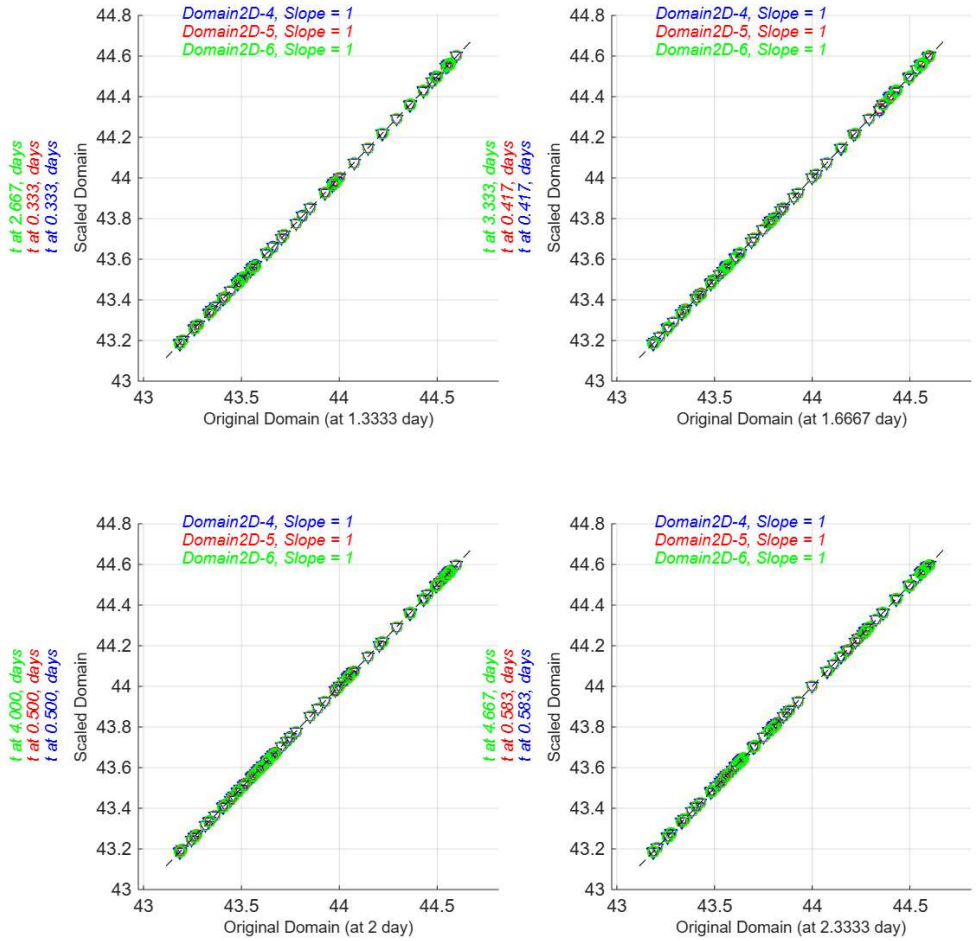

Figure 6.9. Scatter plots comparing water content (%) values in Domain 2D-0 (prototype domain) with those in scaled Domains 2D-4, 2D-5, and 2D-6 at time steps from t = 0 to 3 days in the original domain and at the corresponding scaled times in the scaled domains for two-dimensional flow with different hydraulic conductivity values (Case 2). The slope of the regression line is 1, reflecting the water content scaling ratio. (continued)

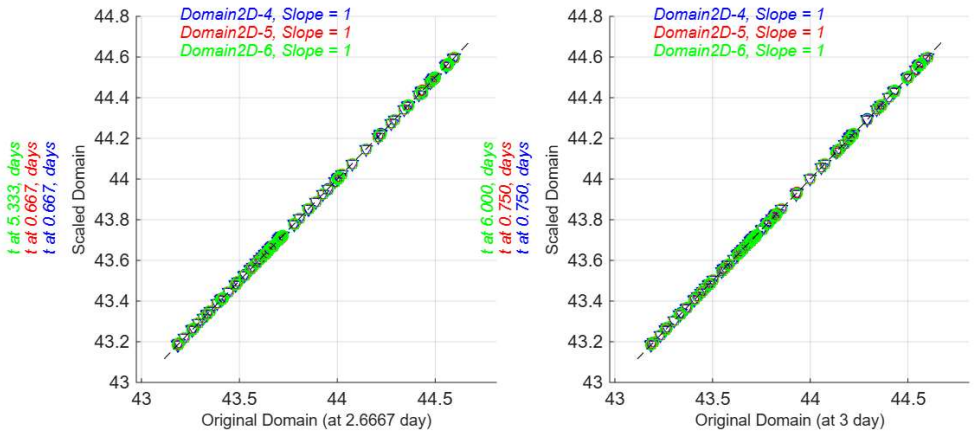

Original Domain at 3 days	R2	RMSE	NSE	NRMSE
Domain 1D-1 vs 1D-0	1.00000000	0.00000000	1.00000000	0.00000000
Domain 1D-2 vs 1D-0	1.00000000	0.00000000	1.00000000	0.00000000
Domain 1D-3 vs 1D-0	1.00000000	0.00000000	1.00000000	0.00000000

Figure 6.9. Scatter plots comparing water content (%) values in Domain 2D-0 (prototype domain) with those in scaled Domains 2D-4, 2D-5, and 2D-6 at time steps from t = 0 to 3 days in the original domain and at the corresponding scaled times in the scaled domains for two-dimensional flow with different hydraulic conductivity values (Case 2). The slope of the regression line is 1, reflecting the water content scaling ratio.

CHAPTER 7

CONCLUSIONS

6.1 Summary and Concluding Remarks

Researchers have explored scaling and self-similarity in hydrologic and hydraulic processes governed by nonlinear partial differential equations to better understand and represent their complexity. In this study, a theoretical scaling framework based on Lie group point transformations was developed, under which one-, two-, and three-dimensional unsteady flow in unsaturated porous media admits self-similar behavior. The proposed analysis extends classical scaling and self-similarity theory to initial and boundary value problems of multi-dimensional unsteady unsaturated flow, therefore bridging a critical gap between traditional hydrodynamic scaling concepts and porous media flow theory. Originally developed by Sophus Lie in the 19th century for solving differential equations, the Lie group theory provides a powerful foundation for identifying self-similarity conditions in complex physical processes. A key advantage of the proposed approach is its ability to obtain self-similarity of the unsteady flow not only based on the governing equations but also in relation to the initial and boundary conditions, offering a more comprehensive understanding of the problem's scaling and self-similarity behavior.

Numerical simulations were employed to demonstrate the existence of self-similar solutions across multiple space-time domains under the derived scaling transformations, confirming that self-similarity can be achieved under the proposed conditions. In engineering practice, the configuration of experimental studies is often constrained by factors such as available laboratory space, accessible materials, and feasible experimental durations. The resulting scaling relations provide a theoretical basis for enhanced spatial and temporal flexibility in physical modeling and offer new insights into the structure of unsteady flow in unsaturated

porous media. The resulting scaling relations provide a theoretical basis for enhanced spatial and temporal flexibility in physical modeling and offer new insights into the structure of unsteady flow in unsaturated porous media.

Scaling and self-similarity conditions for the one-, two-, and three-dimensional forms of the Richards equation were derived using Lie point group transformations as a novel scaling methodology. For the one- and two-dimensional cases, two benchmark problems reported in the literature were adopted as prototype domains. These problems provided computational grids, material parameters, and associated initial and boundary conditions. Scaling conditions obtained by the Lie group transformations were applied to these problems to generate scaled and self-similar domains. The validity of the proposed scaling framework was assessed by comparing numerical solutions between the prototype and scaled domains. Comparisons were conducted for the temporal evolution during the unsteady flow regime. For each one- and two-dimensional case, two scenarios were examined: Case 1, in which the hydraulic conductivity remained unchanged between the prototype and scaled domains (representing identical porous media), and Case 2, in which hydraulic conductivity varied (representing different porous media).

In both cases, self-similarity was visually confirmed through consistent geometric patterns and solution structures in the transient evolution of the flow fields. Scatter plots of corresponding flow variables from the prototype and scaled domains exhibited linear alignment, indicating expected scaling behavior. Beyond visual agreement, quantitative verification was performed by comparing solution values from the prototype and scaled domains at matching time steps using scatter plots. These comparisons demonstrated linear relationships consistent with the derived scaling conditions. To rigorously evaluate the accuracy of the scaling, the coefficient of determination (R^2) was employed as a statistical metric. An R^2 value of unity was consistently obtained, indicating perfect linear correlation between the corresponding datasets. This result provides strong evidence that the scaled solutions precisely reproduce the behavior of the prototype solutions under the defined scaling transformations; therefore, confirming the robustness and

effectiveness of the proposed scaling approach through both graphical and statistical validation.

It was observed that water content did not scale under the derived transformations. This outcome is theoretically expected, as the scaling analysis based on Lie point group transformations reveals that the water content variable does not acquire a scaling exponent. Specifically, the mathematical structure of the Richards equation does not introduce a scaling factor for water content under the admitted symmetry transformations. Consequently, water content remains invariant, in contrast to other variables such as pressure head or hydraulic conductivity that exhibit explicit scaling behavior. This theoretical result is fully consistent with the numerical observations and further validates the symmetry-based scaling framework developed in this study.

6.2 Limitations and Recommendations for Future Research

There are several limitations to this study that should be acknowledged. Firstly, the scaling conditions derived using Lie point group transformations were formulated for the three-dimensional Richards equation (Section 4.2.3). However, the numerical verification presented in Chapters 5 and 6 is limited to one- and two-dimensional example problems. The three-dimensional case was not numerically investigated; only the theoretical scaling conditions of the three-dimensional case were established in Chapter 4. Consequently, future studies should include three-dimensional numerical simulations to explicitly verify the proposed scaling conditions for the 3D Richards equation. Secondly, no experimental demonstration was illustrated in this study. Only the numerical examples, which were performed in literature, were used as the basis to verify the proposed scaling framework based on Lie group point transformations.

Lastly, porous media heterogeneity was not considered in the numerical example problems, although the proposed scaling framework is theoretically valid for both

homogeneous and heterogeneous porous media. In practice, homogeneous porous media with constant hydraulic properties are rarely encountered. The vadose zone typically exhibits substantial heterogeneity, including macropores, fractures, sand lenses, rock inclusions, layered clay-silt sequences, root channels, organic matter variability, and anthropogenic disturbances such as compacted layers. These heterogeneities can strongly influence infiltration processes, flow paths, and moisture redistribution in unsaturated soils. As such, effects of heterogeneous porous media on the proposed scaling relations should also be investigated by numerical or laboratory experiments in the future.

REFERENCES

Assouline, S., Ciriello, V., & Tartakovsky, D. M. (2017). Estimation of intrinsic length scales of flow in unsaturated porous media. Water Resources Research, 53(11), 9980-9987.

Barry, D. A., Lisle, I. G., Li, L., Prommer, H., Parlange, J. Y., Sander, G. C., & Griffioen, J. W. (2001). Similitude applied to centrifugal scaling of unsaturated flow. Water Resources Research, 37(10), 2471-2479.

Baroghel-Bouny, V. (2007). Water vapour sorption experiments on hardened cementitious materials. Part II: Essential tool for assessment of transport properties and for durability prediction. Cement and Concrete Research, 37(3), 438-454.

Bear, J. (1972). Dynamics of Fluids in Porous Media. American Elsevier Publishing Company. A more advanced theoretical treatment of fluid flow in porous media, including unsaturated conditions.

Bear, J. (2018). Modeling Phenomena of Flow and Transport in Porous Media. Springer International Publishing AG, Switzerland. https://doi.org/10.1007/978-3-319-72826-1

Bear, J., & Cheng, A. H. D. (2010). Modeling groundwater flow and contaminant transport (Vol. 23, p. 834). Dordrecht: Springer.

Bluman, C.E., Cole, J.D., (1974). Similarity Methods for Differential Equations. Springer-Verlag, New York.

Bluman, G. W., & Anco, S. C. (2002). Symmetry and integration methods for differential equations. New York, NY: Springer New York.

Brooks, R.H. & Corey, A.T. (1964). Hydraulic properties of porous media. Hydrology Paper No. 3, Colorado State University, Fort Collins, Colo.

Buckingham, E. (1914). On physically similar systems; illustrations of the use of dimensional equations. Physical Review, 4(4), 345-376.

Carr, K. J., Ercan, A., and Kavvas, M. L. (2015). Scaling and self-similarity of one-dimensional unsteady suspended sediment transport with emphasis on unscaled sediment material properties. Journal of Hydraulic Engineering, 141(5), (ASCE)HY.1943-7900.0000994.

Catucci, D., Briganti, R., & Heller, V. (2021). Numerical validation of novel scaling laws for air entrainment in water. Proceedings of the Royal Society A, 477(2255), 20210339.

Catucci, D., Briganti, R., & Heller, V. (2023). Numerical validation of novel scaling laws for air–water flows including compressibility and heat transfer. Journal of Hydraulic Research, 61(4), 517-531.

Darcy, H (1856). Les Fontaines Publiques de la Ville de Dijon, Dalmont, Paris.

Ercan, A., Kavvas, M.L. & Haltas, I. (2014). Scaling and self-similarity in one-dimensional unsteady open channel flow. Hydrol. Process., 28, 2721-2737.

Ercan, A., Kavvas, M.L. (2015a). Scaling and self-similarity in two-dimensional hydrodynamics. Chaos 25 (7), 075404.

Ercan, A., Kavvas, M.L. (2015b.). Self-similarity in Navier-Stokes equations. Chaos 25 (12), 123126.

Ercan, A., Kavvas, M.L. (2017). Scaling Relations and Self-Similarity of 3-Dimensional Reynolds-Averaged Navier-Stokes Equations. Sci Rep 7, 6416

Ercan, A. (2020). Self-similarity in fate and transport of contaminants in groundwater. Science of The Total Environment, 706, 135738.

Fetter Jr, C. W. (2001). Applied Hydrogeology Fetter Fourth Edition.

Freeze, R.A. and Cherry, J.A. (1979). Groundwater. Prentice-Hall, Englewood Cliffs, NJ.

Hall, C. (1989). Water sorptivity of mortars and concretes: a review. Magazine of Concrete Research, 41(147), 51-61.

Haltas I., Kavvas M.L. (2011) Scale Invariance and Self-Similarity in Hydrologic Processes in Space and Time, Journal of Hydrologic Engineering 16(1), 51-63.

Hodson, T. O. (2022). Root mean square error (RMSE) or mean absolute error (MAE): When to use them or not. Geoscientific Model Development Discussions, 2022, 1-10.

Holzbecher, E. (2012). Environmental modeling: Using MATLAB®. Environmental Modeling: Using MATLAB®, 9783642220425, 1–410.

Hornberger, G. & Wiberg, P. (2005). Numerical Methods in Hydrological Sciences. Am. Geophys. Union, Washington D.C., e-book.

Ibragimov, N.H. (1994). CRC Handbook of Lie Group Analysis of Differential Equations. CRC Press.

Knoben, W. J. M., Freer, J. E., & Woods, R. A. (2019). Technical note: Inherent problems of the Nash–Sutcliffe efficiency for model evaluation. Hydrology and Earth System Sciences.

Lie, S. (1888). Theorie der transformationsgruppen. 1. Teubner, Leipzig. – CROSS REFERENCE: Lie, S. (2015). *Theory of Transformation Groups I: General Properties of Continuous Transformation Groups. A Contemporary Approach and Translation*. Springer.

List, F., & Radu, F. A. (2016). A study on iterative methods for solving Richards' equation. Computational Geosciences, 20(2), 341-353.

Mandelbrot, B. B. (1982). The fractal geometry of nature (Vol. 1, pp. 25-74). New York: WH freeman.

Miller, E. E., & Miller, R. D. (1956). Physical theory for capillary flow phenomena. Journal of Applied Physics, 27(4), 324-332.

Moriasi, D. N., Arnold, J. G., Van Liew, M. W., Bingner, R. L., Harmel, R. D., & Veith, T. L. (2007). Model evaluation guidelines for systematic quantification of accuracy in watershed simulations. Transactions of the ASABE.

Mualem, Y. (1976). A new model for predicting the hydraulic conductivity of unsaturated porous media. Water Resources Research, 12(3), 513-522.

Newman, A. J., et al. (2015). Development of a large-sample watershed-scale hydrometeorological data set for the contiguous US: data set characteristics and regional model performance. Hydrology and Earth System Sciences.

Nimmo, J.R. (2004). Porosity and pore size distribution. In Hillel, D. (Ed.), Encyclopedia of Soils in the Environment (pp. 295–303). Elsevier.

Pearson, K. (1896). VII. Mathematical contributions to the theory of evolution.—III. Regression, heredity, and panmixia. Philosophical Transactions of the Royal Society of London. Series A, containing papers of a mathematical or physical character, (187), 253-318.

Polsinelli, J. & Kavvas, M. L. (2016). A comparison of the modern Lie scaling method to classical scaling techniques. Hydrol. Earth Syst. Sci., 20, 2669–2678.

Polyanin AD, Manzhirov AV. (2006). Handbook of Mathematics for Engineers and Scientists, 1st edn. Chapman & Hall/CRC: FL, USA; ISBN-10 1584885025.

Reichardt, K., Nielsen, D. R., & Biggar, J. W. (1972). Scaling of horizontal infiltration into homogeneous soils. Soil Science Society of America Journal, 36(2), 241-245.

Richards, L. A. (1931). Capillary conduction of liquids through porous mediums. Physics, 1(5), 318–333.

Rodriguez-Iturbe, I., & Rinaldo, A. (1997). Fractal River Basins: Chance and Self-Organization. Cambridge University Press.

Russo, D., & Bresler, E. (1980). Scaling soil hydraulic properties of a heterogeneous field soil. Soil Science Society of America Journal, 44(4), 681-684.

Sadeghi, M., Ghahraman, B., Davary, K., Hasheminia, S. M., & Reichardt, K. (2011). Scaling to generalize a single solution of Richards' equation for soil water redistribution. Scientia Agricola, 68, 582-591.

Sadeghi, M., Ghahraman, B., Ziaei, A. N., Davary, K., & Reichardt, K. (2012a). Invariant solutions of Richards' equation for water movement in dissimilar soils. Soil Science Society of America Journal, 76(1), 1-9.

Sadeghi, M., Ghahraman, B., Ziaei, A. N., Davary, K., & Reichardt, K. (2012b). Additional scaled solutions to Richards' equation for infiltration and drainage. Soil and Tillage research, 119, 60-69.

Saeid E., Faezeh E. (2025) Handbook of Hydrosystem Restoration Groundwater Natural Recharge (GNR) 1st Edition - August 29, 2025 Imprint: Elsevier Paperback ISBN: 9780443288265, eBook ISBN: 9780443288272.

Scanlon, B. R., Healy, R. W., Davis, J. M., Anderson, T., & Fahlquist, L. (2002). Choosing appropriate techniques for quantifying groundwater recharge. Hydrogeology Journal, 10(1), 18-39.

Selker, J. S., McCord, J. T., & Keller, C. K. (1999). Vadose zone processes. CRC Press.

Sharma, M. L., Gander, G. A., & Hunt, C. G. (1980). Spatial variability of infiltration in a watershed. Journal of Hydrology, 45(1-2), 101-122.

Simmons, C. S., Nielsen, D. R., & Biggar, J. W. (1979). Scaling of field-measured soil water properties. Hilgardia, 47(4), 77-173.

Šimůnek, J., van Genuchten, M. T., & Šejna, M. (2016). Recent developments and applications of the HYDRUS computer software packages. Vadose Zone Journal, 15(7).

Suciu, N., Illiano, D., Prechtel, A., & Radu, F. A. (2021). Global random walk solvers for fully coupled flow and transport in saturated/unsaturated porous media. Advances in Water Resources, 152, 103935.

Sposito, G. (1990). Lie group invariance of the Richards equation. IN: Dynamics of Fluids in Hierarchical Porous Media. Academic Press, Inc., San Diego, California. 1990. p 327-347, 1 tab, 40 ref, append. NSF Grant.Sposito, G. (1995). Recent advances associated with soil water in the unsaturated zone.

Sposito, G., & Jury, W. A. (1985). Inspectional analysis in the theory of water flow through unsaturated soil. Soil Science Society of America Journal, 49(4), 791-798.Sposito, G., and Jury, W. A. (1990). Miller similitude and generalized scaling analysis.

Taylor, R.G., Scanlon, B., Döll, P., Rodell, M., van Beek, R., Wada, Y., Longuevergne, L., et al. (2013). Ground water and climate change. Nature Climate Change, 3(4), 322-329.

Toride, N., Leij, F. J., & Van Genuchten, M. T. (1995). The CXTFIT code for estimating transport parameters from laboratory or filed tracer experiments. US Salinity Laboratory.

Trenberth, K. E. (2011). Changes in precipitation with climate change. Climate Research, 47(1-2), 123-138.

Turcotte, D. L. (1989). Fractals in geology and geophysics. Pure and Applied Geophysics, 131(1-2), 171-196.

Van Genuchten, M.T. (1980). A closed-form equation for predicting the hydraulic conductivity of unsaturated soils. Soil Sci. Soc. Am. J., 44, 892–898.

Wang, Z. (2021). Scaling analysis of Richards equation for horizontal infiltration and its approximate solution. Soil Science Society of America Journal, 85(5), 1555-1565.

Warrick, A. W., Mullen, G. J., & Nielsen, D. R. (1977). Scaling field-measured soil hydraulic properties using a similar media concept. Water Resources Research, 13(2), 355-362.

Warrick, A. W., & Amoozegar-Fard, A. (1979). Infiltration and drainage calculations using spatially scaled hydraulic properties. Water Resources Research, 15(5), 1116-1120.

Warrick, A. W. (1990). Application of scaling to the characterization of spatial variability in soils. In D. Hillel & D. E. Elrick (Eds.), Scaling in Soil Physics: Principles and Applications (pp. 39-51). Soil Science Society of America.

Warrick, A. W., & Hussen, A. A. (1993). Scaling of Richards' equation for infiltration and drainage. Soil Science Society of America Journal, 57(1), 15-18.

CURRICULUM VITAE

PERSONAL INFORMATION
Surname, Name: Basa, Mustafa Mazhar

EDUCATION

Degree	Institution	Year of Graduation
MS	METU Civil Engineering	2006
BS	METU Civil Engineering	2002
High School	Atatürk Anadolu High School, Ankara	1997

WORK EXPERIENCE

Year	Place	Enrollment
2009-Present	Gulermak	Project Controls Manager
2006-2009	Ekatek	Design and Software Development Engineer
2003-2006	Ertugrul-Kur Insaat	Site Engineer, Design Engineer
2002-2003	Albatros Technologies	Software Sales Engineer

FOREIGN LANGUAGES
Fluent English, Intermediate Polish

PUBLICATIONS

1. Basa, M. M. (2006). Determination of computational domain boundaries for viscous flow around two dimensional bodies (Master's thesis, Middle East Technical University, Civil Engineering, Hydromechanics, Turkey.)

HOBBIES

Cycling, Flight Simulators, Cooking